

**ISTANBUL TECHNICAL UNIVERSITY ★ INFORMATICS INSTITUTE**

**HYPERSPECTRAL DATA CLASSIFICATION  
USING CONTOURLET TRANSFORM**

**M.Sc. Thesis by  
Bedrettin Erbil KONUK**

**Department : Institute of Science and Technology**

**Programme : Satellite Communication and Remote Sensing**

**OCTOBER 2010**



**HYPERSPECTRAL DATA CLASSIFICATION  
USING CONTOURLET TRANSFORM**

**M.Sc. Thesis by  
Bedrettin Erbil KONUK  
(705071003)**

**Date of submission : 30 September 2010  
Date of defence examination: 11 October 2010**

**Supervisor (Chairman) : Assoc.Prof. Işın ERER (ITU)  
Members of the Examining Committee : Prof.Dr. Ahmet Hamdi KAYRAN (ITU)  
Assoc.Prof. İbrahim ALTUNBAŞ (ITU)**

**October 2010**



**İSTANBUL TEKNİK ÜNİVERSİTESİ ★ BİLİŞİM ENSTİTÜSÜ**

**CONTOURLET DÖNÜŞÜMÜ İLE  
HİPERSPEKTRAL VERİ SINIFLANDIRMA**

**YÜKSEK LİSANS TEZİ  
Bedrettin Erbil KONUK  
(705071003)**

**Tezin Enstitüye Verildiği Tarih : 30 Eylül 2010  
Tezin Savunulduğu Tarih : 11 Ekim 2010**

**Tez Danışmanı : Doç.Dr. Işın ERER (İTÜ)  
Diğer Jüri Üyeleri : Prof.Dr. Ahmet Hamdi KAYRAN (İTÜ)  
Doç.Dr. İbrahim ALTUNBAŞ (İTÜ)**

**Ekim 2010**



## **FOREWORD**

I would like to express my deep appreciation and thanks for my advisor Assoc.Prof. Işın Erer who guided me during the thesis research. I would like to thank also assistant Özgür Gültekin for both practical and theoretical ideas during the hard times. Colonel Kemal Denктаş is another person to thank for helping me discover my academic potential and encouraging me for pursuing the graduate study. Finally and most importantly, I wish to thank my parents and sister, Dr. Sara Banu Akkaş and Ebru Buharalıođlu who gave me precious support during the thesis preparation times. Without them, this work would not be as it has finally become.

I would like to dedicate this work to my friend and my former colleague 2<sup>nd</sup> Lieutenant Zafer Oluk who passed away after a tragic accident on 5th May 2008 during his military duty. I wished you could read this work and discuss with me its flaws.

September 2010

Bedrettin Erbil KONUK  
Electrical & Electronics Engineer





## TABLE OF CONTENTS

	<u>Page</u>
<b>ABBREVIATIONS</b> .....	<b>ix</b>
<b>LIST OF TABLES</b> .....	<b>xi</b>
<b>LIST OF FIGURES</b> .....	<b>xiii</b>
<b>SUMMARY</b> .....	<b>xv</b>
<b>ÖZET</b> .....	<b>xvii</b>
<b>1. INTRODUCTION</b> .....	<b>1</b>
<b>2. DISCRETE WAVELET AND STATIONARY WAVELET TRANSFORM</b> ..	<b>5</b>
2.1 Continuous Wavelet Transform .....	7
2.2 Discrete Wavelet Transform .....	7
2.3 Discrete Wavelet Coefficients.....	8
2.4 2-D Discrete Wavelet Decomposition.....	9
2.5 Stationary Wavelet Transform .....	13
2.6 2-D Stationary Wavelet Decomposition .....	13
<b>3. CONTOURLET AND NONSUBSAMPLED CONTOURLET TRANSFORM</b> .....	<b>17</b>
3.1 Laplacian Pyramid Decomposition .....	17
3.2 Directional Filter Bank Decomposition .....	20
3.3 Contourlet Transform.....	24
3.4 Nonsubsampled Laplacian Pyramid Decomposition .....	27
3.5 Nonsubsampled Directional Filter Bank Decomposition.....	30
3.6 Nonsubsampled Contourlet Transform .....	33
<b>4. HYBRID CONTOURLET TRANSFORMS</b> .....	<b>37</b>
4.1 Wavelet Based Contourlet Transform.....	37
4.2 Stationary Wavelet Based Contourlet Transform .....	41
<b>5. FEATURE EXTRACTION AND CLASSIFICATION</b> .....	<b>45</b>
5.1 Introduction .....	45
5.2 Feature Extraction .....	45
5.2.1 Spectral Features .....	45
5.2.2 Shape Features .....	45
5.2.3 Texture Features.....	46
5.3 Classification Algorithms.....	46
5.3.1 Supervised and Unsupervised Learning.....	46
5.3.2 Discriminative and Generative Approaches .....	46
5.4 K-Nearest Neighbour Algorithm.....	48
5.5 Textures .....	48
5.5.1 Regular Textures .....	48
5.5.2 Statistical Textures .....	49
5.5.3 Synthetic Textures.....	49
5.5.4 Natural Textures.....	49
5.6 Brodatz Textures .....	49
5.7 Brodatz Texture Matrix Classification Algorithm .....	51

5.7.1 Discrete Wavelet Decomposition Features .....	53
5.7.2 Stationary Wavelet Decomposition Features .....	53
5.7.3 Contourlet Decomposition Features.....	54
5.7.4 Nonsubsampled Contourlet Decomposition Features .....	54
5.7.5 Wavelet Based Contourlet Decomposition Features.....	55
5.7.6 Stationary Wavelet Based Contourlet Decomposition Features .....	55
5.8 AVIRIS Indiana’s Indian Pine Hyperspectral Data.....	56
5.9 AVIRIS Hyperspectral Data Classification Algorithm .....	58
5.9.1 Discrete Wavelet Decomposition Features .....	60
5.9.2 Stationary Wavelet Decomposition Features .....	61
5.9.3 Contourlet Decomposition Features.....	62
5.9.4 Nonsubsampled Contourlet Decomposition Features .....	62
5.9.5 Wavelet Based Contourlet Decomposition Features.....	63
5.9.6 Stationary Wavelet Based Contourlet Decomposition Features .....	63
<b>6. RESULTS AND DISCUSSION.....</b>	<b>65</b>
6.1 Discrete Wavelet Transform Brodatz Results .....	66
6.2 Stationary Wavelet Transform Brodatz Results .....	67
6.3 Contourlet Transform Brodatz Results.....	68
6.4 Nonsubsampled Contourlet Transform Brodatz Results .....	69
6.5 Wavelet Based Contourlet Transform Brodatz Results.....	70
6.6 Stationary Wavelet Based Contourlet Transform Brodatz Results .....	71
6.7 Brodatz Results and Discussion .....	72
6.8 Discrete Wavelet Transform AVIRIS Results .....	74
6.9 Stationary Wavelet Transform AVIRIS Results .....	75
6.10 Contourlet Transform AVIRIS Results .....	76
6.11 Nonsubsampled Contourlet Transform AVIRIS Results .....	77
6.12 Wavelet Based Contourlet Transform AVIRIS Results.....	78
6.13 Stationary Wavelet Based Contourlet Transform AVIRIS Results .....	79
6.14 AVIRIS Results and Discussion.....	80
<b>7. RESULTS OVERVIEW AND CONCLUSION .....</b>	<b>83</b>
<b>REFERENCES .....</b>	<b>85</b>
<b>CURRICULUM VITAE .....</b>	<b>89</b>

## ABBREVIATIONS

<b>1-D</b>	: 1-Dimensional
<b>2-D</b>	: 2-Dimensional
<b>BT</b>	: Brodatz Textures
<b>CBF</b>	: Checker-Board Filter
<b>CD</b>	: Contourlet Decomposition
<b>CT</b>	: Contourlet Transform
<b>db4</b>	: Daubechies-4 Wavelet
<b>db6</b>	: Daubechies-6 Wavelet
<b>DWD</b>	: Discrete Wavelet Decomposition
<b>DWT</b>	: Discrete Wavelet Transform
<b>DFB</b>	: Directional Filter Bank
<b>DFBD</b>	: Directional Filter Bank Decomposition
<b>FT</b>	: Fourier Transform
<b>GT</b>	: Ground Truth
<b>HF</b>	: Hourglass Filter
<b>HPF</b>	: High-Pass Filter
<b>KNN</b>	: K-Nearest Neighbour
<b>LP</b>	: Laplacian Pyramid
<b>LPD</b>	: Laplacian Pyramid Decomposition
<b>LPF</b>	: Low-Pass Filter
<b>MLP</b>	: Multilayer Perceptrons
<b>MRA</b>	: Multiresolution Analysis
<b>NN</b>	: Neural Network
<b>NSCD</b>	: Nonsampled Contourlet Decomposition
<b>NSCT</b>	: Nonsampled Contourlet Transform
<b>NSDFB</b>	: Nonsampled Directional Filter Bank
<b>NSDFBD</b>	: Nonsampled Directional Filter Bank Decomposition
<b>NSLP</b>	: Nonsampled Laplacian Pyramid
<b>NSLPD</b>	: Nonsampled Laplacian Pyramid Decomposition
<b>PDFB</b>	: Pyramidal Directional Filter Bank
<b>QDF</b>	: Quincunx Downsampling Filter
<b>RVM</b>	: Relevance Vector Machines
<b>STFT</b>	: Short Time Fourier Transform
<b>SVM</b>	: Support Vector Machines
<b>SWBCD</b>	: Stationary Wavelet Based Contourlet Decomposition
<b>SWBCT</b>	: Stationary Wavelet Based Contourlet Transform
<b>SWD</b>	: Stationary Wavelet Decomposition
<b>SWT</b>	: Stationary Wavelet Transform
<b>WBCD</b>	: Wavelet Based Contourlet Decomposition
<b>WBCT</b>	: Wavelet Based Contourlet Transform
<b>WFT</b>	: Windowed Fourier Transform
<b>WT</b>	: Wavelet Transform



## LIST OF TABLES

	<b><u>Page</u></b>
<b>Table 5.1 :</b> AVIRIS Hyperspectral Data Classes. ....	57
<b>Table 6.1 :</b> BT Classification Results. ....	81
<b>Table 6.2 :</b> AVIRIS Hyperspectral Data Classification Results.....	81



## LIST OF FIGURES

	<u>Page</u>
<b>Figure 2.1 :</b> Examples of Wavelet Functions – Part 1. ....	5
<b>Figure 2.2 :</b> Examples of Wavelet Functions – Part 2. ....	6
<b>Figure 2.3 :</b> Multiresolution Analysis. ....	6
<b>Figure 2.4 :</b> 2-D Discrete Wavelet Decomposition. ....	10
<b>Figure 2.5 :</b> Frequency Division of the 2-D 2-Level DWD. ....	11
<b>Figure 2.6 :</b> 2-D 3-Level Discrete Wavelet Decomposition. ....	12
<b>Figure 2.7 :</b> 2-D Stationary Wavelet Decomposition. ....	14
<b>Figure 2.8 :</b> Frequency Division of the 2-D 2-Level SWD. ....	14
<b>Figure 2.9 :</b> 2-D 3-Level Stationary Wavelet Decomposition. ....	15
<b>Figure 3.1 :</b> 2-D Laplacian Pyramid Decomposition. ....	17
<b>Figure 3.2 :</b> Frequency Division of the 2-D 2-Level LPD. ....	18
<b>Figure 3.3 :</b> 2-D 3-Level Laplacian Pyramid Decomposition. ....	19
<b>Figure 3.4 :</b> Directional Filter Bank Decomposition on the first two levels. ....	20
<b>Figure 3.5 :</b> Directional Filter Bank Decomposition on the remaining levels. ....	20
<b>Figure 3.6 :</b> Directional Filter Bank Decomposition Filters. ....	21
<b>Figure 3.7 :</b> Frequency Division of the 3-Level DFBD. ....	22
<b>Figure 3.8 :</b> 3-Level Directional Filter Bank Decomposition. ....	23
<b>Figure 3.9 :</b> Contourlet Decomposition. ....	24
<b>Figure 3.10 :</b> Frequency Division of the 2-Level Contourlet Decomposition. ....	25
<b>Figure 3.11 :</b> 3-Level Contourlet Decomposition. ....	26
<b>Figure 3.12 :</b> 2-D Nonsubsampled Laplacian Pyramid Decomposition. ....	27
<b>Figure 3.13 :</b> Frequency Division of the 2-D 2-Level NSLPD. ....	28
<b>Figure 3.14 :</b> 2-D 3-Level NSLPD. ....	29
<b>Figure 3.15 :</b> Nonsubsampled Directional Filter Bank Decomposition Filters. ....	30
<b>Figure 3.16 :</b> Nonsubsampled Directional Filter Bank Decomposition. ....	30
<b>Figure 3.17 :</b> Frequency Division of the 3-Level NSDFBD. ....	31
<b>Figure 3.18 :</b> 3-Level NSDFBD. ....	32
<b>Figure 3.19 :</b> Nonsubsampled Contourlet Decomposition. ....	33
<b>Figure 3.20 :</b> Frequency Division of the 2-Level NSCD. ....	34
<b>Figure 3.21 :</b> 3-Level Nonsubsampled Contourlet Decomposition. ....	34
<b>Figure 4.1 :</b> Wavelet Based Contourlet Decomposition. ....	38
<b>Figure 4.2 :</b> Frequency Division of the 2-Level WBCD. ....	38
<b>Figure 4.3 :</b> 3-Level Wavelet Based Contourlet Decomposition. ....	40
<b>Figure 4.4 :</b> Stationary Wavelet Based Contourlet Decomposition. ....	41
<b>Figure 4.5 :</b> Frequency Division of the 2-Level SWBCD. ....	42
<b>Figure 4.6 :</b> 3-Level Stationary Wavelet Based Contourlet Decomposition. ....	43
<b>Figure 5.1 :</b> 4 Class Brodatz Textures Matrix. ....	50
<b>Figure 5.2 :</b> Perfectly Segmented 4 Class Brodatz Textures Matrix. ....	50
<b>Figure 5.3 :</b> 4 Class Brodatz Textures Matrix Classification Algorithm. ....	51
<b>Figure 5.4 :</b> AVIRIS Data on Band 32 and its GT. ....	56
<b>Figure 5.5 :</b> AVIRIS Data GT before and after the class reduction. ....	56

<b>Figure 5.6 :</b>	AVIRIS Hyperspectral Data Classification Algorithm. ....	58
<b>Figure 6.1 :</b>	DWT BT Segmentation Results. ....	66
<b>Figure 6.2 :</b>	SWT BT Segmentation Results. ....	67
<b>Figure 6.3 :</b>	CT BT Segmentation Results. ....	68
<b>Figure 6.4 :</b>	NSCT BT Segmentation Results. ....	69
<b>Figure 6.5 :</b>	WBCT BT Segmentation Results. ....	70
<b>Figure 6.6 :</b>	SWBCT BT Segmentation Results. ....	71
<b>Figure 6.7 :</b>	DWT AVIRIS Segmentation Results. ....	74
<b>Figure 6.8 :</b>	SWT AVIRIS Segmentation Results. ....	75
<b>Figure 6.9 :</b>	CT AVIRIS Segmentation Results. ....	76
<b>Figure 6.10 :</b>	NSCT AVIRIS Segmentation Results. ....	77
<b>Figure 6.11 :</b>	WBCT AVIRIS Segmentation Results. ....	78
<b>Figure 6.12 :</b>	SWBCT AVIRIS Segmentation Results. ....	79



# **HYPERSPECTRAL DATA CLASSIFICATION USING CONTOURLET TRANSFORM**

## **SUMMARY**

For many years, Wavelet Transform was the major feature extraction method for image classification. Since the means of feature extraction process directly affects the performance of the classification, it is vital to choose an appropriate method for different types of images. Although the Wavelet Transform provides a basic and generic method for this, recent techniques are being studied that can capture further image properties hidden from the Wavelet Transform.

One of the alternatives to the Wavelet Transform is the Contourlet Transform, also known as the Pyramidal Directional Filter Banks. The Contourlet Transform performs better on detecting the smoothness along the edges which is encountered on the boundaries of smooth regions of the image. Furthermore, it has more directionality than the Wavelet counterpart that can improve classification performance significantly when the image has classes with many different directions.

This graduate thesis applies the Contourlet Transform and its variations to the classification of the AVIRIS image data taken from Indiana's Indian Pine test site in June 1992. The data is hyperspectral in nature and hence this work additionally provides new research results on hyperspectral data classification by using also the directionality properties of the image classes.



## CONTOURLET DÖNÜŞÜMÜ İLE HİPERSPEKTRAL VERİ SINIFLANDIRMA

### ÖZET

Dalgacık Dönüşümü yıllardır görüntü sınıflandırmasında kullanılan öznelik çıkarım yöntemlerinden biridir. Öznelik çıkarım yöntemleri sınıflandırma başarısında büyük rol oynadığından, görüntülerin çeşidine uygun bir yöntem seçmek önem taşımaktadır. Dalgacık Dönüşümü temel ve genellenebilir bir yöntem sağlamakta, bununla beraber Dalgacık Dönüşümü'nün ortaya çıkaramadığı özellikleri de saptayabilen daha yeni yöntemler araştırılmaktadır.

Dalgacık Dönüşümü'nün alternatiflerinden biri de aynı zamanda Piramit Yönlü Filtre Bankası olarak da bilinen Contourlet Dönüşümü'dür. Contourlet Dönüşümü görüntülerin yumuşak bölgelerinin sınırlarında karşılaşılan kenar yumuşaklıklarını saptamada daha başarılıdır. Bunlara ek olarak Dalgacık Dönüşümü'nden daha fazla yöne duyarlıdır. Bu özelliği, görüntünün birçok farklı yönlerde sınıflara sahip olduğu durumlarda sınıflandırma başarısını yükseltmektedir.

Bu yüksek lisans tezi Contourlet Dönüşümü ve çeşitlerini Haziran 1992 tarihinde alınan Indiana'daki Indian Pine AVIRIS görüntüsünün sınıflandırılmasında kullanılmaktadır. Görüntü veri yapısı itibariyle hiperspektraldır ve bu nedenle çalışma aynı zamanda görüntü sınıflarının yön bilgilerini de kullanarak hiperspektral veri sınıflandırması konusunda yeni araştırma sonuçları sağlamaktadır.



## 1. INTRODUCTION

Image processing is the major area of research in remote sensing since it is a vital part of the information extraction of remote objects. The image processing techniques vary in their purpose such that they can be used to enhance the image quality, combine two or more of the different instances of the same image, compress the image to reduce its size, detect and recognize the objects in the image or classify the regions on the image. These different tasks are named in the terminology as the image enhancement/denoising, the image fusion, image coding/compression, object detection/recognition and image classification respectively.

To be able to carry out these tasks, one will need image information called the features. The extraction methods of these features vary and the most widely accepted methods are the transform based methods due to their ease of implementation where the features hidden in the spatial domain can be extracted from the transformed frequency domain.

Over the last three decades, the Wavelet Transform has been the major transform method for these tasks mentioned above. Mallat proposed the Wavelet Transform which enables a scale-invariant pyramidal decomposition/reconstruction utilizing orthogonal/biorthogonal Wavelets [1][2]. Shensa combined later the Wavelet Transform with the A Trous algorithm to propose the Nonsubsampled Wavelet Transform; also known as the Stationary Wavelet Transform; and achieve less shift-sensitivity and redundancy [3].

Despite its many advantages like multiresolution nature, critical sampling property and localization in both spatial and frequency domain, it has few directionality and lacks detection of the smoothness along the contours which are encountered on the boundaries between objects. Due to these facts, new transform methods were and are still being researched. Bamberger and Smith proposed the Directional Filter Bank which enabled image decomposition into as many directions as one wishes [4]. The method was then improved by Park, Smith and Mersereau but it was still not the ultimate alternative to the Wavelet Transform due to the poor directionality on low

frequencies [5]. Do and Vetterli proposed later the Pyramidal Directional Filter Bank, which was later renamed as the Contourlet Transform [6], where the Laplacian Pyramid proposed by Burt and Adelson [7] and the Directional Filter Bank are combined to compensate each other's disadvantages and serve as a multiresolution representation[8].

The lack of multidirectional properties on the Wavelet Transform forced the researchers on the Wavelet Domain to propose new types of Wavelet Transforms and as a result, the Directional Wavelet Transform, also known as the Steerable Wavelet Transform, was introduced by Antoine, Carrette, Murenzi and Piette utilizing the linear combination of two orthogonal Wavelets [9]. The Complex Directional Wavelet Transform was proposed by Kingsbury to enable shift-invariant analysis of the images which was not possible using the Contourlet Transform [10]. In the mean time, another transform method called the Curvelet Transform was pioneered by Candes and Donoho combining the subband decomposition with the Ridgelet Transform defined in the polar coordinate system [11]. The Curvelet Transform was and is still being compared with the Contourlet Transform due to their similar application areas like detection of the smooth contours and boundaries but its implementation is limited by its high redundancy and difficult implementation [12][13].

The more recent works during the last decade propose combination of the known transform methods to introduce new techniques and also concentrate on the high redundancy and shift/rotation invariance. Li and Taylor showed that the combination of the features provide better texture classification results than the individual usage of the ones extracted by the Wavelet and the Contourlet Transform [14]. Duan, Man and Chen applied a special type of the Directional Filter Bank to achieve high classification performance of both non-rotated and rotated images [15]. Eslami and Radha proposed the Wavelet Based Contourlet Transform to overcome the remaining small redundancy of the Contourlet Transform and provide more efficient image coding [16]. Later, they enhanced this concept and introduce the Hybrid Wavelets and Directional Filter Bank Transform family where they employ Wavelets for the subband decomposition and use modified versions of the Directional Filter Bank to achieve small redundancy [17]. Cunda, Zhou and Do proposed the Nonsubsampled Contourlet Transform to achieve a fully shift-invariant, multiscale and

multidirectional expansion and designed nonsubsampling counterparts of the Pyramid Filter Bank and Fan Filter Bank [18]. Hu, Hou, Wang and Jiao introduced the Stationary Wavelet Based Contourlet Transform and showed that it outperforms all the other known alternative texture classification methods due to its high redundancy [19]. Tanaka, Ikehara and Nguyen proposed the combination of the 1-D, 2-D Directional Filter Bank with the Quincunx Filter Bank [20].

Considering the literature so far, there are few number of research results on the hyperspectral data classification. Tadjudin and Landgrebe classified AVIRIS hyperspectral data using different classifiers including the covariance estimator with limited number of training samples [21]. Benediktsson, Garcia, Waske, Chanussot, Sveinsson and Fauvel used ensemble methods for the classification of the same data [22]. Mojaradi, Emami, Varshosaz and Jamali utilized novel band selection method for the classification of the same data [23].





## 2. DISCRETE WAVELET AND STATIONARY WAVELET TRANSFORM

The Wavelet Transform (WT) gained popularity in the last three decades due to its flexibility on the Multiresolution Analysis (MRA). The WT is highly inspired from the Short Time Fourier Transform (STFT), also known as the Windowed Fourier Transform (WFT). Unlike the STFT and its predecessor, the Fourier Transform (FT) which utilizes sinusoidals having infinite duration and constant frequencies, the WT uses window functions with variable scaling factors. These window functions are typically a pulse that continues for a period of time and vanishes outside its interval. They are called the Wavelets that satisfy the following admissibility condition:

$$c_{\Psi} = 2\pi \int_{-\infty}^{+\infty} \frac{|\Psi(\omega)|^2}{|\omega|} d\omega < +\infty \quad (2.1)$$

which means that the Wavelet  $\Psi$  has zero mean, i.e. it has no DC components. Examples of the basic Wavelet Functions are shown in Figures 2.1 and 2.2.

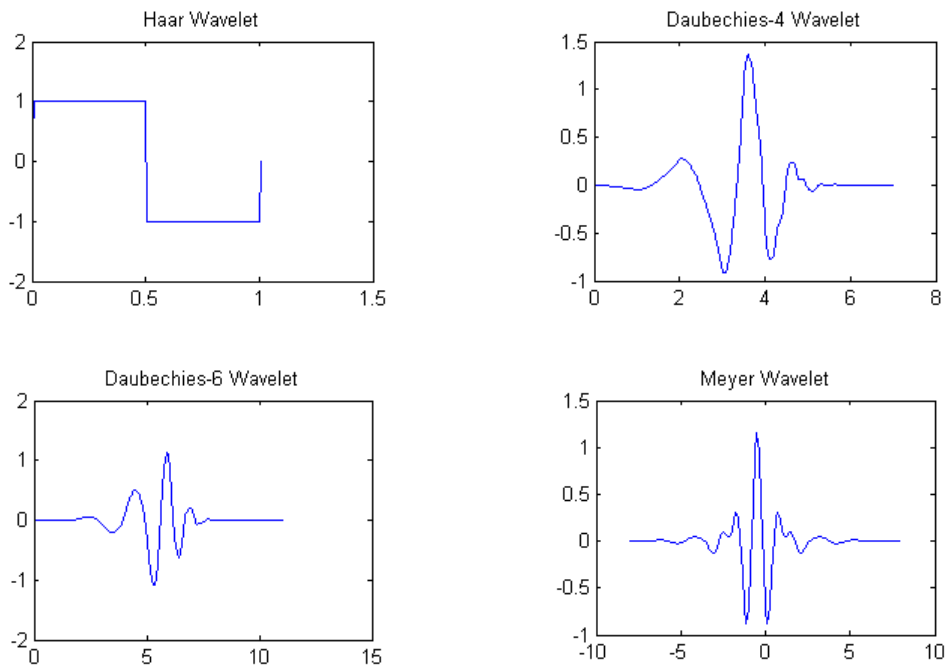


**Figure 2.1** : Examples of Wavelet Functions – Part 1.

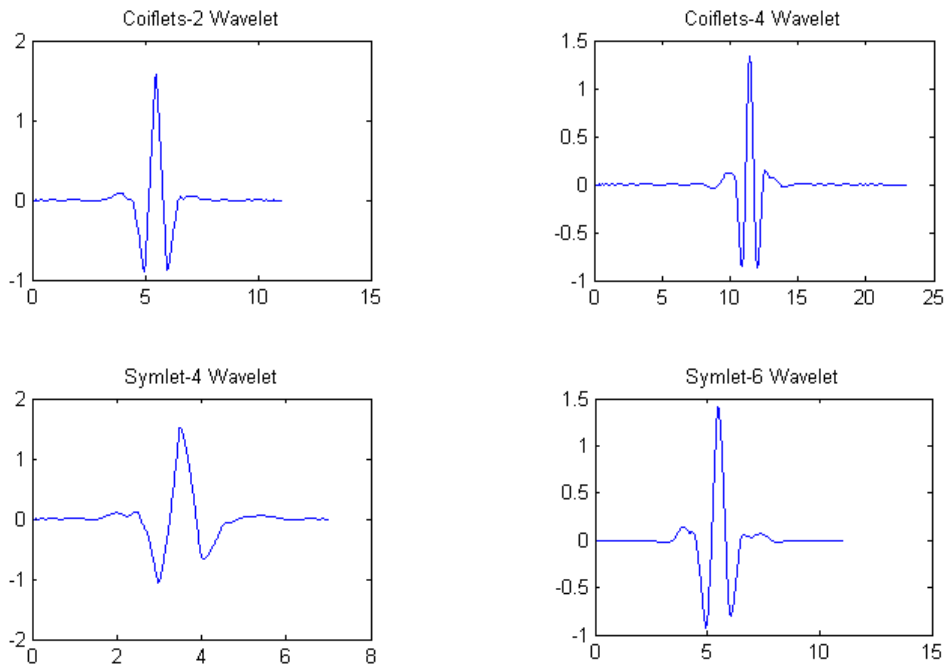


**Figure 2.2 :** Examples of Wavelet Functions – Part 2.

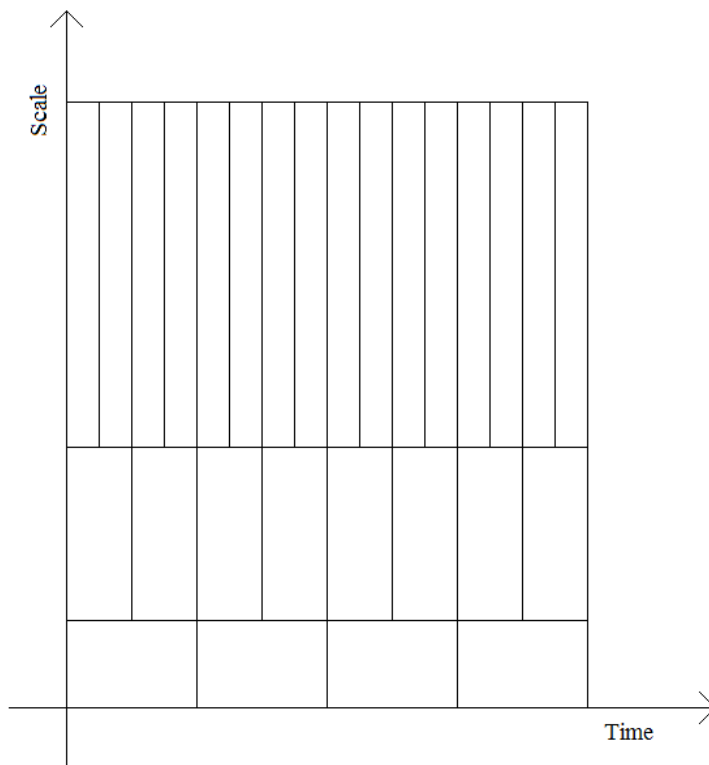


**Figure 2.3 :** Multiresolution Analysis.

Scaling of a Wavelet can be regarded as changing its width. The time-frequency resolutions  $\Delta_t$  and  $\Delta_f$  are not fixed, instead they change accordingly so that the ratio of  $\Delta_f$  over  $f$  remains constant to achieve the MRA.

## 2.1 Continuous Wavelet Transform

The forward and backward WT; also known as the analysis or the decomposition; for 1-D signals are defined as:

$$C(a, b) = \int_{t=-\infty}^{+\infty} I(t)\Psi_{a,b}(t)dt \quad (2.2)$$

where  $\Psi_{a,b}(t)$  are the scaled versions of the Mother Wavelet  $\Psi(t)$  as follows:

$$\Psi_{a,b}(t) = \frac{1}{\sqrt{|a|}} \Psi\left(\frac{t-b}{a}\right) \quad (2.3)$$

where  $a \in \mathbb{R}^+ - \{0\}$ ,  $b \in \mathbb{R}$

The Inverse WT; also known as the synthesis of the reconstruction; for 1-D signals are defined as:

$$I(t) = \frac{1}{K_\Psi} \int_{\mathbb{R}^+} \int_{\mathbb{R}} \frac{1}{\sqrt{|a|}} \Psi\left(\frac{t-b}{a}\right) \frac{dad b}{a^2} \quad (2.4)$$

where  $0 < K_\Psi < \infty$  for the perfect reconstruction is:

$$K_\Psi = \int_{-\infty}^{+\infty} \frac{|\Psi(t)|^2}{|t|} dt \quad (2.5)$$

During the Continuous WT Analysis, the signal is decomposed into a family of analyzing signals by changing the scale and the position of the Mother Wavelets. This results in the redundant information in the reconstruction case.

## 2.2 Discrete Wavelet Transform

The Discrete Wavelet Transform (DWT) is derived by using discrete scaling and time-shifting parameters  $a$  and  $b$  respectively. Then the DWT for 1-D signals becomes:

$$C(a, b) = \int_{t=-\infty}^{+\infty} I(t) \frac{1}{\sqrt{|a|}} \Psi\left(\frac{t-b}{a}\right) dt \quad (2.6)$$

where  $a = 2^j, b = k2^j, (j, k) \in Z^2$

The synthesis equation of the signal is the following:

$$I(t) = \sum_j \sum_k C(j, k) \Psi_{j,k}(t) \quad (2.7)$$

The Dyadic WT is a special case where the scaling is performed in the powers of 2.

$$I(t) = \sum_j \sum_k C(j, k) 2^{-\frac{j}{2}} \Psi(2^{-j}t - k) \quad (2.8)$$

The reconstruction equation shows that the signal itself is the linear combination of the basis vectors, the shifted versions of the Mother Wavelet, over the basis vector space B. If the set  $\Psi_{j,k}$  is orthonormal and complete, then the space B is orthonormal, hence the basis and its dual are the same. The Haar, Daubechies-4 and Daubechies-6 Wavelets are some examples of the orthonormal Wavelets.

### 2.3 Discrete Wavelet Coefficients

The WT can be implemented by using the Filter Bank approach where the signal is the decomposed representation of the shifted versions of the scaling function:

$$\Phi_{j,k} = 2^{-\frac{j}{2}} \Phi(2^{-j}t - k) \quad (2.9)$$

for  $-\infty < k < +\infty$

where the signal at resolution  $j_0$  is the following:

$$I_{j_0}(t) = \sum_{k=-\infty}^{+\infty} I_{j_0}(k) \Phi_{j_0,k}(t) \quad (2.10)$$

The lower resolution scaling function filter can be derived by the weighted linear combination of the shifted versions of the next higher resolution as the following:

$$\Phi(t) = \sqrt{2} \sum_{k=-\infty}^{+\infty} g(k)\Phi(2t - k) \quad (2.11)$$

The Mother Wavelet can also be constructed as follows:

$$\Psi(t) = \sqrt{2} \sum_{k=-\infty}^{+\infty} h(k)\Phi(2t - k) \quad (2.12)$$

where  $g$  and  $h$  are Low-Pass and High-Pass Wavelet Filters respectively which have the following relation:

$$g(k) = (-1)^k h(1 - k) \quad (2.13)$$

Then, the DWT for the 1-D signal can be rewritten as:

$$I(t) = \sum_{k=-\infty}^{+\infty} c_{j_0}(k)\Phi_{j_0,k}(t) + \sum_{j=j_0}^{+\infty} \sum_{k=-\infty}^{+\infty} d_j(k)\Psi_{j,k}(t) \quad (2.14)$$

where  $c_{j_0}(k)$  and  $d_j(k)$  are the approximation and detail coefficients respectively.

It is shown that the Discrete Wavelet Coefficients at scale  $j-1$  are related to the ones at scale  $j$  by the following relations:

$$c_{j-1}(k) = \sum_m g(m - 2k)c_j(m) \quad (2.15)$$

$$d_{j-1}(k) = \sum_m h(m - 2k)c_j(m) \quad (2.16)$$

where  $j = J, J - 1, \dots, j_0 + 1$

This relation makes the cascaded Filter Bank approach possible and hence the higher scale Discrete Wavelet Coefficients can be calculated from the lower scale ones.

## 2.4 2-D Discrete Wavelet Decomposition

The High-Pass Filter (HPF) and Low-Pass Filter (LPF) for the 2-D Discrete Wavelet Decomposition (DWD) can be either separable or non-separable. For separable

cases, the decomposition is performed first on the rows, then on the columns of the signal which results in the decomposition of the signal into one approximation and directional coefficients in three different directions; horizontal, vertical and diagonal ones. Since the HPF and LPF disregards the half of the frequency response of the row and column signal, the half of the information is also lost in the spatial domain. To eliminate the redundant spatial information, the downsampling operations in horizontal and vertical directions are performed.

For the decomposition into more than one level, The DWD is performed in the Pyramidal fashion. The Pyramidal Decomposition assumes that the most of the energy of a signal exists in the low frequency portion and the next level of decomposition should be performed using the approximation coefficients. So, the overall process becomes:

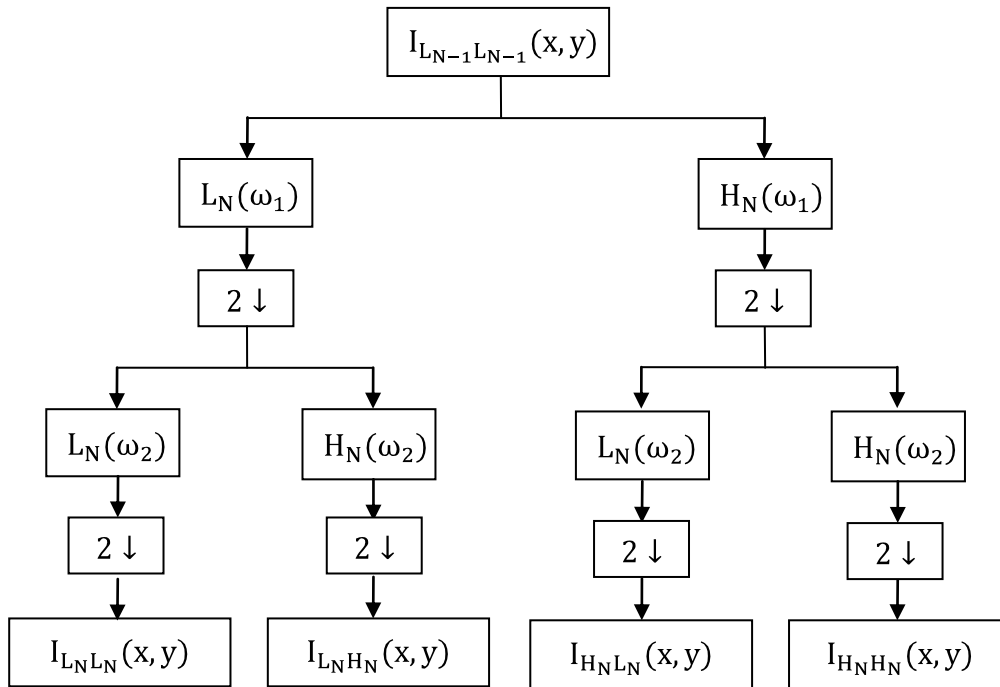


**Figure 2.4 :** 2-D Discrete Wavelet Decomposition.

Beginning from the first level, the input image can be considered as the approximation image. First, the rows of the image are filtered by the High-Pass and Low-Pass Wavelet Decomposition Filters. Both resultant filtered rows do not contain the half of the frequency band so they can be downsampled to avoid redundancy. After the row-wise filtering, the column-wise filtering is performed, following with the downsampling of the rows and columns. The resulting images after one level decomposition are the four subband images.  $I_{L_N H_N}(x, y)$ ,  $I_{L_N L_N}(x, y)$ ,  $I_{H_N H_N}(x, y)$  are

the horizontally, vertically and diagonally decomposed subband images, whereas  $I_{L_N L_N}(x,y)$  is the approximated image that will be carried into the next level of decomposition.

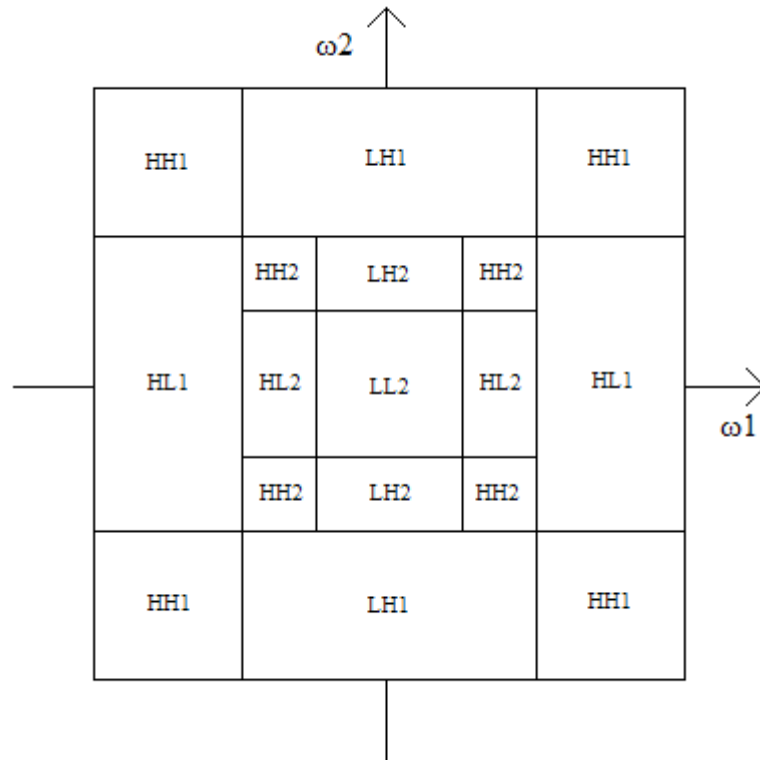


**Figure 2.5 :** Frequency Division of the 2-D 2-Level DWD.

The frequency division of the 2-D 2-Level DWD is presented in the Figure 2.5. The frequency plane is divided into 4 diagonal, 2 vertical and 2 horizontal regions on every level whereas there is one approximation region on the last level.

As an example, the 2-D 3-Level DWD of an image is the following:

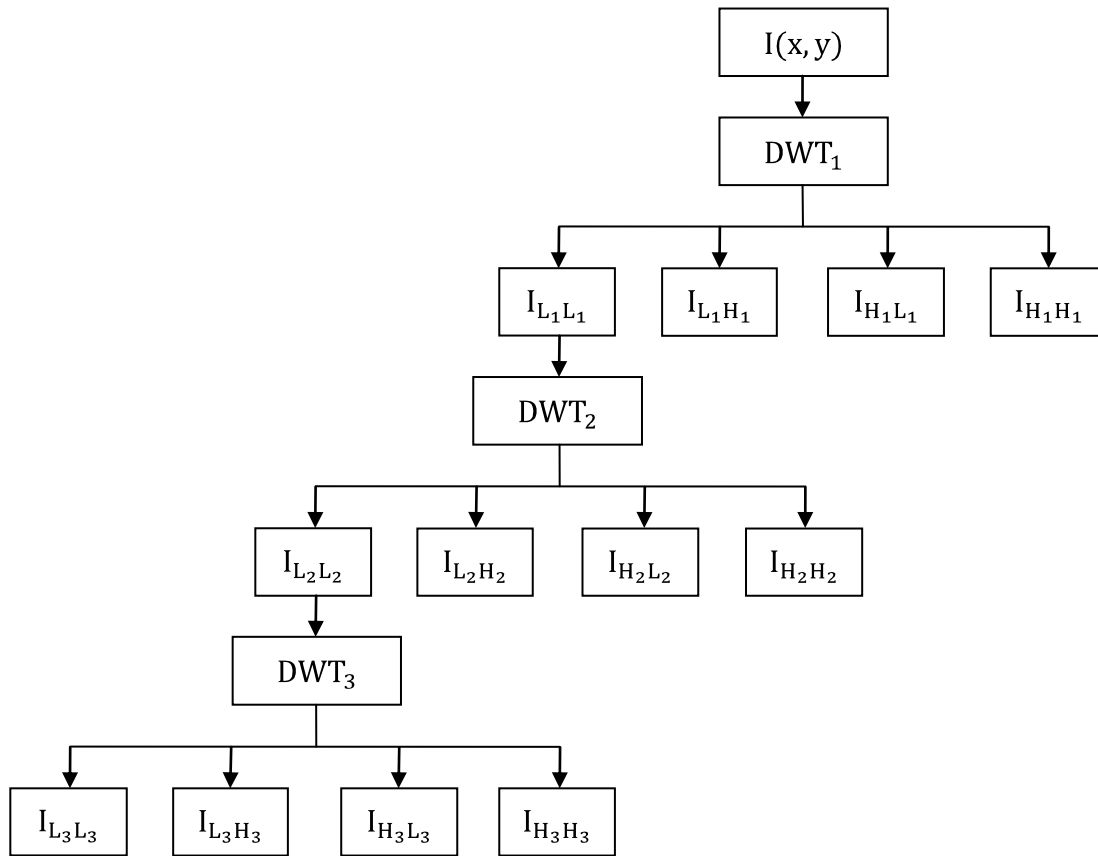


**Figure 2.6 :** 2-D 3-Level Discrete Wavelet Decomposition.

The 3-Level DWD inherently produces 12 subbands including 3 approximation subbands. The information from the approximation subbands of the first and the second level are carried into the next level since they will be decomposed into 4 subbands on the next level. Due to this fact, the smallest subset of the subbands for perfect reconstruction includes all the subband images/coefficients from the last level and the remaining directional subband images/coefficients from the upper remaining levels. This property is considered during the feature set selection to avoid unnecessary redundant information.

The inverse operation of the DWD is called the Discrete Wavelet Reconstruction which can be performed by using the inverse LPF/HPF and upsampling the rows/columns after each reconstruction level.



## 2.5 Stationary Wavelet Transform

The Stationary Wavelet Transform (SWT) is the high redundant counterpart of the DWT. Redundancy is useful in image processing such as during edge detection, denoising and image reconstruction. In fact, after a certain level of the DWT depending on the initial signal size, the subbands gets so narrow so that the local features of the same class differ significantly. This results in the increased misclassification on higher levels. Due to the redundant information, the SWT outperforms the DWT in texture analysis and classification on higher levels.

The downsampling and upsampling operations during the SWT decomposition and reconstruction respectively are omitted to avoid information loss. Instead, the LPF and HPF are upsampled by a factor  $2^{N-1}$  in the Nth level where the expansion of the Wavelet filters occur due to the inserted zeros between every consecutive filter coefficients.

$$g_{N,k_1,k_2} = g_{1,\frac{k_1}{2^N},\frac{k_2}{2^N}} \text{ for } k_1 = k_2 = 2^N m, m \in \mathbb{Z}, N > 1 \quad (2.17)$$

$$g_{N,k_1,k_2} = 0 \text{ for else} \quad (2.18)$$

$$h_{N,k_1,k_2} = h_{1,\frac{k_1}{2^N},\frac{k_2}{2^N}} \text{ for } k_1 = k_2 = 2^N m, m \in \mathbb{Z}, N > 1 \quad (2.19)$$

$$h_{N,k_1,k_2} = 0 \text{ for else} \quad (2.20)$$

where  $N$  denotes the current level of decomposition and  $k_1, k_2$  are the indices of the LPF/HPF.

## 2.6 2-D Stationary Wavelet Decomposition

The HPF and LPF for the 2-D Stationary Wavelet Decomposition (SWD) can be either separable or non-separable. For separable cases, the decomposition is performed first on the rows, then on the columns of the signal which results in the decomposition of the signal into one approximation and directional coefficients in three different directions; horizontal, vertical and diagonal ones. Since the SWD does not downsample the filtered rows and columns, the subband images have the same

dimensions as the input image. The HPFs and LPFs are upsampled after each consecutive level to achieve coarse subband decomposition.

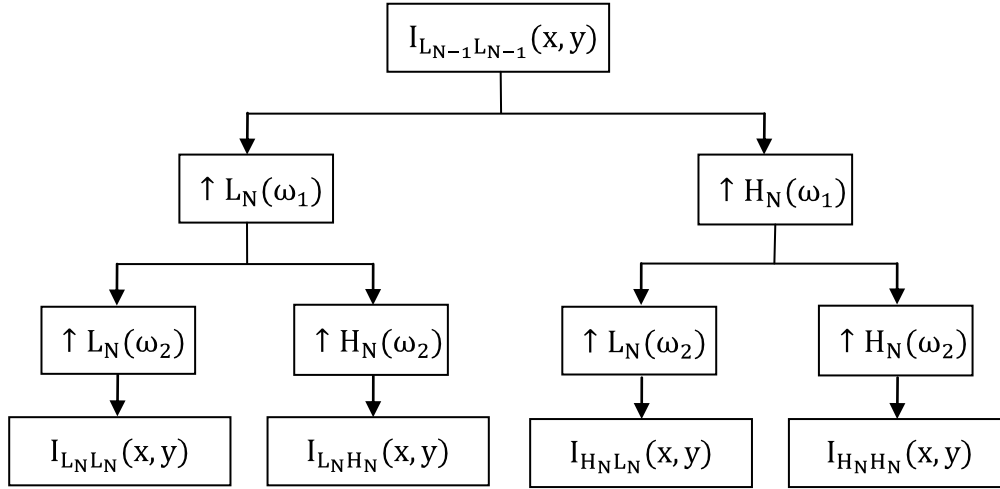


**Figure 2.7 :** 2-D Stationary Wavelet Decomposition.

As in the DWD, the input image can be considered as the approximation image on the first level. First, the rows of the image are filtered by the High-Pass and Low-Pass Wavelet Decomposition Filters that are upsampled after each level. After the row-wise filtering, the column-wise filtering is performed. The resulting images after one level decomposition are the four subband images.  $I_{L_NH_N}(x, y)$ ,  $I_{L_NH_N}(x, y)$ ,  $I_{H_NH_N}(x, y)$  are the horizontally, vertically and diagonally decomposed subband images, whereas  $I_{L_NL_N}(x, y)$  is the approximated image that will be carried into the next level of decomposition.

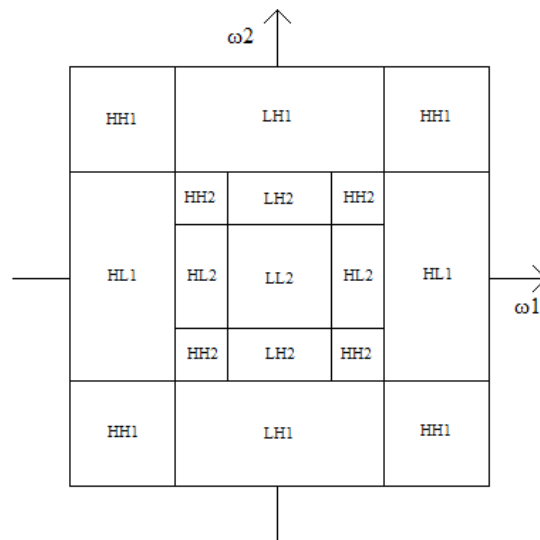


**Figure 2.8 :** Frequency Division of the 2-D 2-Level SWD.

As seen in the Figure 2.9, the frequency division of the 2-D 2-Level SWD is the same as the 2-D 2-Level DWD case. The frequency plane is divided into 4 diagonal, 2 vertical and 2 horizontal regions on every level whereas there is one approximation region on the last level.

As an example, the 2-D 3-Level SWD of an image is the following:

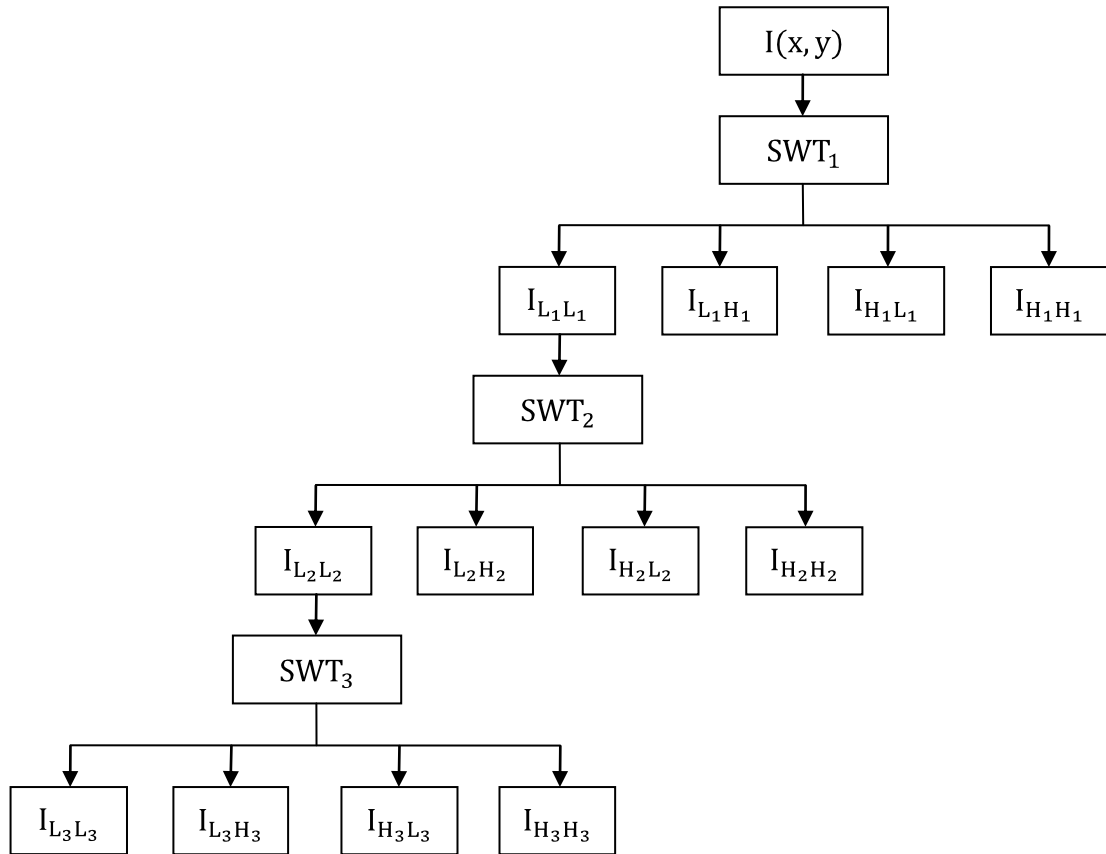


**Figure 2.9 :** 2-D 3-Level Stationary Wavelet Decomposition.

The 3-Level SWD inherently produces 12 subbands with the original input image dimensions including 3 approximation subbands. As in the DWD, the smallest subset of the subbands for perfect reconstruction includes all the subband images/coefficients from the last level and the remaining directional subband images/coefficients from the upper remaining levels.

The inverse operation of the SWD is called the Stationary Wavelet Reconstruction which can be performed by using the inverse LPF and HPF that are downsampled after each reconstruction level.



### 3. CONTOURLET AND NONSUBSAMPLED CONTOURLET TRANSFORM

The Contourlet Transform (CT) consists of two cascaded operations; the sub-band decomposition and the directional decomposition. The main advantage of the CT is that features in desirable number of directions can be extracted depending on the number of directions used on each level.

#### 3.1 Laplacian Pyramid Decomposition

The Laplacian Pyramid Decomposition (LPD) is the application of a LPF on the signal and subsampling the low frequency portion for each level desired. The LPF can be a variety of filters including the Gaussian LPF and the Wavelet LPF. The high-pass portion of the signal is the redundant part of this level and its information will not be passed into the coarse levels. As in the DWD, the low-pass filtered image contains unnecessary information that can be avoided by downsampling operation [7].

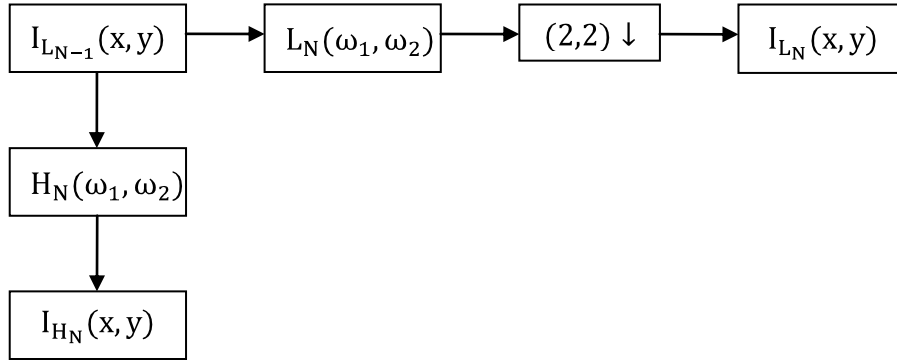


**Figure 3.1** : 2-D Laplacian Pyramid Decomposition.

The HPF  $H_N(\omega_1, \omega_2)$  is actually not needed for the decomposition; instead the difference of the input signal from its low-pass filtered one can be used [7].

$$I_{H_N}(x, y) = I_{L_{N-1}}(x, y) - I_{L_{N-1}}(x, y) ** L_N(\omega_1, \omega_2) \quad (3.1)$$

$$H_N(\omega_1, \omega_2) = 1 - L_N(\omega_1, \omega_2) \quad (3.2)$$

Noting that after each level, the frequency characteristics of the signal are separated into high and low frequency portions and hence, many subbands occur dividing the low frequency portions into finer scales. As a result, the frequency response of the signal is decomposed into one high frequency band, N-1 subbands and one remaining low frequency band. The main advantage of this approach is that the resolution of the low frequency portions is increased after each level.

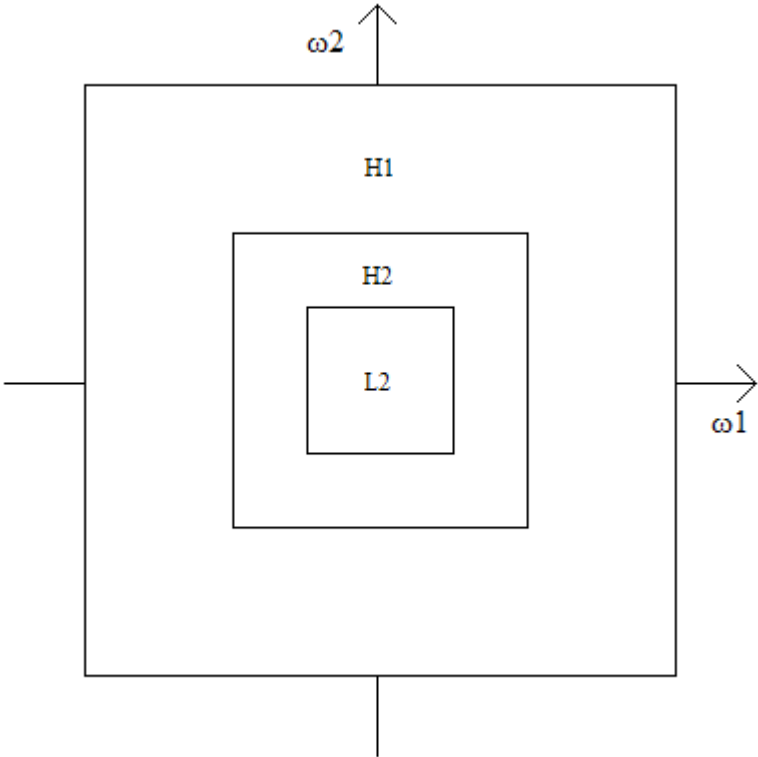


**Figure 3.2 :** Frequency Division of the 2-D 2-Level LPD.

The frequency division of the 2-D 2-Level LPD is presented in the Figure 3.2. The frequency plane is divided into one high frequency region on every level whereas there is one approximation region on the last level.

The 2-D 3-Level LPD is given as:

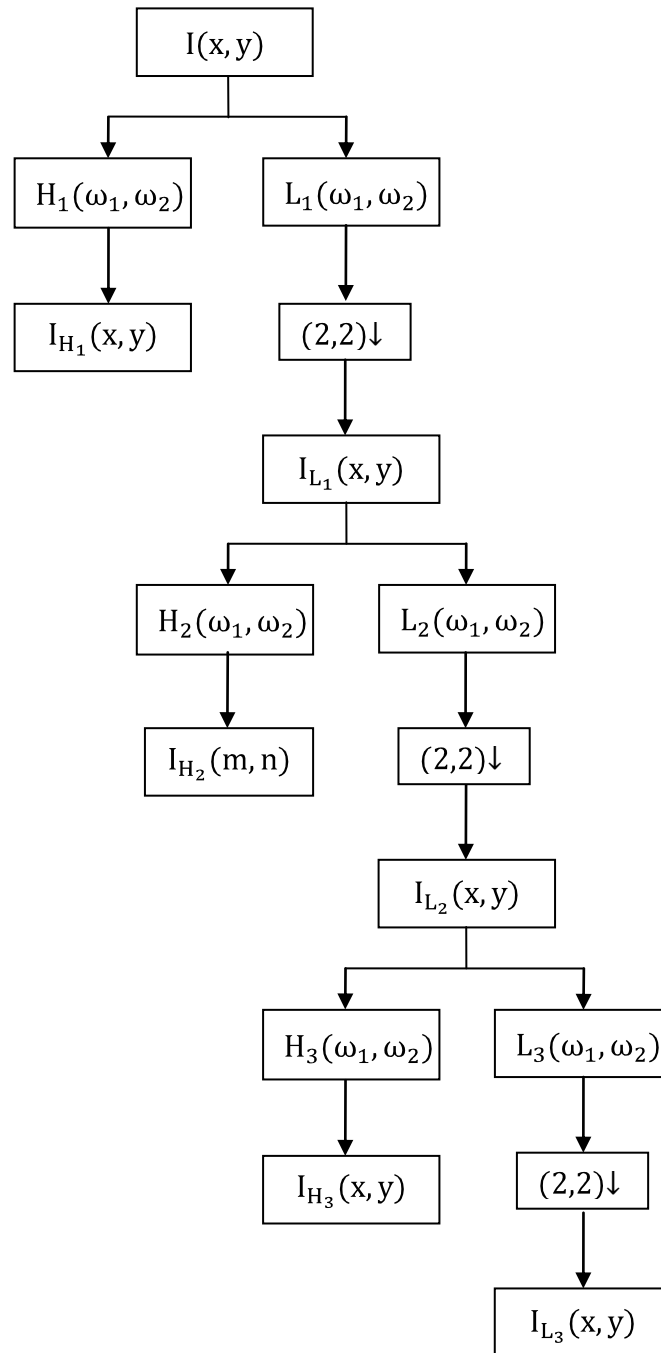


**Figure 3.3 :** 2-D 3-Level Laplacian Pyramid Decomposition.

The 2-D 3-Level LPD inherently produces 3 high-pass and 3 low-pass subbands. The information from the low-pass subbands on the first and the second level are carried into the next level since they will be decomposed into 2 subbands on the next level. Due to this fact, the smallest subset of the subbands for perfect reconstruction includes all the subband images from the last level and the remaining high-pass

subband images from the upper remaining levels. This property is considered during the feature set selection to avoid unnecessary redundant information.

The inverse operation of the LPD is called the Laplacian Pyramid Reconstruction and can be performed by upsampling the low frequency decompositions and using the inverse LPF/HPF.

### 3.2 Directional Filter Bank Decomposition

The Directional Filter Bank Decomposition (DFBD) is the method used for dividing the frequency response of the signal into wedge shaped slices. An  $N$  Level Directional Filter Bank (DFB) divides the frequency response of the signal into  $2^N$  wedges. An immediate observation is that the DFB does not perform well on low frequencies. The low frequency portions are diverted into many directions whereas the directional distinction between the individual high frequency portions can be obtained more easily. So, the DFB performs poor on low frequencies but it captures the directionality on high frequencies [5].

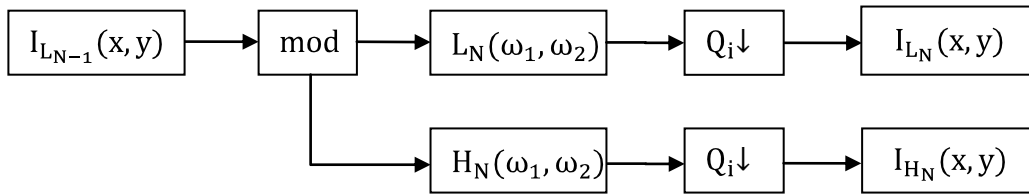


**Figure 3.4 :** Directional Filter Bank Decomposition on the first two levels.

On the first two levels, the above structure can be used where  $L_N(\omega_1, \omega_2) = H_0(\omega_1, \omega_2)$  and  $H_N(\omega_1, \omega_2) = 1 - H_0(\omega_1, \omega_2)$ . The Hourglass Filter (HF) can be used if the modulator is omitted such that  $L_N(\omega_1, \omega_2) = H_{m_1} = H_{m_0}(\omega_1, \omega_2)$  and  $H_N(\omega_1, \omega_2) = 1 - H_{m_1} = 1 - H_{m_0}(\omega_1, \omega_2)$  [5].

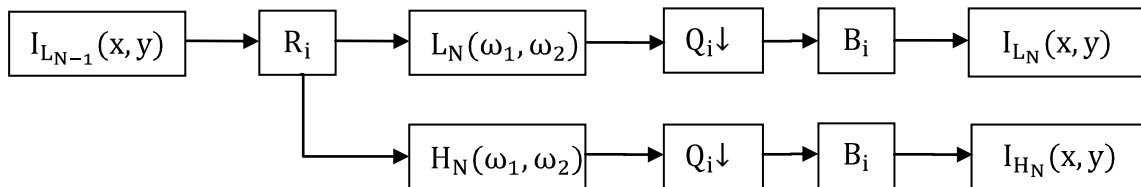


**Figure 3.5 :** Directional Filter Bank Decomposition on the remaining levels.



On the remaining levels, the above structure can be used where  $L_N(\omega_1, \omega_2)$  and  $H_N(\omega_1, \omega_2)$  are one of the Parallelogram Filters from  $A_0(\omega_1, \omega_2)$  to  $D_0(\omega_1, \omega_2)$  if the modulator was used in the first 2 levels. If the modulator was omitted, the filters from  $A_{m_0}(\omega_1, \omega_2)$  to  $D_{m_0}(\omega_1, \omega_2)$  and from  $A_{m_1}(\omega_1, \omega_2) = 1 - A_{m_0}(\omega_1, \omega_2)$  to  $D_{m_1}(\omega_1, \omega_2) = 1 - D_{m_0}(\omega_1, \omega_2)$  can be used [5].

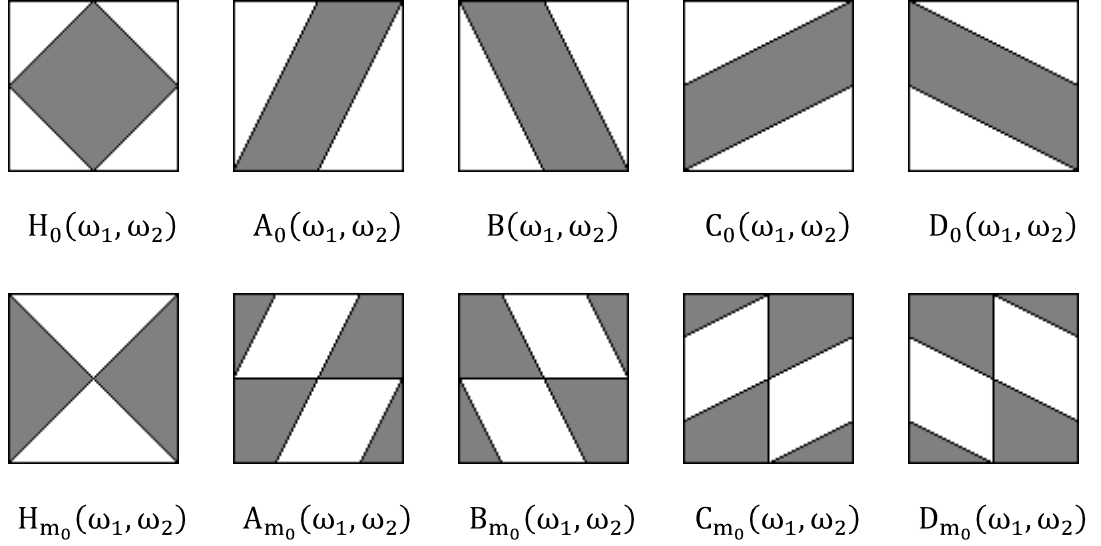


**Figure 3.6 :** Directional Filter Bank Decomposition Filters.

The  $Q_i \downarrow$  is the Quincunx Downsampling Filter (QDF) which downsamples and rotates the image 45 degrees counter-clockwise and is defined as the following [5]:

$$q_1 = \begin{bmatrix} 1 & 1 \\ -1 & 1 \end{bmatrix} \quad q_2 = \begin{bmatrix} 1 & -1 \\ 1 & 1 \end{bmatrix} \quad q_3 = \begin{bmatrix} -1 & 1 \\ 1 & 1 \end{bmatrix} \quad q_4 = \begin{bmatrix} 1 & 1 \\ 1 & -1 \end{bmatrix} \quad (3.3)$$

$q_1$  is typically used for the first 2 levels. For the remaining levels, the QDF will be defined by using the following equations [5]:

$$Q_i = q_2 \text{ for } i = 1 \text{ or } i = 4 \quad (3.4)$$

$$Q_i = q_1 \text{ for } i = 2 \text{ or } i = 3 \quad (3.5)$$

The  $R_i$  is the Resampling Matrix defined as [5]:

$$r_1 = \begin{bmatrix} 1 & 1 \\ 0 & 1 \end{bmatrix} \quad r_2 = \begin{bmatrix} 1 & -1 \\ 0 & 1 \end{bmatrix} \quad r_3 = \begin{bmatrix} 1 & 0 \\ 1 & 1 \end{bmatrix} \quad r_4 = \begin{bmatrix} 1 & 0 \\ -1 & 1 \end{bmatrix} \quad (3.6)$$

The  $B_i$  is the Backsampling Matrix defined as [5]:

$$B_i^{T_N} = \left[ [B^{T(N-1)}]^{-1} R_i \cdot Q_i \right]^{-1} \cdot D_i \quad (3.7)$$

$$D_i = \begin{bmatrix} 1 & 0 \\ 0 & 2 \end{bmatrix} \text{ for } i = 1 \text{ or } 2 \quad (3.8)$$

$$D_i = \begin{bmatrix} 2 & 0 \\ 0 & 1 \end{bmatrix} \text{ for } i = 3 \text{ or } 4 \quad (3.9)$$

$$B_i^{T_3} = R_{5-i} \text{ where } i = 1, 2, 3, 4 \quad (3.10)$$

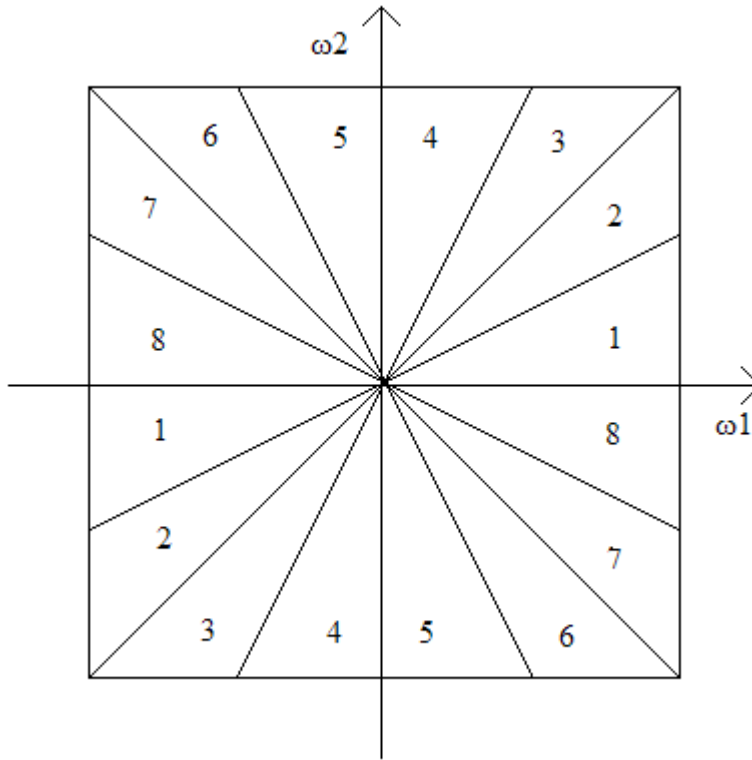


**Figure 3.7 :** Frequency Division of the 3-Level DFBD.

The frequency division of the 3-Level DFBD is presented in the Figure 3.7. The frequency plane is divided into  $2^4$  wedges that represent the directionalities in  $2^3$  directions.

Then, the 3-Level DFBD can be constructed by omitting the modulator as the following:

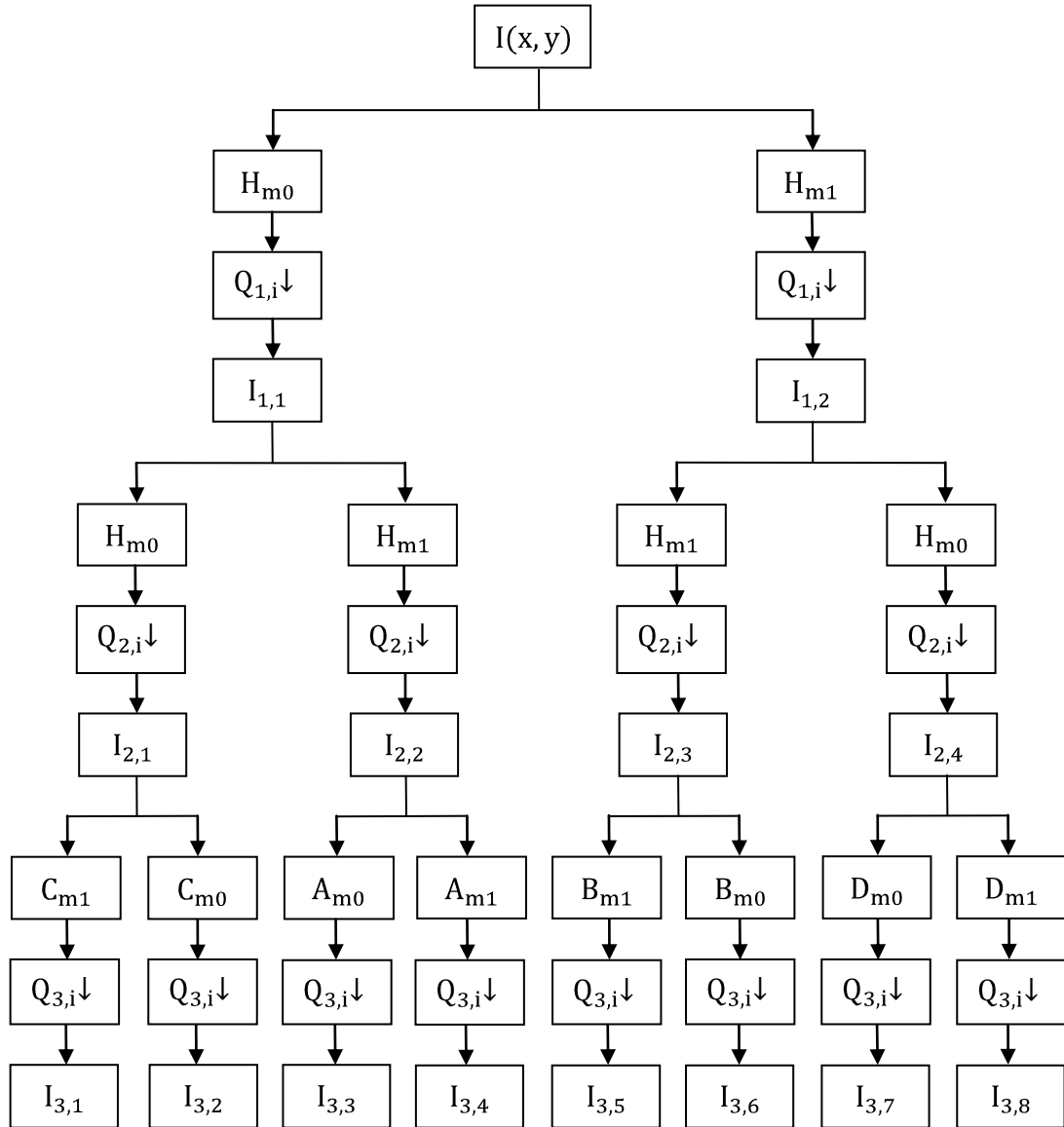


**Figure 3.8 :** 3-Level Directional Filter Bank Decomposition.

The 3-Level DFBD inherently produces 14 subbands. The input image is first directionally decomposed into 2 directions resulting in 4 slices in the frequency domain. On the second level, the number of directions doubles and becomes 4 resulting in 8 slices in the frequency domain. The last level produces 8 directional subbands that divide the frequency domain in 16 slices.

The first 2 levels utilize the HFs whereas the last level uses specially designed filters presented in the Figure 3.6. Cascading an HF with a QDF results in a filtering operation with checkerboard support and filtering with an HF again on the second

level enables the division of the frequency domain into 4 directions. The special filters used at the third and last level gets input images filtered with supports in 4 different directions and the outputs are as a result 8 different directional subbands. The smallest subset of the subbands for perfect reconstruction includes only the directional subband decompositions on the last level.

The inverse operation of the DFBD is called the DFB Reconstruction and can be performed by using the inverse DFBD filters.

### 3.3 Contourlet Transform

The CT is basically the resulting transform of applying multiscale decomposition by the Laplacian Pyramid (LP) and cascading the output with the DFB. The DFB divides the frequency band of the image into wedge-shaped slices and performs well on capturing the high frequency components in a direction but the low frequency components are miscaptured due to decreased resolution. To avoid this disadvantage, the LP is applied first to the image which divides the image frequency band into a low-pass and as many as desired subband decompositions, which are fed into the DFB. The number of directions increases as the number of subbands increase and by this, the same accuracy of capturing the frequency components of each resulting regions are achieved [6][8].

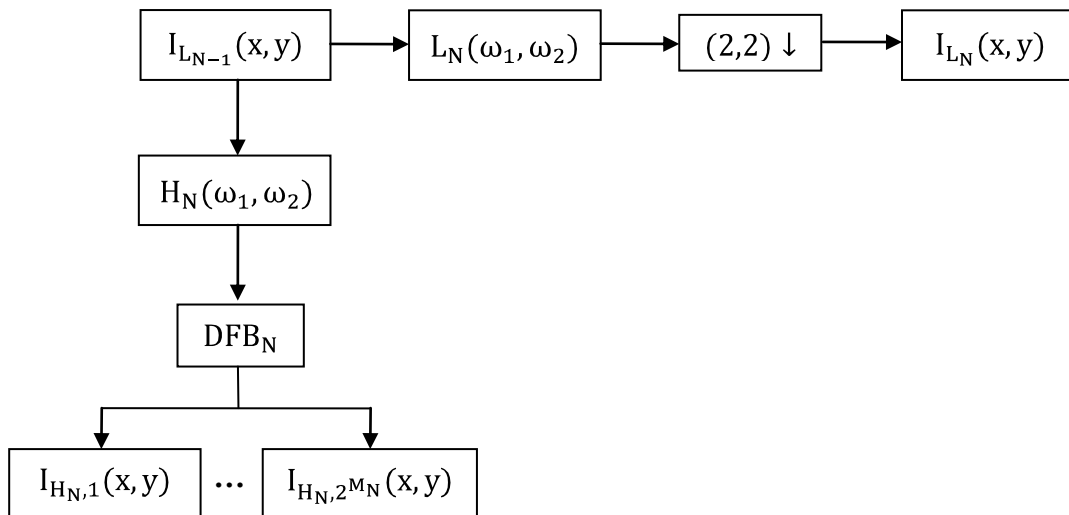


**Figure 3.9 :** Contourlet Decomposition.

Beginning from the first level, the input image is decomposed into high-pass and low-pass subbands. The resultant high-pass subband is decomposed into directional

subbands since the DFB performs better on high frequencies. The low-pass subband will be downsampled and passed into the next level. The common practice is to decompose the high-pass subbands into many directions on the first levels and into fewer directions on the coarse levels, since the frequency domain will be divided into smaller chunks on the coarse levels [6][8].

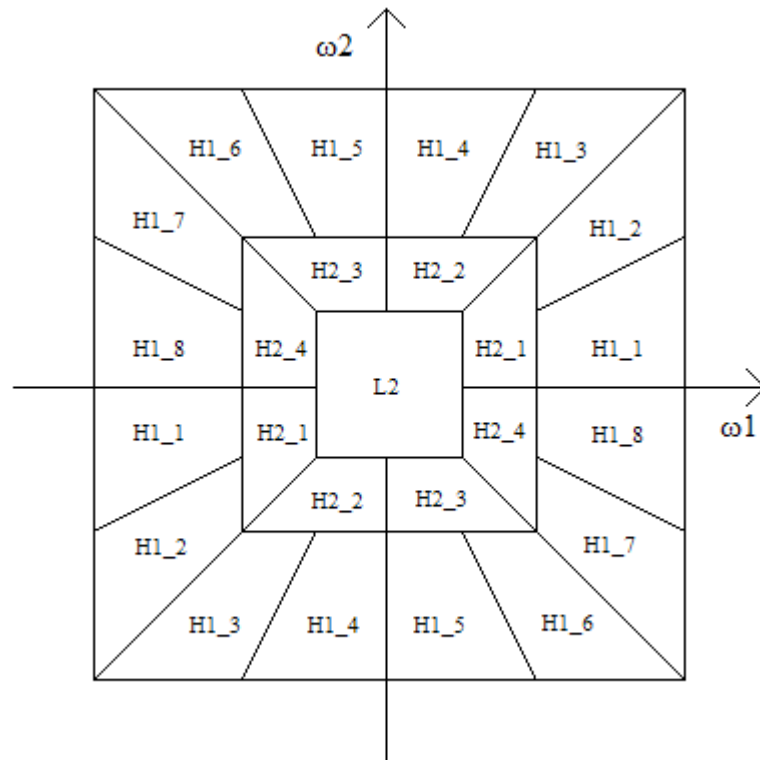


**Figure 3.10 :** Frequency Division of the 2-Level Contourlet Decomposition.

The frequency division of the 2-Level CD is presented in the Figure 3.10. The frequency plane is divided into 8 directional regions on the first level whereas there are 4 directional regions and one approximation region on the last level.

The 3-Level Contourlet Decomposition (CD) can be structured as the following:

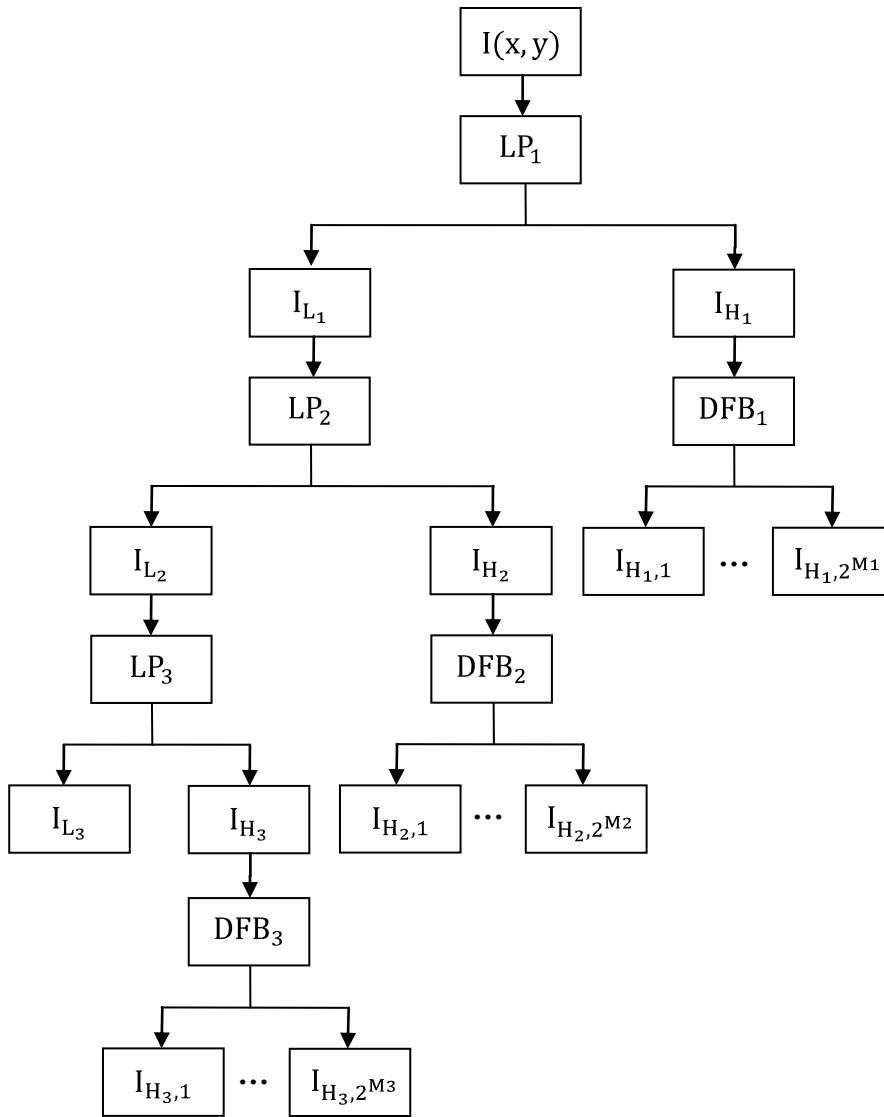


**Figure 3.11 :** 3-Level Contourlet Decomposition.

The 3-Level CD inherently produces  $6 + 2^{M_1} + 2^{M_2} + 2^{M_2}$  subbands.  $I_{H_3}, I_{H_2}, I_{H_1}, I_{L_2}, I_{L_1}$  are the redundant subbands whereas the smallest subset of the subbands for the perfect reconstruction is the low-pass subband from the last level and the directional subband decompositions from all levels. Only the high-pass portions of the LPD are directionally decomposed by the DFB since it performs better on high frequencies [5].

The inverse operation of the CD is called the Contourlet Reconstruction which can be performed by using both the LP and the DFB Reconstruction.

### 3.4 Nonsubsampled Laplacian Pyramid Decomposition

The Nonsubsampled Laplacian Pyramid Decomposition (NSLPD) is similar to its subsampled counterpart except that the upsamplers and downsamplers are omitted and it utilizes the application of a LPF on the signal where the LPF is upsampled by the factor of  $2^{N-1}$  in the Nth level. After each level, the expansion of the LPF occurs due to the inserted zeros between every consecutive LPF coefficients [18].

$$g_{N,k_1,k_2} = g_{1,\frac{k_1}{2^{N-1}},\frac{k_2}{2^{N-1}}} \text{ for } k_1 = k_2 = 2^N m, m \in \mathbb{Z}, N > 1 \quad (3.11)$$

$$g_{N,k_1,k_2} = 0 \text{ for else} \quad (3.12)$$

where  $N$  denotes the current level of decomposition and  $k_1, k_2$  are the indices of the LPF.

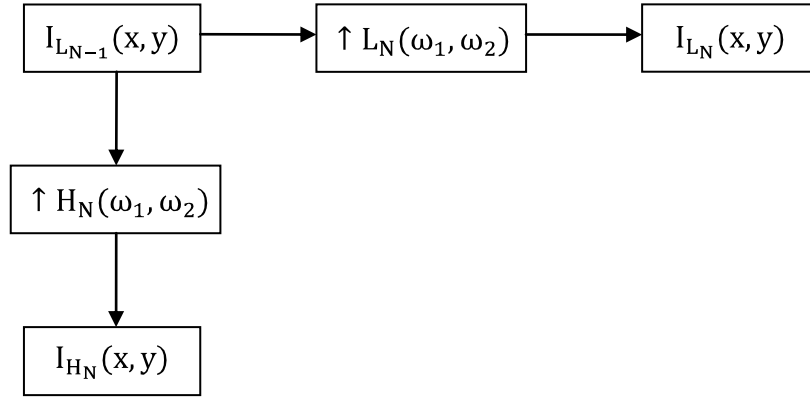


**Figure 3.12** : 2-D Nonsubsampled Laplacian Pyramid Decomposition.

Like in the LPD, the HPF or the high-pass filtered input can be deduced from the LPF or the low-pass filtered input respectively [7].

$$I_{H_N}(x, y) = I_{L_{N-1}}(x, y) - I_{L_{N-1}}(x, y) ** \uparrow L_N(\omega_1, \omega_2) \quad (3.13)$$

$$\uparrow H_N(\omega_1, \omega_2) = 1 - \uparrow L_N(\omega_1, \omega_2) \quad (3.14)$$

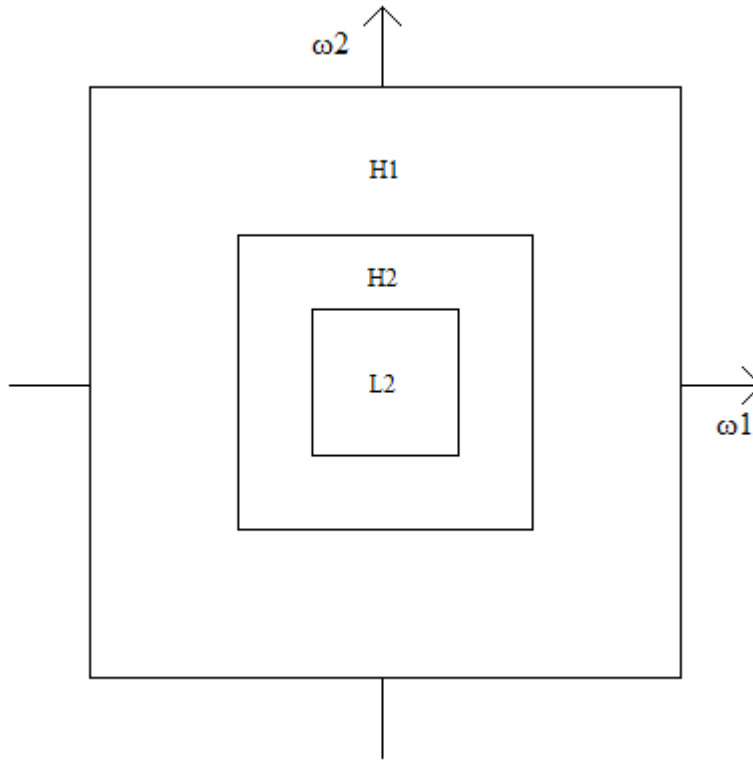


**Figure 3.13 :** Frequency Division of the 2-D 2-Level NSLPD.

As seen in the Figure 3.13, the frequency division of the 2-D 2-Level NSLPD is the same as the 2-D 2-Level LPD case. The frequency plane is divided into one high frequency region on every level whereas there is one approximation region on the last level.



Then, the 2-D 3-Level NSLPD is the following:

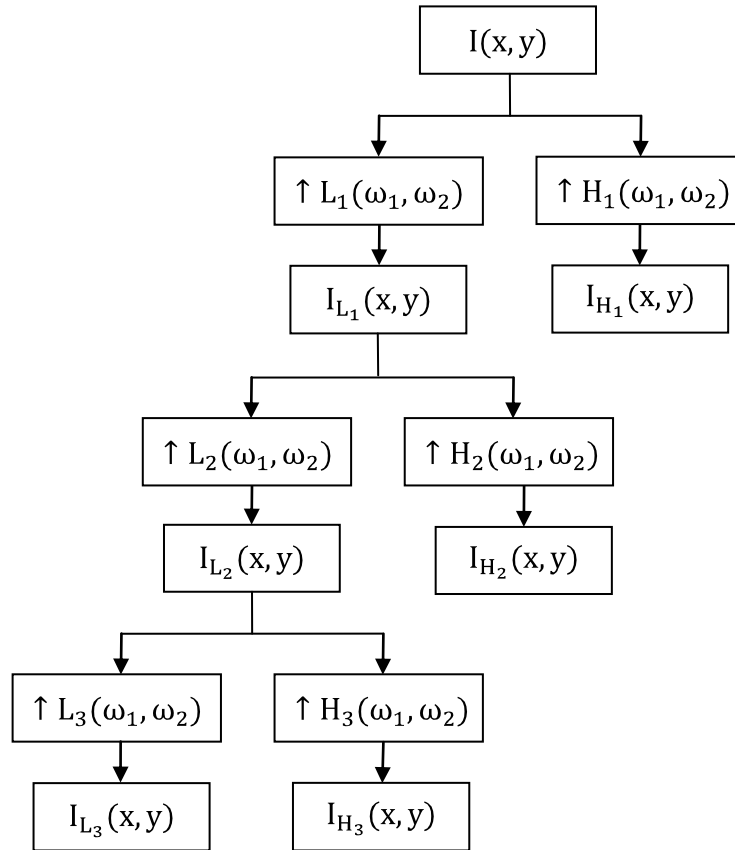


**Figure 3.14 :** 2-D 3-Level NSLPD.

The 2-D 3-Level NSLPD inherently produces 3 high-pass and 3 low-pass subbands. The information from the low-pass subbands on the first and the second level are carried into the next level since they will be decomposed into 2 subbands on the next level. Due to this fact, the smallest subset of the subbands for perfect reconstruction includes all the subband images from the last level and the remaining high-pass subband images from the upper remaining levels. This property is considered during the feature set selection to avoid unnecessary redundant information.

The inverse operation of the NSLPD is called the NSLP Reconstruction and can be performed by using the inverse LPF/HPF that are downsampled after each reconstruction level.

### 3.5 Nonsubsampled Directional Filter Bank Decomposition

The Nonsubsampled Directional Filter Bank Decomposition (NSDFBD) is similar to its subsampled counterpart except that the Modulator, QDFs are omitted and different special Directional Filters are used.

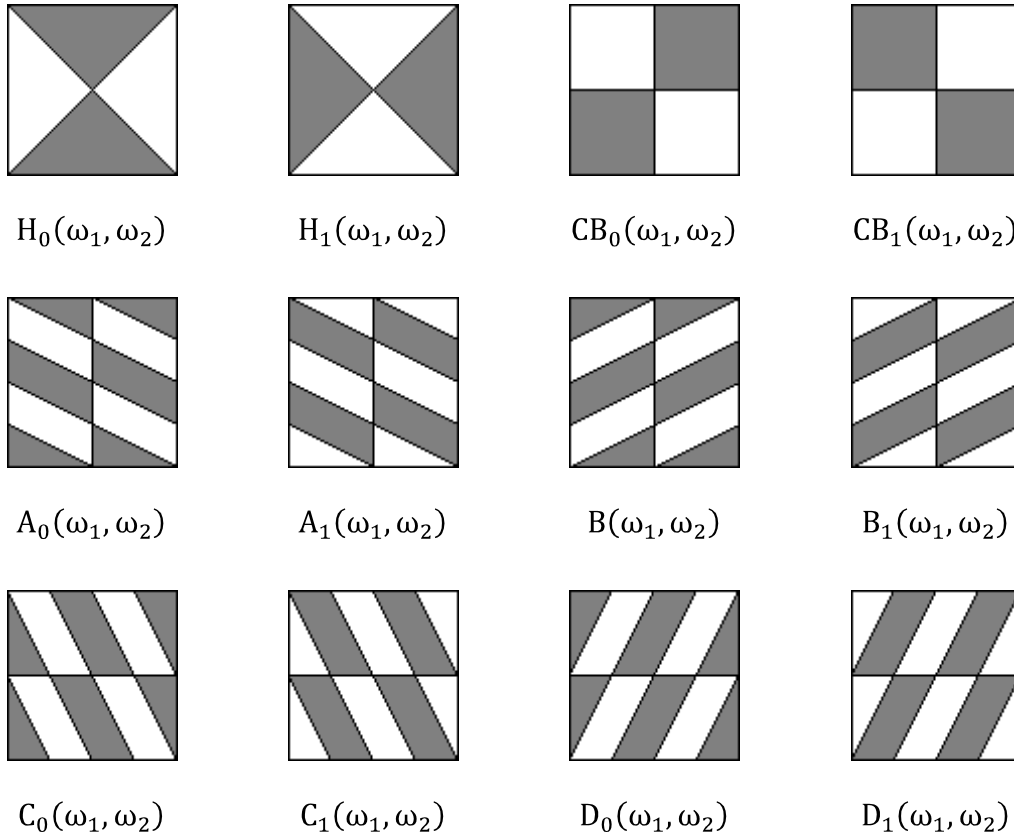


**Figure 3.15 :** Nonsubsampled Directional Filter Bank Decomposition Filters.

Upsampled versions of the filters  $CB_0(\omega_1, \omega_2)$  and  $CB_1(\omega_1, \omega_2)$  are used on the second level whereas the special filters  $A_0(\omega_1, \omega_2)$ ,  $B_0(\omega_1, \omega_2)$ ,  $C_0(\omega_1, \omega_2)$ ,  $D_0(\omega_1, \omega_2)$ ,  $A_1(\omega_1, \omega_2)$ ,  $B_1(\omega_1, \omega_2)$ ,  $C_1(\omega_1, \omega_2)$  and  $D_1(\omega_1, \omega_2)$  are upsampled by the factor of  $2^2$  on the third level [18][36].

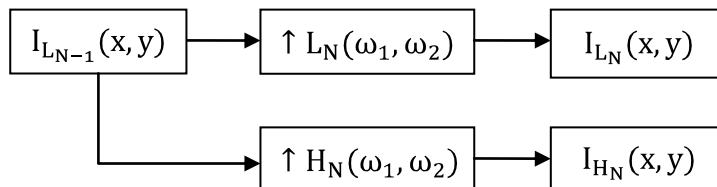


**Figure 3.16 :** Nonsubsampled Directional Filter Bank Decomposition.

For all the levels, the above structure can be used where  $\uparrow L_N(\omega_1, \omega_2)$  and  $\uparrow H_N(\omega_1, \omega_2)$  are the HFs, Checker-Board Filters (CBFs), special Directional Filters on the first, second and third level respectively [18][36].

The upsampling of the Directional Filters is necessary and critical to avoid the phenomena called as the Aliasing Effect due to the imperfection of the Directional Filters. Without the upsampling, the transition bands of the Directional Filters coincide with the coarser upsampled LP subbands and will cause distortion of the signal output [18]. This effect is studied in detail by Nguyen and Oraintara[24].

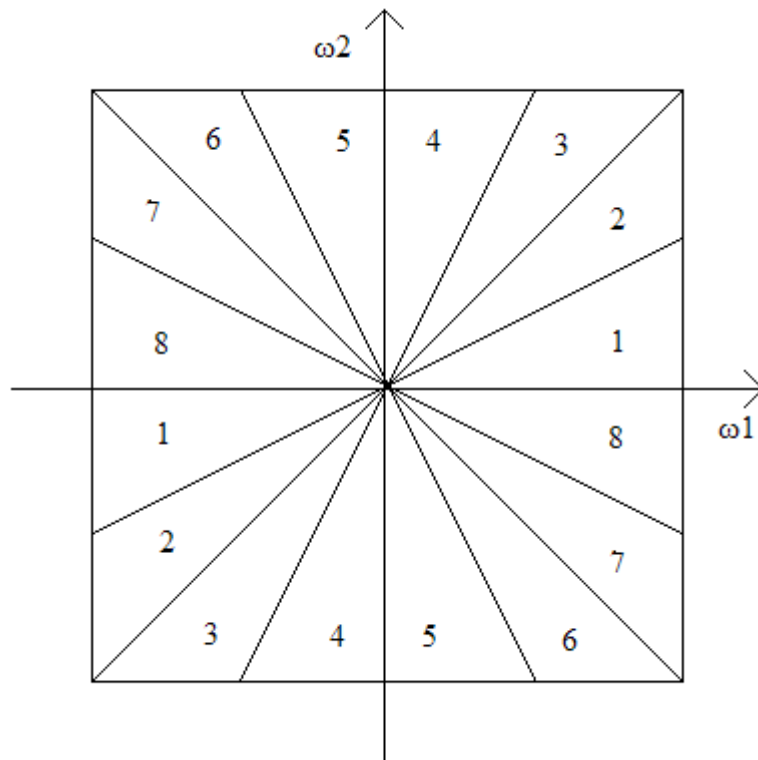


**Figure 3.17 :** Frequency Division of the 3-Level NSDFBD.

As seen in the Figure 3.17, the frequency division of the 3-Level NSDFBD is the same as the 2-Level DFBD case. The frequency plane is divided into  $2^4$  wedges that represent the directionalities in  $2^3$  directions.

The 3-Level NSDFBD is as the following:

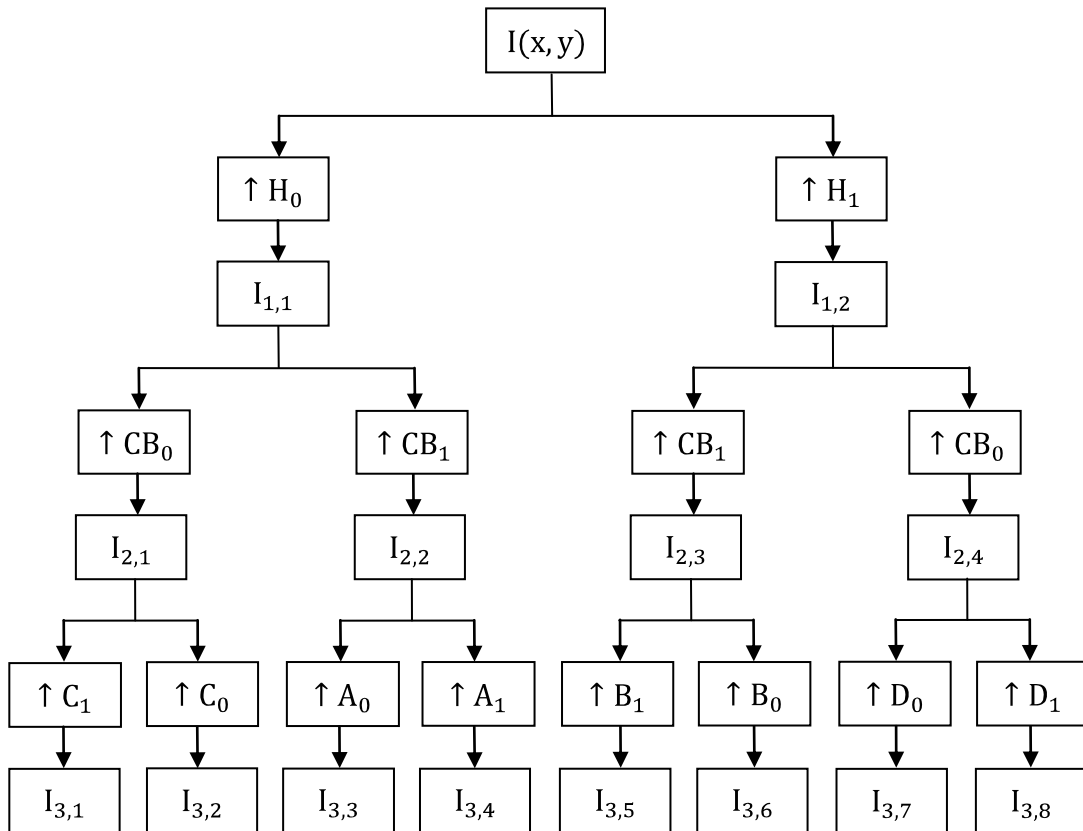


**Figure 3.18** : 3-Level NSDFBD.

The 3-Level NSDFBD inherently produces 14 subbands. The input image is first directionally decomposed into 2 directions resulting in 4 slices in the frequency domain. On the second level, the number of directions doubles and becomes 4 resulting in 8 slices in the frequency domain. The last level produces 8 directional subbands that divide the frequency domain in 16 slices.

The first level utilizes the HFs, the second one uses the CBFs whereas the last level utilizes the specially designed filters presented in the Figure 3.15. Cascading an HF with the CBFs results in the division of the frequency domain into 4 directions. The special filters used on the third and last level gets input images filtered with supports in 4 different directions and the outputs are as a result 8 different directional subbands. The smallest subset of the subbands for perfect reconstruction includes only the directional subband decompositions from the last level.

The inverse operation of the NSDFBD is called the NSDFB Reconstruction and can be performed by using the inverse NSDFBD filters.

### 3.6 Nonsubsampled Contourlet Transform

The Nonsubsampled Contourlet Transform (NSCT) is similar to the subsampled counterpart except the omitted upsamplers/downsamplers and upsampling of both the LP and the DFBD Filters successively after each level. In other words, the NSCT is obtained by cascading the NSLP with the Nonsubsampled Directional Filter Bank (NSDFB) [18].

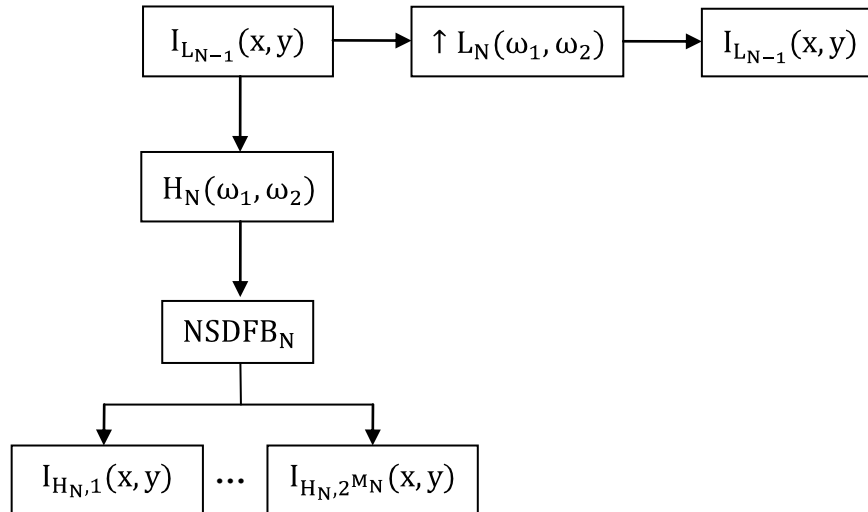


**Figure 3.19 :** Nonsubsampled Contourlet Decomposition.

Beginning from the first level, the input image is decomposed into high-pass and low-pass subbands. The resultant high-pass subband is decomposed into directional subbands since the DFB performs better on high frequencies [5]. The low-pass subband will be downsampled and passed into the next level. The common practice is to decompose the high-pass subbands into many directions on the first levels and into fewer directions on the coarse levels, since the frequency domain will be divided into smaller chunks on the coarse levels.

As seen in the Figure 3.20, the frequency division of the 2-Level NSCD is the same as the 2-Level CD case. The frequency plane is divided into 8 directional regions on the first level whereas there are 4 directional regions and one approximation region on the last level.

The 3-Level Nonsubsampled Contourlet Decomposition (NSCD) can be constructed as in the Figure 3.21.

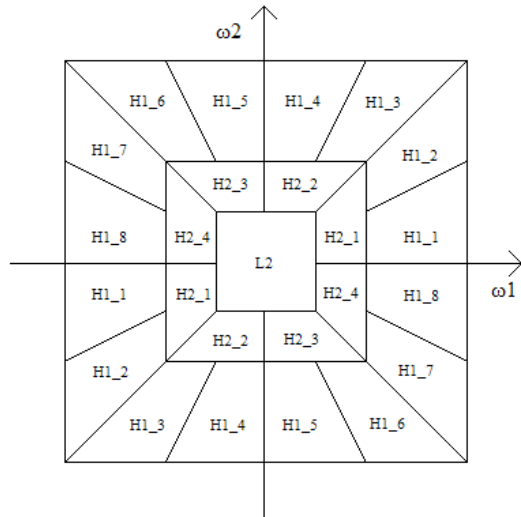


**Figure 3.20 :** Frequency Division of the 2-Level NSCD.

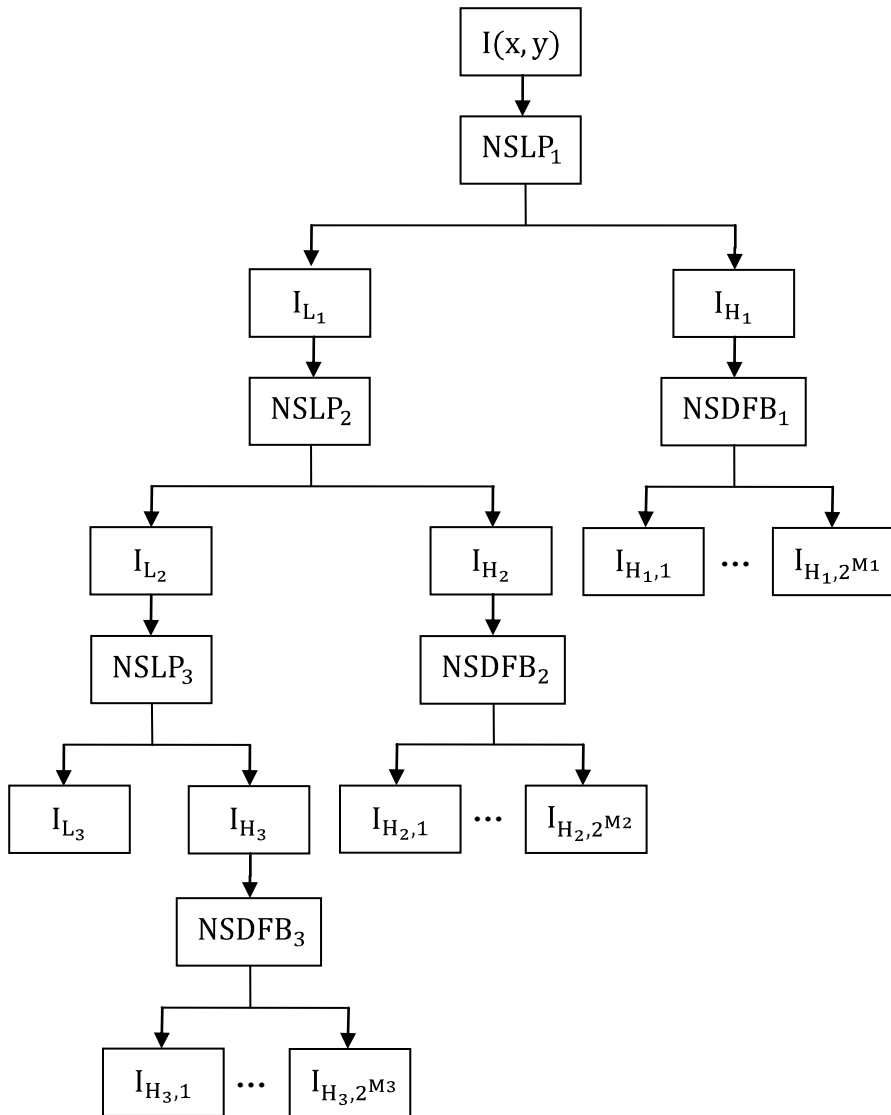


**Figure 3.21 :** 3-Level Nonsampled Contourlet Decomposition.

The 3-Level NSCD inherently produces  $6 + 2^{M_1} + 2^{M_2} + 2^{M_2}$  subbands.  $I_{H_3}, I_{H_2}, I_{H_1}, I_{L_2}, I_{L_1}$  are the redundant subbands whereas the smallest subset of the subbands for perfect reconstruction is the low-pass subband from the last level and the directional subband decompositions from all levels. Only the high-pass portions of the NSLPD are directionally decomposed by the NSDFB since it performs better on high frequencies [5].

The inverse operation of the NSCD is called the Nonsampled Contourlet Reconstruction which can be performed by using both the NSLP and the NSDFB Reconstruction.





## **4. HYBRID CONTOURLET TRANSFORMS**

The fashion of combining or cascading the different transform methods began with the introduction of the CT. Whereas the CT is the resulting transform of the combination of the rather simpler transforms, the more advanced and complex combinations were and are recently being researched. The major purpose of this strategy is to achieve better feature extraction by eliminating the individual weaknesses of each cascaded transform methods through compensation. The Hybrid Contourlet Transforms are one of the important members of this Hybrid Transform Families [16][17].

### **4.1 Wavelet Based Contourlet Transform**

The Wavelet Based Contourlet Transform (WBCT) is achieved by utilizing the DWT for subband decomposition and reconstruction, followed by the DFB for directional decomposition and reconstruction. During the decomposition, the Discrete Wavelet approximation signal is passed into the next level whereas the directional subbands are directionally decomposed [16][17].

The Wavelet Based Contourlet Decomposition (WBCD) is performed by using the DWD instead of the LPD to achieve directional decompositions on low-pass portions as well. Only the approximated image is passed into the next level, whereas the horizontal, vertical and diagonal subbands are decomposed by the DFB [16][17].

The block diagram for single level WBCD and its frequency division are shown in Figures 4.1 and 4.2 respectively.

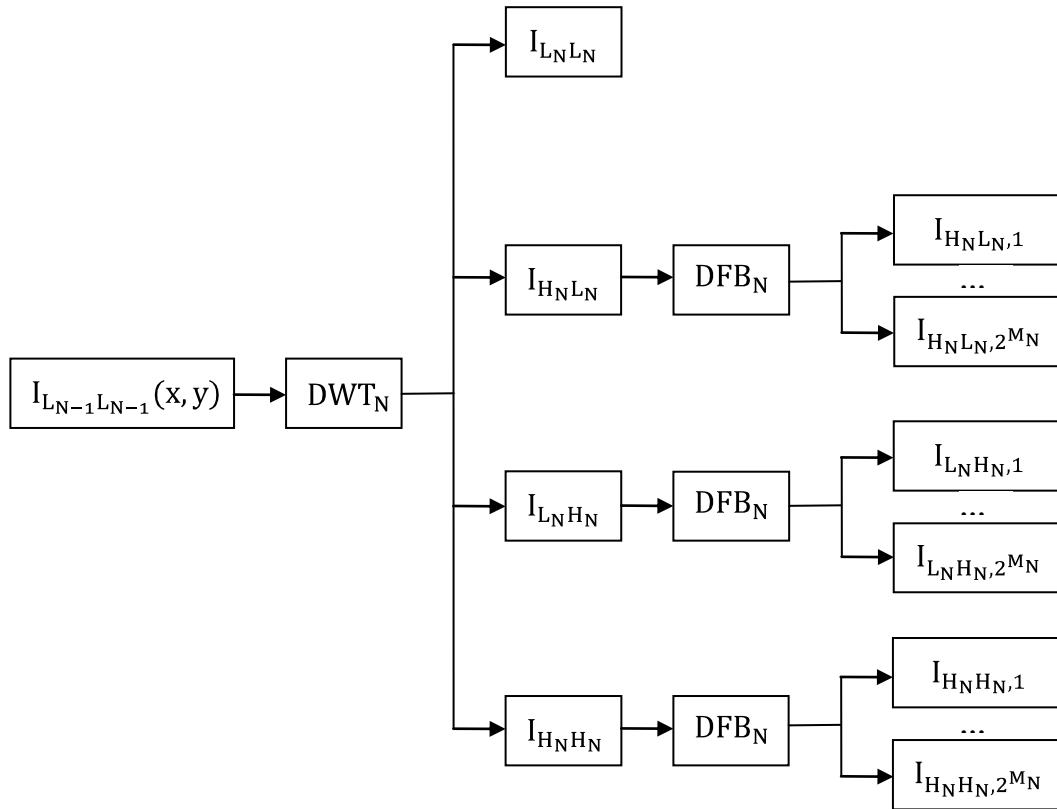


**Figure 4.1 :** Wavelet Based Contourlet Decomposition.

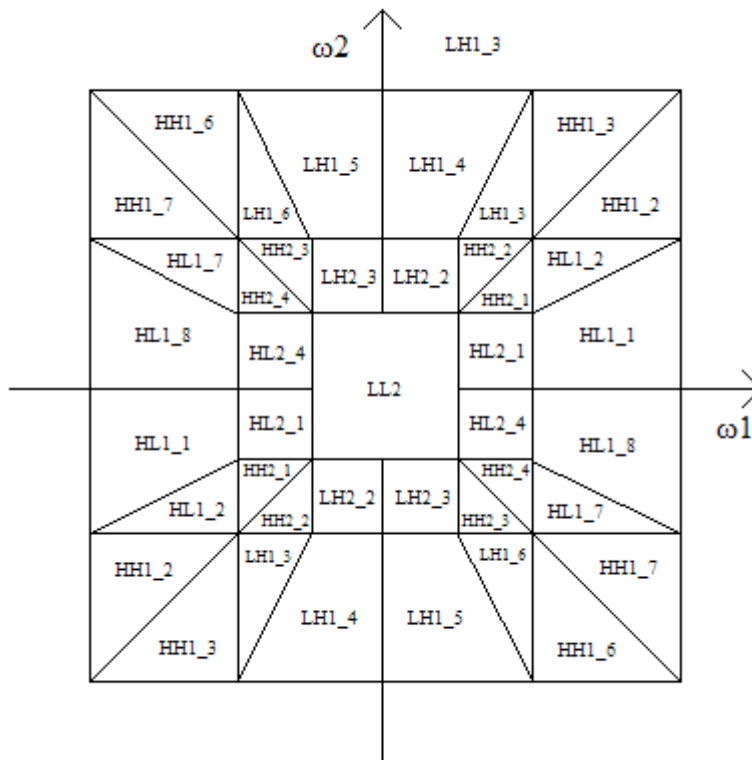


**Figure 4.2 :** Frequency Division of the 2-Level WBCD.

The frequency division of the 2-Level WBCD is presented in the Figure 4.2. The frequency plane is divided into 24 directional regions on the first level whereas there are 16 directional regions and one approximation region on the last level.

The 3-Level WBCD is constructed as in the Figure 4.3. The decomposition inherently produces  $12 + 2^{M_1} + 2^{M_2} + 2^{M_2}$  subbands. All the DWD subbands except  $I_{L_3L_3}$  are the redundant subbands whereas the smallest subset of the subbands for perfect reconstruction contains  $I_{L_3L_3}$  and all the directional subbands produced by DFBS on all levels. Horizontal, vertical and diagonal portions of the DWDs are directionally decomposed by the DFB since it performs better on high frequencies [5].

The inverse operation of the WBCD is called the Wavelet Based Contourlet Reconstruction which can be performed by using both the Discrete Wavelet and the NSDFB Reconstruction.

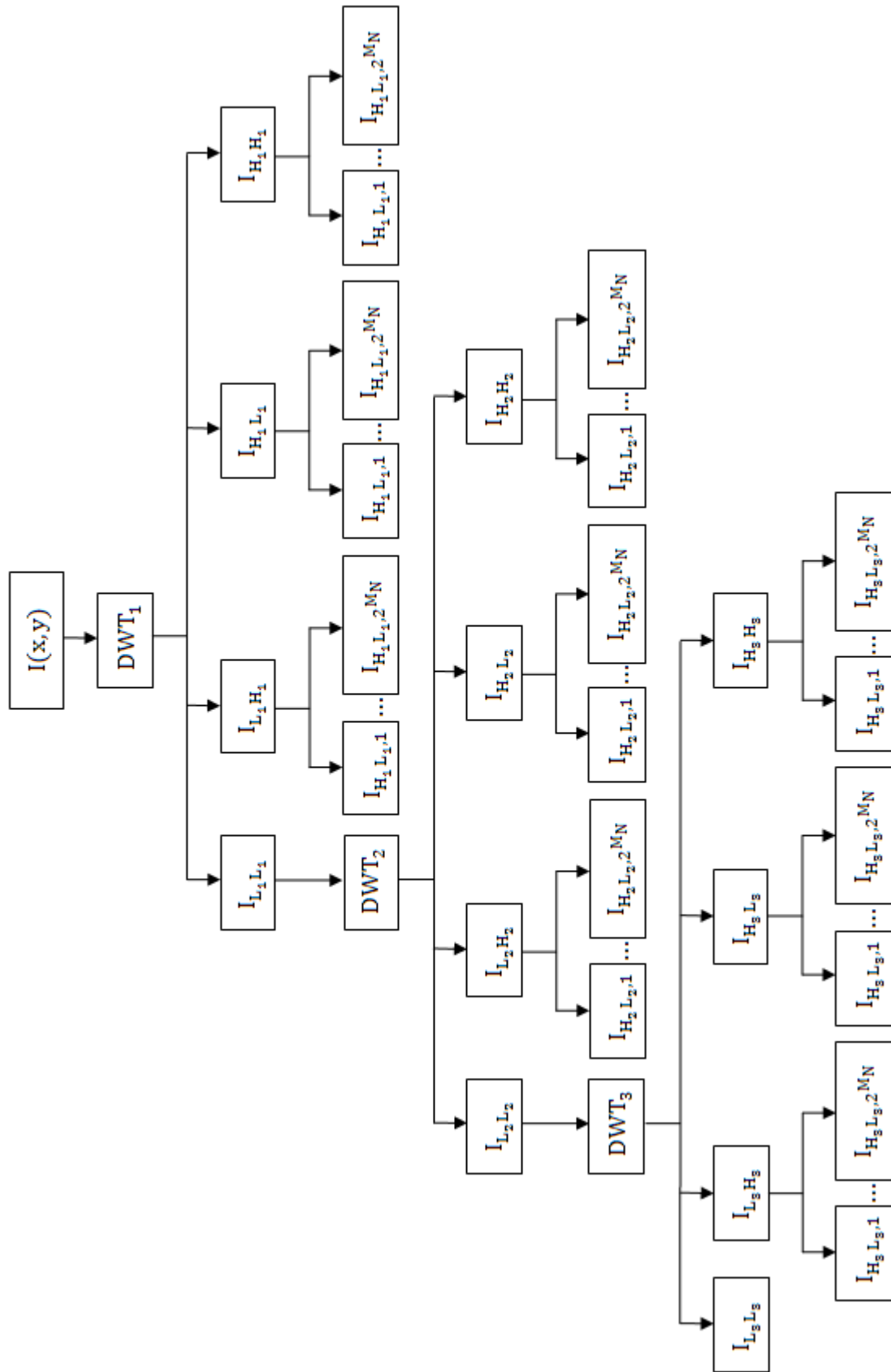


**Figure 4.3 :** 3-Level Wavelet Based Contourlet Decomposition.

## 4.2 Stationary Wavelet Based Contourlet Transform

The Stationary Wavelet Based Contourlet Transform (SWBCT) is achieved by utilizing the SWT for subband decomposition and reconstruction, followed by the DFB decomposition and reconstruction. During the decomposition, the SWT approximation is passed into the next level whereas the directional subbands are directionally decomposed [19].

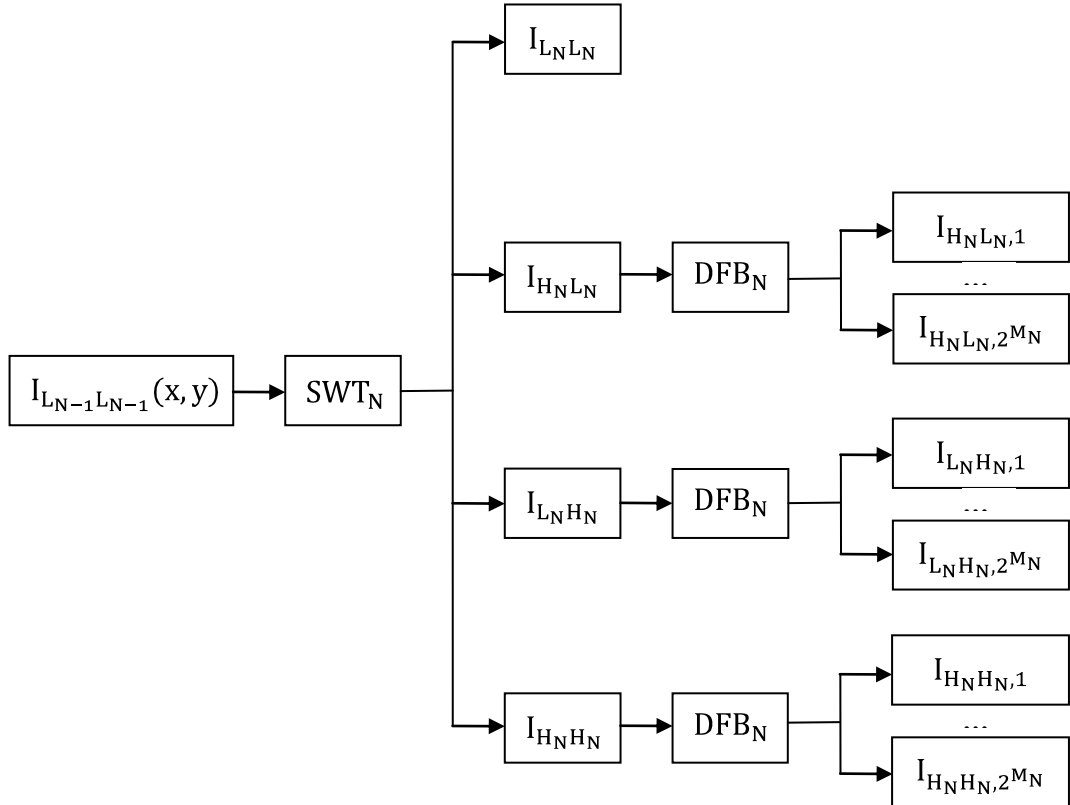


**Figure 4.4 :** Stationary Wavelet Based Contourlet Decomposition.

The Stationary Wavelet Based Contourlet Decomposition (SWBCD) is performed by using the SWD instead of the NSLPD to achieve directional decompositions on low pass portions as well. Only the approximated image is passed into the next level, whereas the horizontal, vertical and diagonal subbands are decomposed by the NSDFB [19].

The 3-Level SWBCD is constructed as in the Figure 4.4. The decomposition inherently produces  $12 + 2^{M_1} + 2^{M_2} + 2^{M_2}$  subbands. All the SWD subbands except  $I_{L_3L_3}$  are the redundant subbands whereas the smallest subset of the subbands for perfect reconstruction contains  $I_{L_3L_3}$  and all the directional subbands produced by

NSDFBs on all levels. Horizontal, vertical and diagonal portions of the SWDs are directionally decomposed by the NSDFB since it performs better on high frequencies [5].

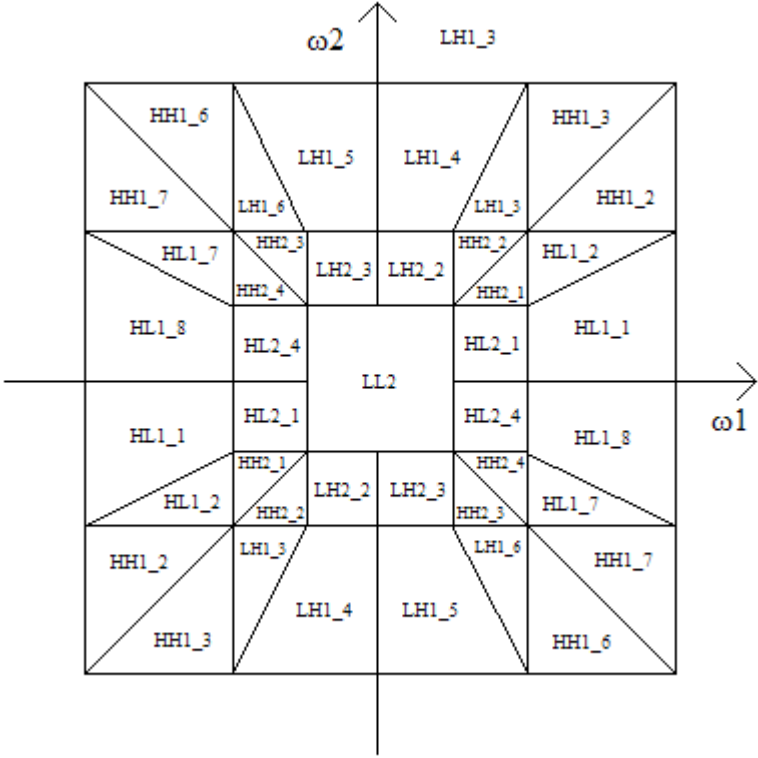


**Figure 4.5 :** Frequency Division of the 2-Level SWBCD.

As seen in the Figure 4.5, the frequency division of the 2-Level SWBCD is the same as the 2-Level WBCD case. The frequency plane is divided into 24 directional regions on the first level whereas there are 16 directional regions and one approximation region on the last level.

The inverse operation of the SWBCD is called the Stationary Wavelet Based Contourlet Reconstruction which can be performed by using both the Stationary Wavelet and the DFB Reconstruction.

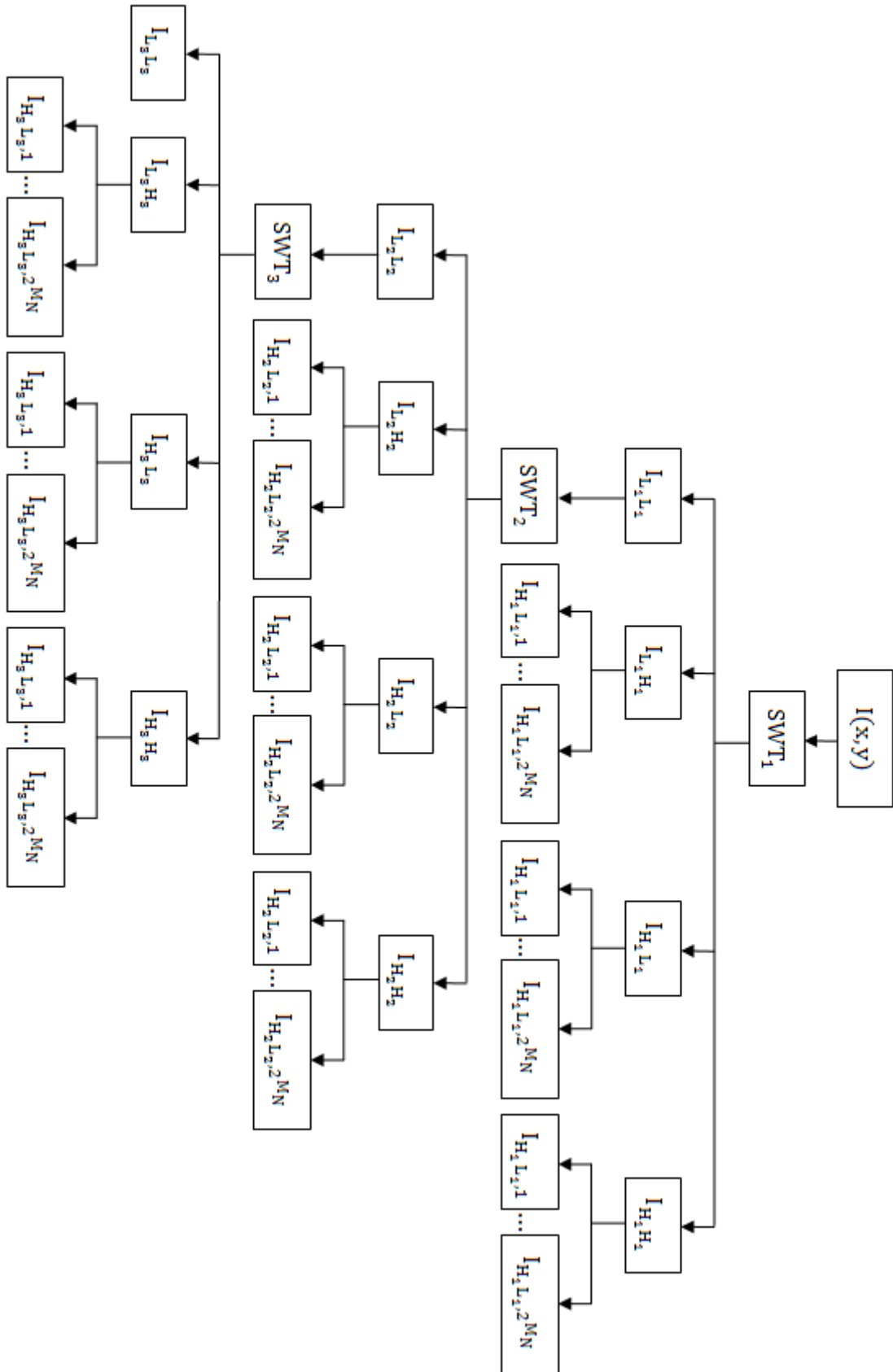


**Figure 4.6 :** 3-Level Stationary Wavelet Based Contourlet Decomposition.





## **5. FEATURE EXTRACTION AND CLASSIFICATION**

### **5.1 Introduction**

Classification falls into one of the subsets of machine learning which is a vast area of research closely relevant to the artificial intelligence. Classification has basically three steps. First, the features of the signal are extracted. Then, the classification algorithm is trained using a training set. Finally, the features are fed into the trained classification algorithm which decides upon the classes based on these extracted features [25][26].

### **5.2 Feature Extraction**

The simplest feature extraction method would be using the data itself. For most of the cases, this does not suffice and methods should be used, which extract features that are specifically suitable for the classification problem [25][26].

Generally, types of features can be divided into the following categories:

#### **5.2.1 Spectral Features**

For some classification problems, one is not interested in the spatial domain of the image. Instead, the features on the frequency domain are needed. The most used methods are the colour histogram and the cumulative colour histogram [27].

#### **5.2.2 Shape Features**

For object recognition and classification, most widely used techniques are the edge detection algorithms. Some are Nevati and Babu's Technique, Hysteretic Threshold, Shape Models, Canny's Procedure, Deriche's Procedure and Morphologic Features [27].

### **5.2.3 Texture Features**

Textures are images which have more or less periodic characteristics in the spatial domain [27]. Since they have repeated patterns over the spatial domain, the more successful feature extraction methods should also cover the frequency domain of the image. Therefore, most widely used methods involve analysis methods using 2-D transforms like WFT, DWT and CT. In this work, six different feature extraction methods of this kind are used.

## **5.3 Classification Algorithms**

There are many classification algorithms in the literature. To briefly summarize, the classification algorithms can be categorized by its training strategies and decision approaches.

### **5.3.1 Supervised and Unsupervised Learning**

When a classification algorithm is trained by a smaller subset of samples, a supervised training feeds the classification algorithm with both the feature vectors and the target values. The target values are the correctly assigned classes of the training set so they need to be known before the classification phase. An unsupervised classification however does not require the target values so it only uses the feature vectors [25][26].

### **5.3.2 Discriminative and Generative Approaches**

Discriminative approach based classification algorithms separate classes from each other by forming decision boundaries; also known as hyperplanes; between them. This can be achieved by parametric methods. Parametric methods assume a prior distribution of the classes which is for most of the cases a Gaussian Distribution. After that, the parameters of the distribution are estimated by using the training set. Logistic Discriminants, Support Vector Machines (SVM), Relevance Vector Machines (RVM) and Linear Discriminants, despite its name which can act non-linear as well by utilizing non-linear basis function, use this kind of approach [25][26].

In contrast, the generative approach; also known as the Bayesian approach; does not assume a prior distribution. It lets the data speak itself and applies well known Bayesian Theorem to calculate the posterior probability of the classes [25][26].

### 5.3.2.1 Bayesian Theorem

For  $K$  mutually exclusive and exhaustive classes;  $C_i$ ,  $i = 1, \dots, K$ ; the prior probability, the likelihood and the evidence are defined as [25][26]:

$$\text{prior} = P(C_i) \tag{5.1}$$

$$\text{likelihood} = p(x|C_i) \tag{5.2}$$

$$\text{evidence} = p(x) \tag{5.3}$$

$$\text{posterior} = \frac{\text{prior} \cdot \text{likelihood}}{\text{evidence}} = \frac{p(C_i)p(x|C_i)}{p(x)} \tag{5.4}$$

$$p(x) = \sum_{k=1}^K p(x|C_k)p(C_k) \tag{5.5}$$

Bayesian Networks and K-Nearest Neighbour (KNN) are based upon this generative approach [25][26].

Besides these algorithms, there is another algorithm called Neural Networks (NN); also known as the Multilayer Perceptrons (MLP); which does not assume prior distribution of the classes but estimate its weight parameters according to the training set [25][26].

As a rule of thumb, Bayesian approach is used when there are lots of both training and sample set data available, since the generalization will be more accurate. Furthermore, on the contrary to the discriminative approach, the Bayesian approach does not need to estimate and correct its parameters for every training set data fed; hence it produces results in much less time. Discriminative approach is used in those cases when the training set data is scarce and therefore the generalization is performed directly by the distribution assumption [25][26].

## 5.4 K-Nearest Neighbour Algorithm

KNN algorithm is one of the simplest classification algorithms due to its robustness and easy implementation. The KNN estimator is defined as [26]:

$$p(x|C_i) = \frac{k_i}{N_i V^k(x)} \quad (5.6)$$

where  $k_i$  is the number of neighbours out of the  $k$  nearest that belong to the class  $C_i$  and  $V^k(x)$  is the volume of the  $d$ -dimensional hypersphere centered at  $x$  with radius  $r = \|x - x_k\|$  where  $x_k$  is the  $k$ -th nearest observation to  $x$ .

Then the KNN classifier becomes using the Bayesian Theorem

$$p(C_i|x) = \frac{p(x|C_i)p(C_i)}{p(x)} = \frac{k_i}{k} \quad (5.7)$$

KNN classifier assigns the input to the class having most of examples among the  $k$ -neighbours from the training set. Ties can be broken randomly or using weighted vote. The distance to determine the proximity of the neighbours can be Euclidean Distance, Cosine Similarity, Correlation or Hamming Distance.

A special case of the KNN classifier is the Nearest Neighbour classifier where  $K$  is chosen to be 1. This results in the division of the space in the form of the Voronoi Tessellation, also known as the Thyssen Polygons [26].

This work uses the KNN classification algorithm with different  $K$  values varying from 1 to 5.

## 5.5 Textures

Textures are defined in literature as the images that have measurable characteristics like smoothness, coarseness and regularity which results in regular patterns or distributions of these measurable properties in the spatial domain [27].

The textures can be categorized into the followings.

### 5.5.1 Regular Textures

Regular textures are the ones that have not necessarily exactly but more or less the same spatial patterns that repeat themselves. Their features are constant or slightly

vary over a frame in the spatial domain. The classification of these texture types is very easy since they have more or less the same repeated features over the spatial domain and require less number of training samples [27].

### **5.5.2 Statistical Textures**

Statistical textures are textures that do not have repeated patterns over most of the spatial domain but the distribution of their features can be fit into a statistical function with an acceptable error margin [27].

### **5.5.3 Synthetic Textures**

Synthetic Textures are the ones that have exactly the same spatial patterns that repeat themselves or can be synthesized using predefined distribution functions. The former ones are also considered as regular textures and hence their classification can be performed easily [27].

### **5.5.4 Natural Textures**

Natural textures are textures that are taken directly from the observations of the nature. This type of textures can be both regular or statistical but due to the random nature of the universe, their feature distribution can be fit into a statistical function with an acceptable error margin [27].

## **5.6 Brodatz Textures**

Phil Brodatz has published a photographic album in 1966 which have 112 different textures called since then as the Brodatz Textures (BT) [28]. The BT cover both regular and statistical natural textures. Each BT has unique individual features which make BT very suitable for testing the feature extraction and classification algorithm performances.

In this work, 4 different regular BT are combined as a matrix. The individual textures were 320 by 320 pixel images and they were downsampled to 160 by 160 pixel images before the combination. The resulted BT Matrix and its perfect segmentation are presented in Figures 5.1 and 5.2 respectively.

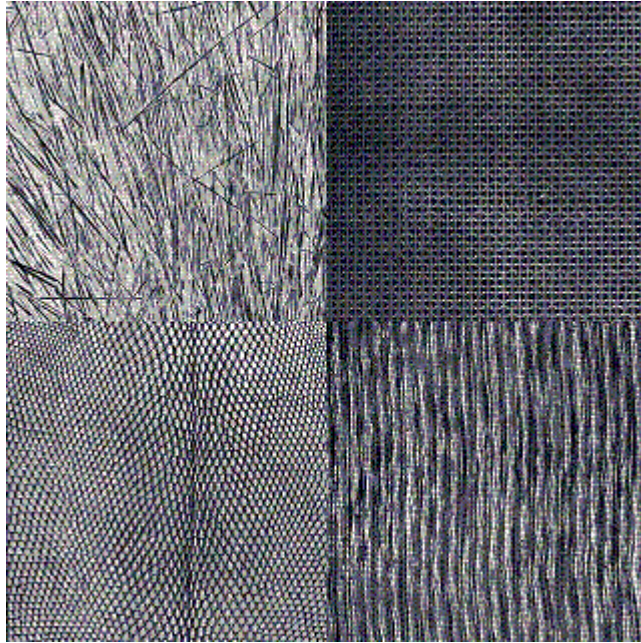


**Figure 5.1** : 4 Class Brodatz Textures Matrix.

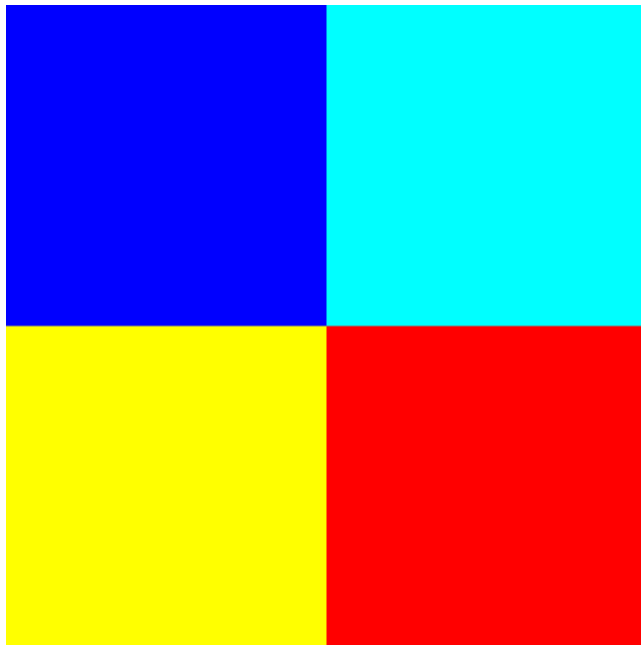


**Figure 5.2** : Perfectly Segmented 4 Class Brodatz Textures Matrix.

## 5.7 Brodatz Texture Matrix Classification Algorithm

The classification algorithm for the BT Matrix can be divided into the following steps some of which have variable inputs:

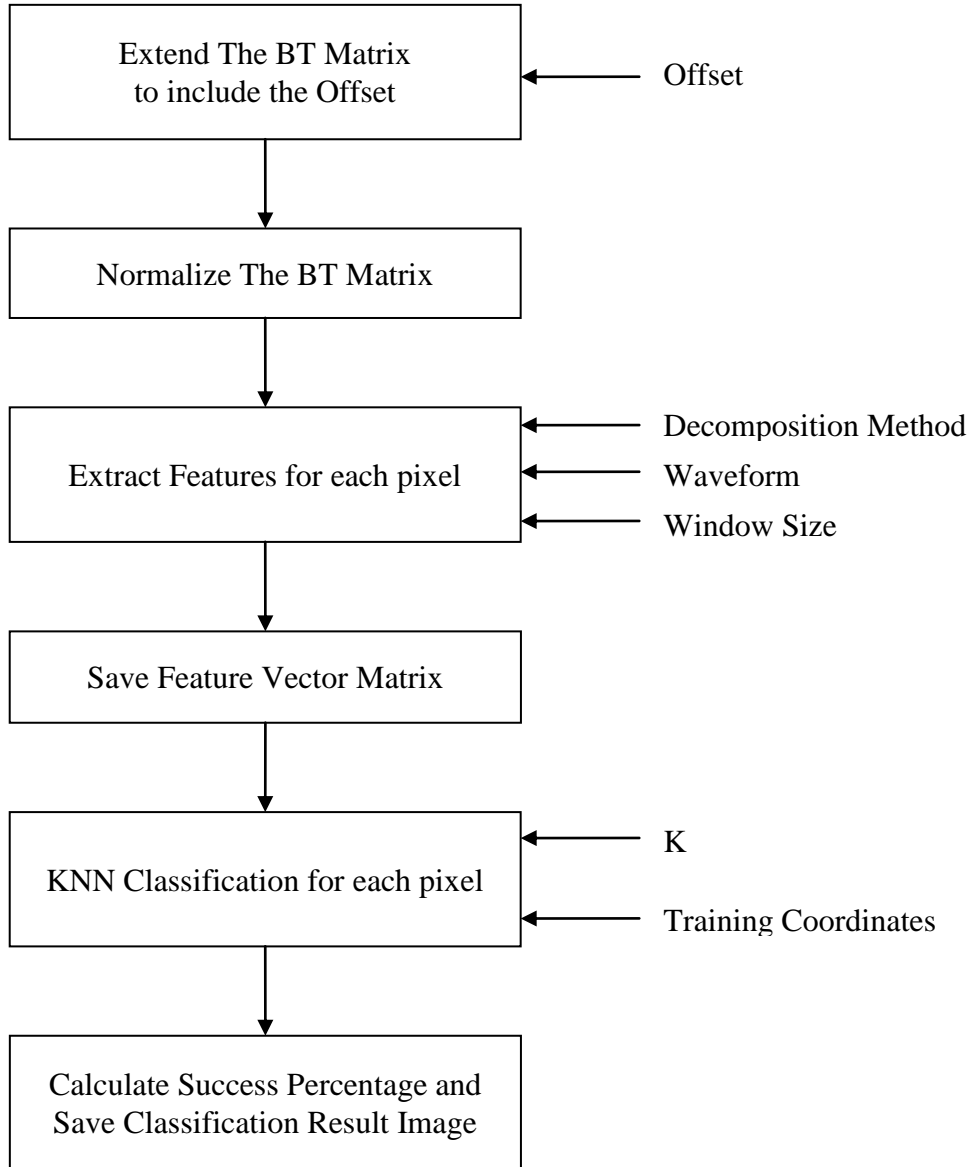


**Figure 5.3 :** 4 Class Brodatz Textures Matrix Classification Algorithm.

1. The BT Matrix size needs to be extended so that the used window has values during traversing the image near its sides. The offset size is directly determined by the size of the window, i.e. the offset is upper rounded value of the half of the window size. The missing pixel values are populated by using the mirror values from the first left and the right image side, then from the top and the bottom image side.

2. The image pixel values are normalized so that image contrast is enhanced.
3. The features are extracted using the Transform Based Decomposition Methods; DWT, SWT, CT, NSCT, WBCT and SWBCT Decompositions. The image is traversed by the used window with predefined size 16 by 16, starting from the left-upper corner and ending on the right-lower corner pixel of the original image. The extracted features are the means and variances of each subband decompositions on every level. The level of decompositions is 2; 1- and 3-level decompositions did not provide satisfactory and consistent results and thus will not be presented in this work. Haar, Daubechies-4 and Daubechies-6 Wavelets are used as waveforms in order to compare the performances of different feature extraction methods more precisely. The formed feature vector represents the features of the pixel on the coordinates (8,8) of the used window. After the traverse of the whole image, the feature matrix is constructed using each feature vector as its rows.

This step applies pixel by pixel shifting of the used window in both horizontal and vertical directions to avoid misclassification on both horizontal and vertical class boundaries. Pixel by pixel shifting is computationally more exhaustive compared to the vertical and horizontal window shifting which however may cause misclassification on the horizontal and vertical class boundaries respectively.

4. The formed feature matrix is stored as a binary file so that it can be used multiple times without having to calculate it over and over again.
5. The feature matrix is read from the file and The KNN Classifier is fed with 10 training feature vectors for each class and the feature vectors of the candidate pixels. The KNN Classifier assigns each pixel to a single class. The classification were performed for K varying from 1 to 5 and the most successful results were achieved for K=1 and K=2. Another approach would be using The Nearest Neighbour Classifier where the mean of each feature vectors of the same class we calculated and fed into the classifier. Its results were unsatisfactory and will not be presented in this work.
6. The resultant segmented image and the classification performance are saved as separate files.



The overall process can be programmed in MATLAB using built-in and custom toolboxes [29][30][31]. Using the MATLAB Parallel Computing Toolbox, this process with different input values can be performed in parallel [32].

### 5.7.1 Discrete Wavelet Decomposition Features

The feature vector for BT-DWT classification includes the mean and standard deviations of the directional subband images on the first level and the mean and standard deviations of both the directional subband and approximation images on the second level.

$$f_{\mu} = [\mu_{L_1H_1}, \mu_{H_1L_1}, \mu_{H_1H_1}, \mu_{L_2L_2}, \mu_{L_2H_2}, \mu_{H_2L_2}, \mu_{H_2H_2}] \quad (5.8)$$

$$f_{\sigma} = [\sigma_{L_1H_1}, \sigma_{H_1L_1}, \sigma_{H_1H_1}, \sigma_{L_2L_2}, \sigma_{L_2H_2}, \sigma_{H_2L_2}, \sigma_{H_2H_2}] \quad (5.9)$$

$$F = [f_{\mu}, f_{\sigma}] \quad (5.10)$$

The resultant feature vector for a single image pixel contains 14 elements.

### 5.7.2 Stationary Wavelet Decomposition Features

The feature vector for BT-SWT classification includes the mean and standard deviations of the directional subband images on the first level and the mean and standard deviations of both the directional subband and approximation images on the second level.

$$f_{\mu} = [\mu_{L_1H_1}, \mu_{H_1L_1}, \mu_{H_1H_1}, \mu_{L_2L_2}, \mu_{L_2H_2}, \mu_{H_2L_2}, \mu_{H_2H_2}] \quad (5.11)$$

$$f_{\sigma} = [\sigma_{L_1H_1}, \sigma_{H_1L_1}, \sigma_{H_1H_1}, \sigma_{L_2L_2}, \sigma_{L_2H_2}, \sigma_{H_2L_2}, \sigma_{H_2H_2}] \quad (5.12)$$

$$F = [f_{\mu}, f_{\sigma}] \quad (5.13)$$

The resultant feature vector for a single image pixel contains 14 elements.

### 5.7.3 Contourlet Decomposition Features

The feature vector for BT-CT classification includes the mean and standard deviations of the directional subband images produced by the DFB on the first level and the mean and standard deviations of the subband images produced by the LP on the second level. The number of directions of the DFB on the first level is 8 whereas there is no directional decomposition performed by the DFB on the second level.

$$f_{\mu} = [\mu_{L_2}, \mu_{H_2}, \mu_{H_{1,1}}, \dots, \mu_{H_{1,8}}] \quad (5.14)$$

$$f_{\sigma} = [\sigma_{L_2}, \sigma_{H_2}, \sigma_{H_{1,1}}, \dots, \sigma_{H_{1,8}}] \quad (5.15)$$

$$F = [f_{\mu}, f_{\sigma}] \quad (5.16)$$

The resultant feature vector for a single image pixel contains 20 elements.

### 5.7.4 Nonsampled Contourlet Decomposition Features

The feature vector for BT-NSCT classification includes the mean and standard deviations of the directional subband images produced by the NSDFB on the first level and the mean and standard deviations of the subband images produced by the NSLP on the second level. The number of directions of the NSDFB on the first level is 8 whereas there is no directional decomposition performed by the NSDFB on the second level.

$$f_{\mu} = [\mu_{L_2}, \mu_{H_2}, \mu_{H_{1,1}}, \dots, \mu_{H_{1,8}}] \quad (5.17)$$

$$f_{\sigma} = [\sigma_{L_2}, \sigma_{H_2}, \sigma_{H_{1,1}}, \dots, \sigma_{H_{1,8}}] \quad (5.18)$$

$$F = [f_{\mu}, f_{\sigma}] \quad (5.19)$$

The resultant feature vector for a single image pixel contains 20 elements.

### 5.7.5 Wavelet Based Contourlet Decomposition Features

The feature vector for BT-WBCT classification includes the mean and standard deviations of the directional subband images produced by the DFB on the first level and the mean and standard deviations of both the directional subband and approximation images produced by the DWD on the second level. The number of directions of the DFB on the first level is 8 whereas there is no directional decomposition performed by the DFB on the second level.

$$f_{\mu} = [\mu_{L_2L_2}, \mu_{L_2H_2}, \mu_{H_2L_2}, \mu_{H_2H_2}, \mu_{H_{1,1}}, \dots, \mu_{H_{1,8}}] \quad (5.20)$$

$$f_{\sigma} = [\sigma_{L_2L_2}, \sigma_{L_2H_2}, \sigma_{H_2L_2}, \sigma_{H_2H_2}, \sigma_{H_{1,1}}, \dots, \sigma_{H_{1,8}}] \quad (5.21)$$

$$F = [f_{\mu}, f_{\sigma}] \quad (5.22)$$

The resultant feature vector for a single image pixel contains 56 elements.

### 5.7.6 Stationary Wavelet Based Contourlet Decomposition Features

The feature vector for BT-SWBCT classification includes the mean and standard deviations of the directional subband images produced by the DFB on the first level and the mean and standard deviations of both the directional subband and approximation images produced by the SWD on the second level. The number of directions of the DFB on the first level is 8 whereas there is no directional decomposition performed by the DFB on the second level.

$$f_{\mu} = [\mu_{L_2L_2}, \mu_{L_2H_2}, \mu_{H_2L_2}, \mu_{H_2H_2}, \mu_{H_{1,1}}, \dots, \mu_{H_{1,8}}] \quad (5.23)$$

$$f_{\sigma} = [\sigma_{L_2L_2}, \sigma_{L_2H_2}, \sigma_{H_2L_2}, \sigma_{H_2H_2}, \sigma_{H_{1,1}}, \dots, \sigma_{H_{1,8}}] \quad (5.24)$$

$$F = [f_{\mu}, f_{\sigma}] \quad (5.25)$$

The resultant feature vector for a single image pixel contains 56 elements.

## 5.8 AVIRIS Indiana's Indian Pine Hyperspectral Data

As the hyperspectral data, the hyperspectral image taken from the AVIRIS satellite in June 1992 is used [33]. The data are composed of the 128 byte image header containing the version, the data type, the number of bands and the pixel dimensions; followed by the non-normalized pixel values of the first line of the image data consequently on each hyperspectral bands, then by the non-normalized pixel values of the second line and so on. The data have 220 bands of 145 by 145 pixel images and the bands are about 10 nm apart from 0.4 to 2.45  $\mu\text{m}$  with a spatial resolution of 20 m. The ground truth (GT) is available on a separate file containing single assigned class for each pixel. The number of total classes is 17 including the background terrain class stone-steel towers [33].

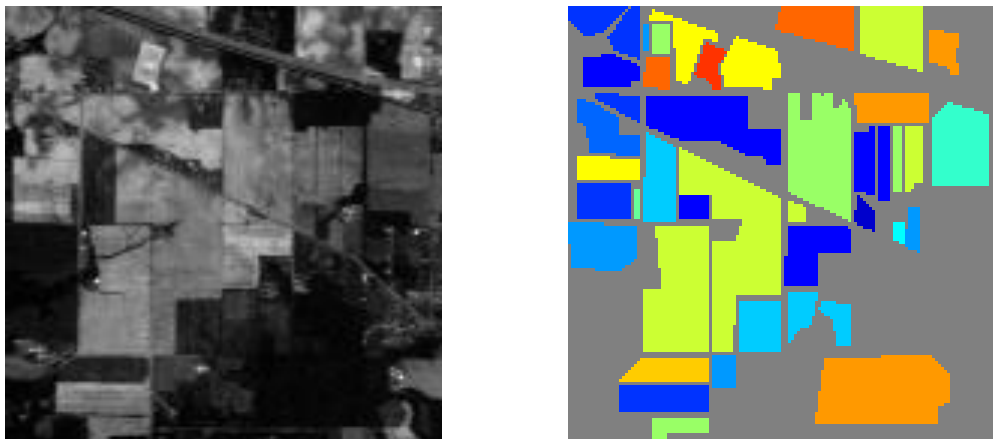


**Figure 5.4 :** AVIRIS Data on Band 32 and its GT.

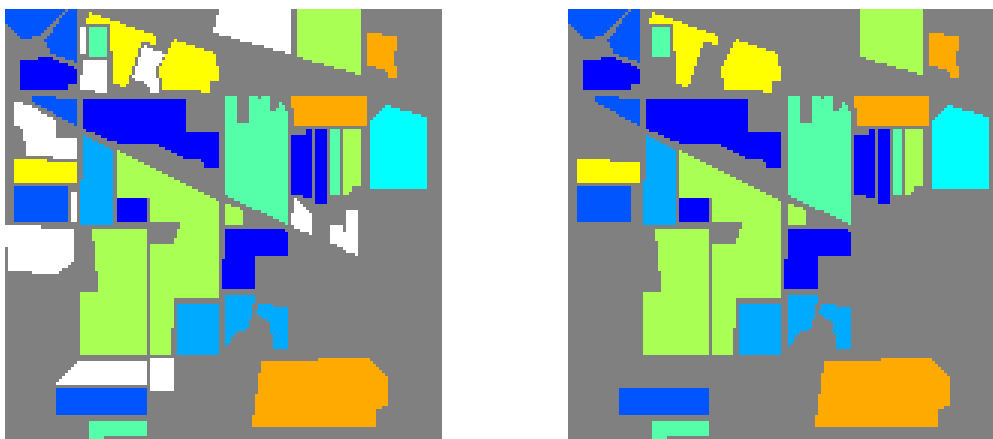


**Figure 5.5 :** AVIRIS Data GT before and after the class reduction.

Considering that the data contains many classes that have small number of counts compared to the ones with large counts, the classes with small counts are removed and assigned to the background class stone-steel towers. The removed classes are 1, 4, 5, 7, 9, 13, 15 and 16. In addition to that, the bands [104-108], [150-163], 220 are marked in the GT file as the water absorption bands and there are fifteen noisy bands [1-3], 103, [109-112], [148-149], [164-165], [217-219]. These bands will not be considered during the feature extraction routines [33].

The original and modified class pixel counts are shown on Table 5.1.

**Table 5.1 :** AVIRIS Hyperspectral Data Classes.

<b>Class No</b>	<b>Class Name</b>	<b>Count (Original)</b>	<b>Count (Modified)</b>
1	Corn-no till	54	0
2	Corn-min till	1434	1434
3	Corn	834	834
4	Soybeans-no till	234	0
5	Soybeans-no till2	497	0
6	Soybeans-min till	747	747
7	Soybeans-clean till	26	0
8	Alfalfa	489	489
9	Grass/Pasture	20	0
10	Grass/Trees	968	968
11	Grass/Pasture-mowed	2468	2468
12	Hay-windrowed	614	614
13	Oats	212	0
14	Wheat	1294	1294
15	Woods	380	0
16	Bldg-Grass-Tree-Drives	95	0
17	Stone-steel towers	10659	12177

## 5.9 AVIRIS Hyperspectral Data Classification Algorithm

The classification algorithm for the AVIRIS Hyperspectral Data is similar to the BT Matrix classification and can be divided into the following steps some of which have variable inputs:

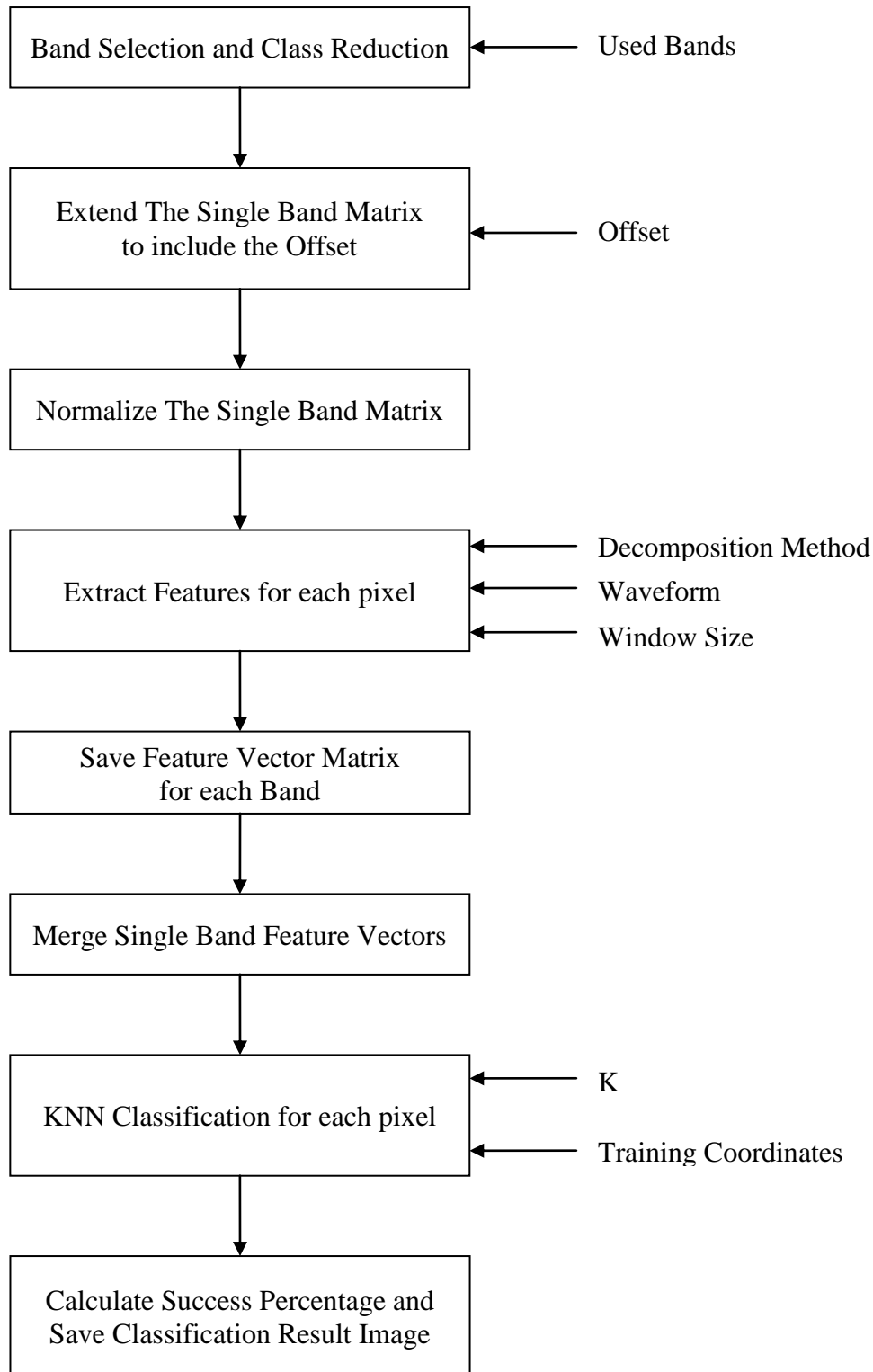


**Figure 5.6 :** AVIRIS Hyperspectral Data Classification Algorithm.

1. The visual inspection of the single-band images and class reduction are performed. The AVIRIS Indiana's Indian Pine data has unignorable number of water absorption and additional noisy bands; some classes of it have small number of pixels that can be ignored due to the resulting insufficient number of training samples. The twenty water absorption bands [104-108], [150-163], 220 marked in the GT file and the fifteen noisy bands [1-3], 103, [109-112], [148-149], [164-165], [217-219] observed by the visual inspection are not considered during the feature extraction.
2. The single-band image size needs to be extended so that the used window has values during traversing the image near its sides. The offset size is directly determined by the size of the window, i.e. the offset is upper rounded value of the half of the window size. The missing pixel values are populated by using the mirror values from the first left and the right image side, then from the top and the bottom image side.
3. The image pixel values are normalized so that image contrast is enhanced.
4. The features are extracted using the Transform Based Decomposition Methods; DWT, SWT, CT, NSCT, WBCT and SWBCT Decompositions. The image is traversed by the used window with predefined size 16 by 16, starting from the left-upper corner and ending on the right-lower corner pixel of the original image. The extracted features are the means and variances of each subband decompositions on every level. The level of decompositions is 2; 1- and 3-level decompositions did not provide satisfactory and consistent results and thus will not be presented in this work. Haar, Daubechies-4 and Daubechies-6 Wavelets are used as waveforms in order to compare the performances of different feature extraction methods more precisely. The formed feature vector represents the features of the pixel on the coordinates (8,8) of the used window. After the traverse of the whole image, the feature matrix is constructed using each feature vector as its rows.

This step applies pixel by pixel shifting of the used window in both horizontal and vertical directions to avoid misclassification on both horizontal and vertical class boundaries. Pixel by pixel shifting is computationally more exhaustive compared to the vertical and horizontal window shifting which

however may cause misclassification on the horizontal and vertical class boundaries respectively.

5. The formed feature matrix is stored as a binary file so that it can be used multiple times without having to calculate it over and over again.
6. The steps from 2 to 5 are performed until all the feature matrices of the selected bands are saved. The saved feature matrices of each selected bands are merged so that the feature vectors of the same pixel are concatenated one by one starting from the first selected band and ending at the last selected band. The final feature matrix is stored again as a binary file to be used multiple times.
7. The final feature matrix is read from the file and The KNN Classifier is fed with 625 training feature vectors of the homogenously distributed pixels and the feature vectors of the candidate pixels. The KNN Classifier assigns each pixel to a single class. The classification were performed for K varying from 1 to 5 and the most successful results were achieved for K=1 and K=2. Another approach would be using The Nearest Neighbour Classifier where the mean of each feature vectors of the same class we calculated and fed into the classifier. Its results were unsatisfactory and will not be presented in this work.
8. The resultant segmented image and the classification performance are saved as separate files.

This overall process can also be programmed in MATLAB using built-in and custom toolboxes where it desperately needs the utilization of parallel programming or GPU based computing due to the large number of used bands [29][30][31][32][34][35].

Using the MATLAB Parallel Computing Toolbox, this process with different input values can be performed in parallel [32].

### **5.9.1 Discrete Wavelet Decomposition Features**

The feature vector for AVIRIS Hyperspectral Data DWT classification includes the mean and standard deviations of the directional subband images on the first level and the mean and standard deviations of both the directional subband and approximation images on the second level.



The sequence of the mean and standard deviations are the same as in the BT-DWT classification. The feature vectors for each used bands are concatenated in the increasing order of band number to form the final feature vector.

$$f_{\mu,B} = [\mu_{L_1H_1}, \mu_{H_1L_1}, \mu_{H_1H_1}, \mu_{L_2L_2}, \mu_{L_2H_2}, \mu_{H_2L_2}, \mu_{H_2H_2}] \quad (5.26)$$

$$f_{\sigma,B} = [\sigma_{L_1H_1}, \sigma_{H_1L_1}, \sigma_{H_1H_1}, \sigma_{L_2L_2}, \sigma_{L_2H_2}, \sigma_{H_2L_2}, \sigma_{H_2H_2}] \quad (5.27)$$

$$F_B = [f_{\mu,B}, f_{\sigma,B}] \quad (5.28)$$

$$F = [F_1, \dots, F_B] \quad (5.29)$$

The resultant feature vector for a single image pixel contains 2590 elements.

### 5.9.2 Stationary Wavelet Decomposition Features

The feature vector for AVIRIS Hyperspectral Data SWT classification includes the mean and standard deviations of the directional subband images on the first level and the mean and standard deviations of both the directional subband and approximation images on the second level.

The sequence of the mean and standard deviations are the same as in the BT-SWT classification. The feature vectors for each used bands are concatenated in the increasing order of band number to form the final feature vector.

$$f_{\mu,B} = [\mu_{L_1H_1}, \mu_{H_1L_1}, \mu_{H_1H_1}, \mu_{L_2L_2}, \mu_{L_2H_2}, \mu_{H_2L_2}, \mu_{H_2H_2}] \quad (5.30)$$

$$f_{\sigma,B} = [\sigma_{L_1H_1}, \sigma_{H_1L_1}, \sigma_{H_1H_1}, \sigma_{L_2L_2}, \sigma_{L_2H_2}, \sigma_{H_2L_2}, \sigma_{H_2H_2}] \quad (5.31)$$

$$F_B = [f_{\mu,B}, f_{\sigma,B}] \quad (5.32)$$

$$F = [F_1, \dots, F_B] \quad (5.33)$$

The resultant feature vector for a single image pixel contains 2590 elements.

### 5.9.3 Contourlet Decomposition Features

The feature vector for AVIRIS Hyperspectral Data CT classification includes the mean and standard deviations of the directional subband images produced by the DFB on the first level and the mean and standard deviations of subband images produced by the LP on the second level. The number of directions of the DFB on the first level is 8 whereas there is no directional decomposition performed by the DFB on the second level.

The sequence of the mean and standard deviations are the same as in the BT-CT classification. The feature vectors for each used bands are concatenated in the increasing order of band number to form the final feature vector.

$$f_{\mu,B} = [\mu_{L_2}, \mu_{H_2}, \mu_{H_1,1}, \dots, \mu_{H_1,8}] \quad (5.34)$$

$$f_{\sigma,B} = [\sigma_{L_2}, \sigma_{H_2}, \sigma_{H_1,1}, \dots, \sigma_{H_1,8}] \quad (5.35)$$

$$F_B = [f_{\mu,B}, f_{\sigma,B}] \quad (5.36)$$

$$F = [F_1, \dots, F_B] \quad (5.37)$$

The resultant feature vector for a single image pixel contains 3700 elements.

### 5.9.4 Nonsampled Contourlet Decomposition Features

The feature vector for AVIRIS Hyperspectral Data NSCT classification includes the mean and standard deviations of the directional subband images produced by the NSDFB on the first level and the mean and standard deviations of subband images produced by the NSLP on the second level. The number of directions of the NSDFB on the first level is 8 whereas there is no directional decomposition performed by the NSDFB on the second level.

The sequence of the mean and standard deviations are the same as in the BT-NSCT classification. The feature vectors for each used bands are concatenated in the increasing order of band number to form the final feature vector.

$$f_{\mu,B} = [\mu_{L_2}, \mu_{H_2}, \mu_{H_1,1}, \dots, \mu_{H_1,8}] \quad (5.38)$$

$$f_{\sigma,B} = [\sigma_{L_2}, \sigma_{H_2}, \sigma_{H_1,1}, \dots, \sigma_{H_1,8}] \quad (5.39)$$

$$F_B = [f_{\mu,B}, f_{\sigma,B}] \quad (5.40)$$

$$F = [F_1, \dots, F_B] \quad (5.41)$$

The resultant feature vector for a single image pixel contains 3700 elements.

### 5.9.5 Wavelet Based Contourlet Decomposition Features

The feature vector for AVIRIS Hyperspectral Data WBCT classification includes the mean and standard deviations of the directional subband images produced by the DFB on the first level and the mean and standard deviations of both the directional subband and approximation images produced by the DWD on the second level.

The sequence of the mean and standard deviations are the same as in the BT-WBCT classification. The feature vectors for each used bands are concatenated in the increasing order of band number to form the final feature vector.

$$f_{\mu,B} = [\mu_{L_2L_2}, \mu_{L_2H_2}, \mu_{H_2L_2}, \mu_{H_2H_2}, \mu_{H_{1,1}}, \dots, \mu_{H_{1,8}}] \quad (5.42)$$

$$f_{\sigma,B} = [\sigma_{L_2L_2}, \sigma_{L_2H_2}, \sigma_{H_2L_2}, \sigma_{H_2H_2}, \sigma_{H_{1,1}}, \dots, \sigma_{H_{1,8}}] \quad (5.43)$$

$$F_B = [f_{\mu,B}, f_{\sigma,B}] \quad (5.44)$$

$$F = [F_1, \dots, F_B] \quad (5.45)$$

The resultant feature vector for a single image pixel contains 10360 elements.

### 5.9.6 Stationary Wavelet Based Contourlet Decomposition Features

The feature vector for AVIRIS Hyperspectral Data SWBCT classification includes the mean and standard deviations of the directional subband images produced by the DFB on the first level and the mean and standard deviations of both the directional subband and approximation images produced by the SWD on the second level.

The sequence of the mean and standard deviations are the same as in the BT-SWBCT classification. The feature vectors for each used bands are concatenated in the increasing order of band number to form the final feature vector.

$$f_{\mu,B} = [\mu_{L_2L_2}, \mu_{L_2H_2}, \mu_{H_2L_2}, \mu_{H_2H_2}, \mu_{H_{1,1}}, \dots, \mu_{H_{1,8}}] \quad (5.46)$$

$$f_{\sigma,B} = [\sigma_{L_2L_2}, \sigma_{L_2H_2}, \sigma_{H_2L_2}, \sigma_{H_2H_2}, \sigma_{H_1,1}, \dots, \sigma_{H_1,8}] \quad (5.47)$$

$$F_B = [f_{\mu,B}, f_{\sigma,B}] \quad (5.48)$$

$$F = [F_1, \dots, F_B] \quad (5.49)$$

The resultant feature vector for a single image pixel contains 10360 elements.

## **6. RESULTS AND DISCUSSION**

The performance difference between the segmentation results can easily be seen for some transform methods whereas for some of them, reference to the performance percentage tables is recommended.

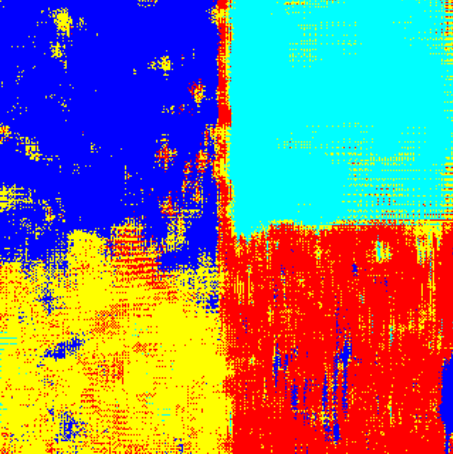
The decomposition and feature extraction routines were run both during the BT Matrix and AVIRIS Hyperspectral Data classification by using the Haar, Daubechies-4 and Daubechies-6 Wavelet Filters for subband decomposition.

The window sizes used during the pixel by pixel feature extraction were 12x12, 16x16 and 20x20. The most satisfactory results were obtained by using the 16x16 window size and the other two window sizes were left out due to this reason.

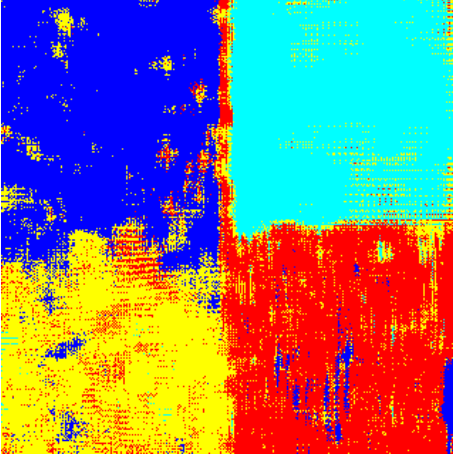
The KNN classification algorithm was run by using K varying from 1 to 5 without taking the average of the training feature vectors belonging to the same classes. The most satisfactory results were demonstrated for K=1 and K=2, the results for other K values will not be shown. The Nearest Neighbour classification algorithm, which uses the average of the training feature vectors belonging to the same classes with K=1 produced inconsistent results and left out due to this reason.

In overall, there were 6 different decomposition methods utilizing 3 different Wavelet Filters applied to 2 different images. Hence, there were 36 different feature sets which were classified using 2 different K values which at the end produced 72 segmentation results.

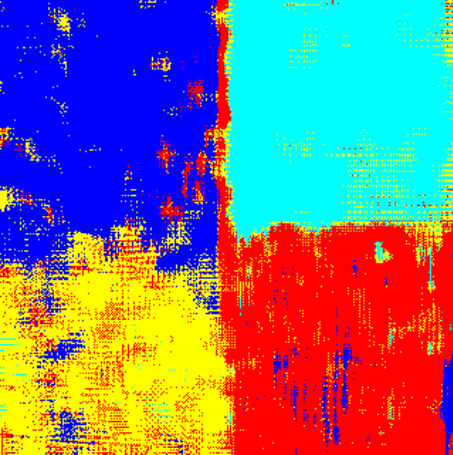
**6.1 Discrete Wavelet Transform Brodatz Results**



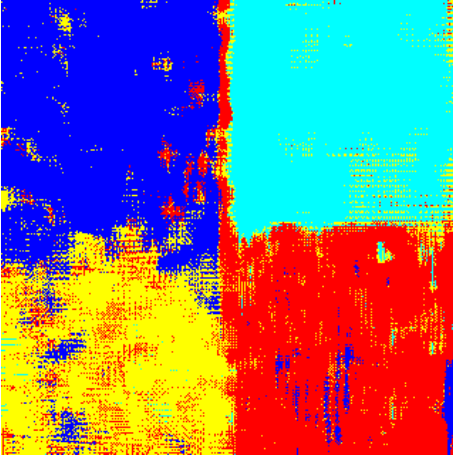
(a) using Haar Wavelet, K=1



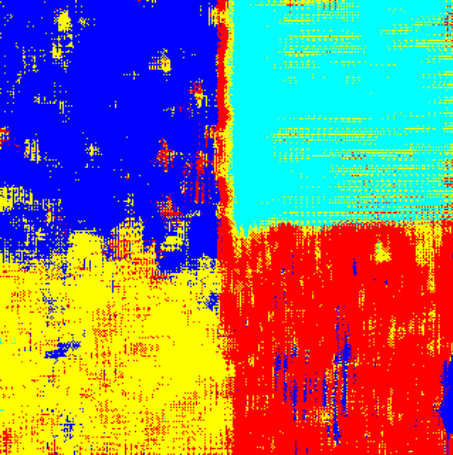
(b) using Haar Wavelet, K=2



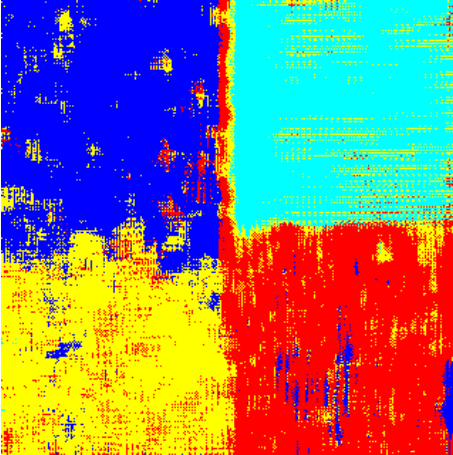
(c) using db4 Wavelet, K=1



(d) using db4 Wavelet, K=2



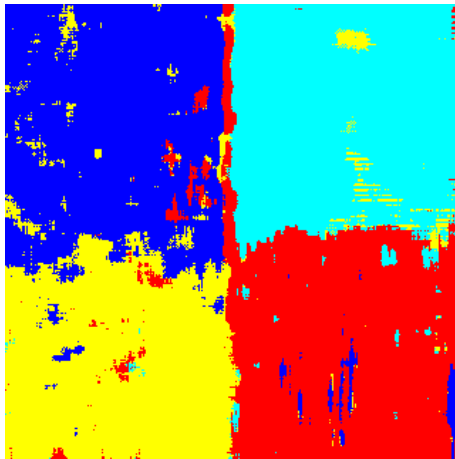
(e) using db6 Wavelet, K=1



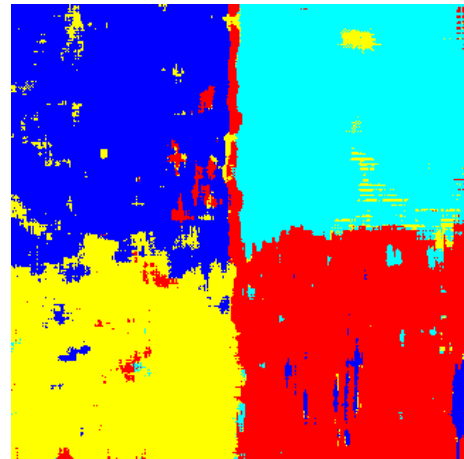
(f) using db6 Wavelet, K=2

**Figure 6.1 : DWT BT Segmentation Results.**

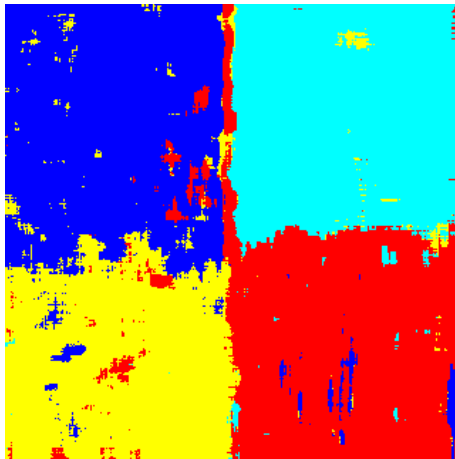
## 6.2 Stationary Wavelet Transform Brodatz Results



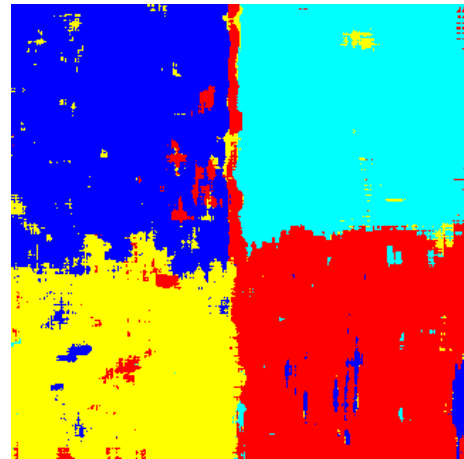
(a) using Haar Wavelet, K=1



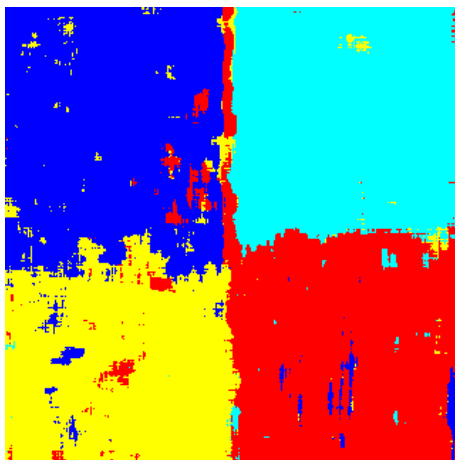
(b) using Haar Wavelet, K=2



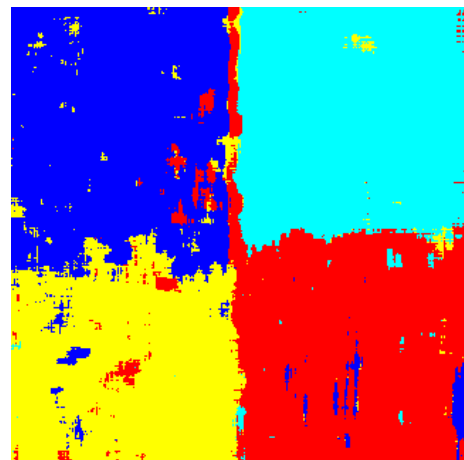
(c) using db4 Wavelet, K=1



(d) using db4 Wavelet, K=2



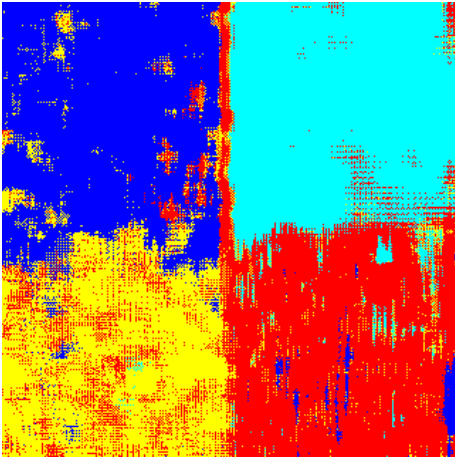
(e) using db6 Wavelet, K=1



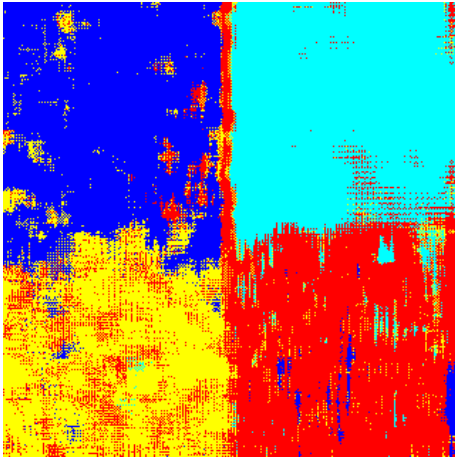
(f) using db6 Wavelet, K=2

**Figure 6.2 :** SWT BT Segmentation Results.

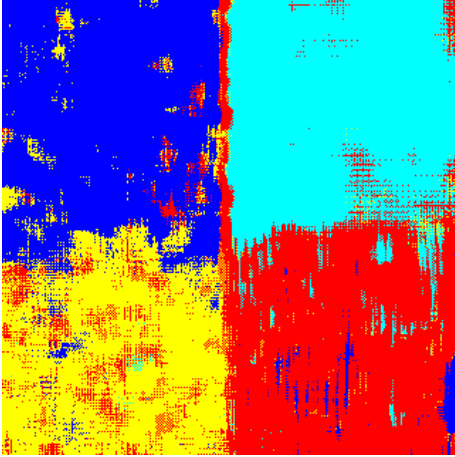
### 6.3 Contourlet Transform Brodatz Results



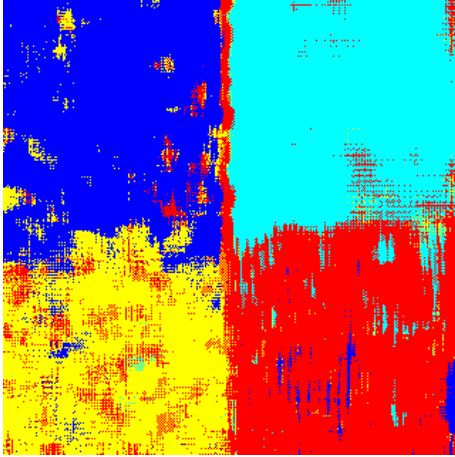
(a) using Haar Wavelet, K=1



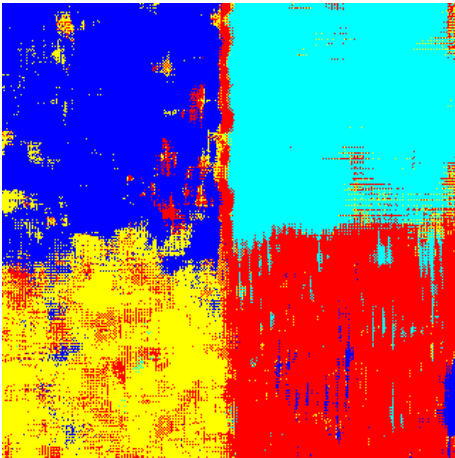
(b) using Haar Wavelet, K=2



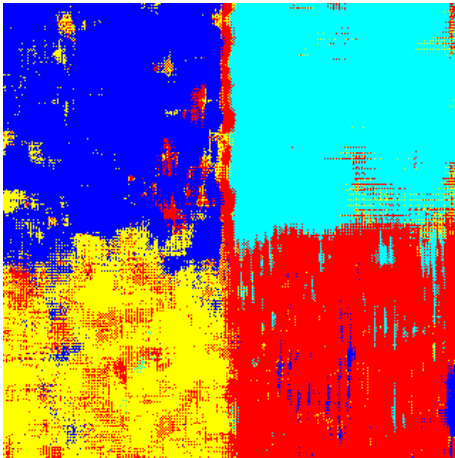
(c) using db4 Wavelet, K=1



(d) using db4 Wavelet, K=2



(e) using db6 Wavelet, K=1

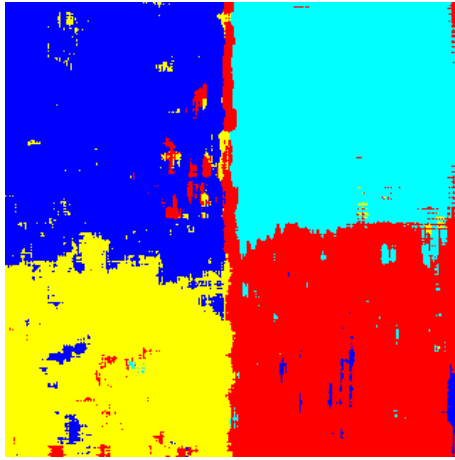


(f) using db6 Wavelet, K=2

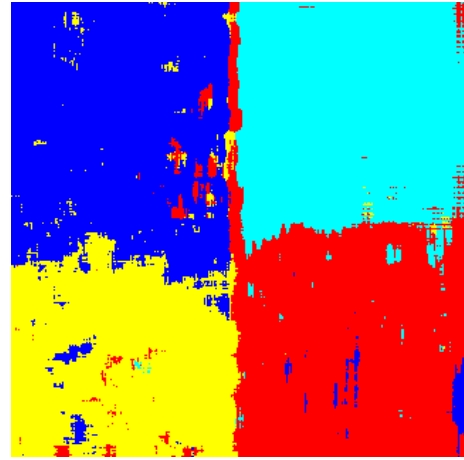
**Figure 6.3 :** CT BT Segmentation Results.



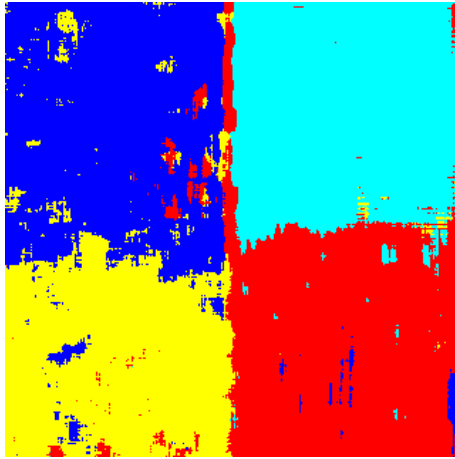
## 6.4 Nonsubsampled Contourlet Transform Brodatz Results



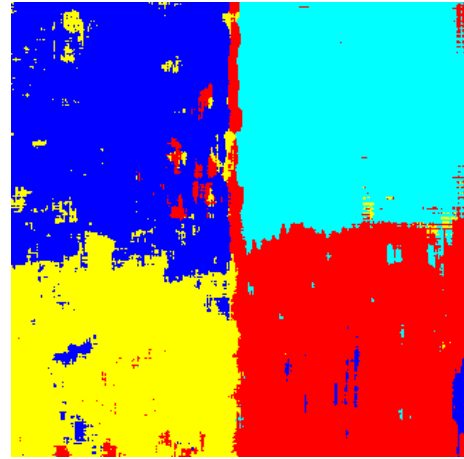
(a) using Haar Wavelet, K=1



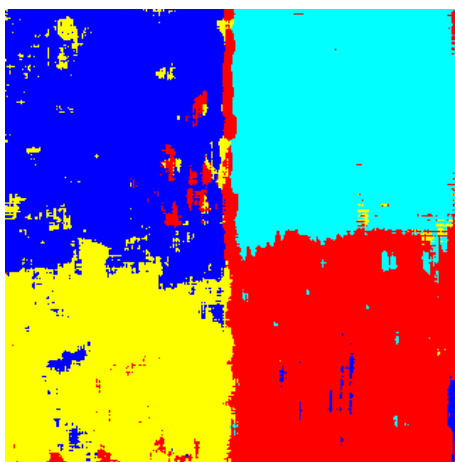
(b) using Haar Wavelet, K=2



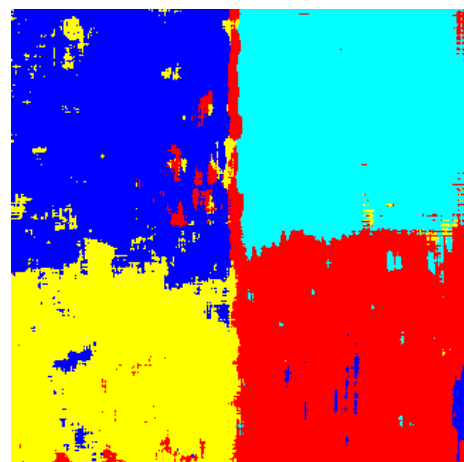
(c) using db4 Wavelet, K=1



(d) using db4 Wavelet, K=2



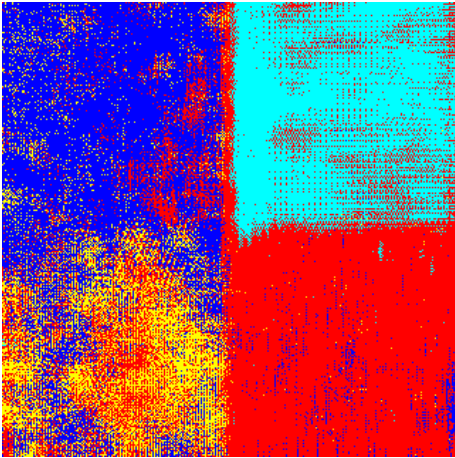
(e) using db6 Wavelet, K=1



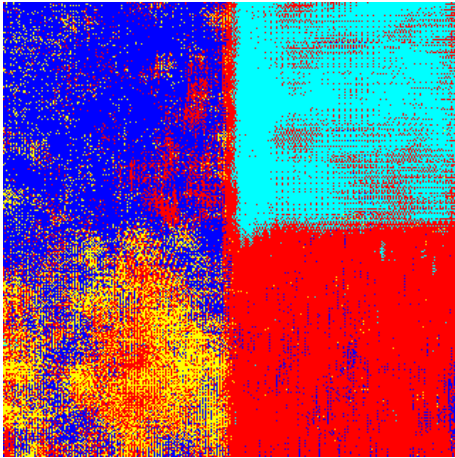
(f) using db6 Wavelet, K=2

**Figure 6.4 :** NSCT BT Segmentation Results.

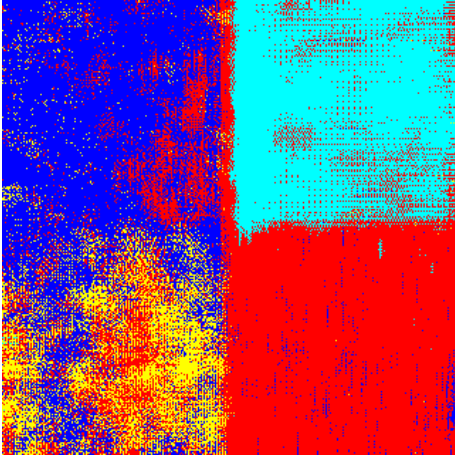
**6.5 Wavelet Based Contourlet Transform Brodatz Results**



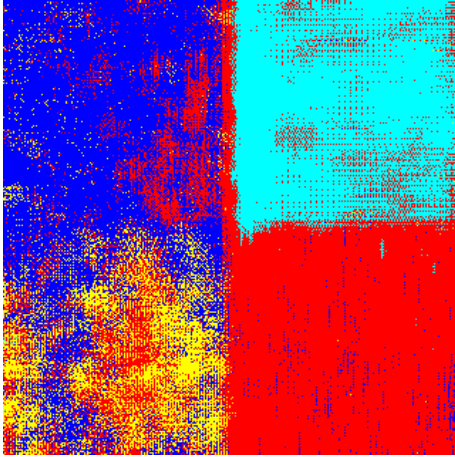
(a) using Haar Wavelet, K=1



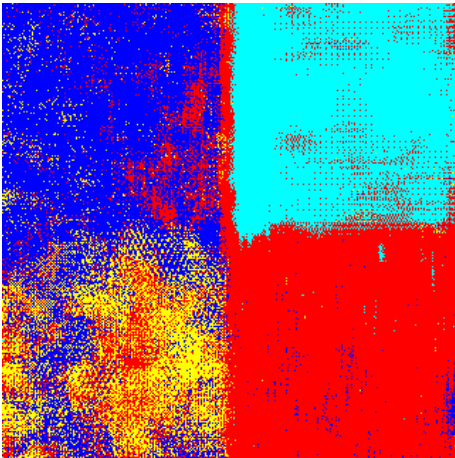
(b) using Haar Wavelet, K=2



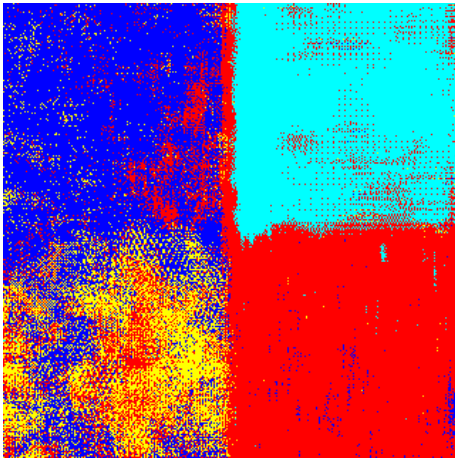
(c) using db4 Wavelet, K=1



(d) using db4 Wavelet, K=2



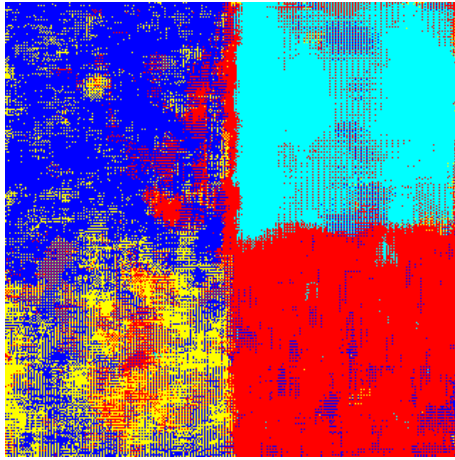
(e) using db6 Wavelet, K=1



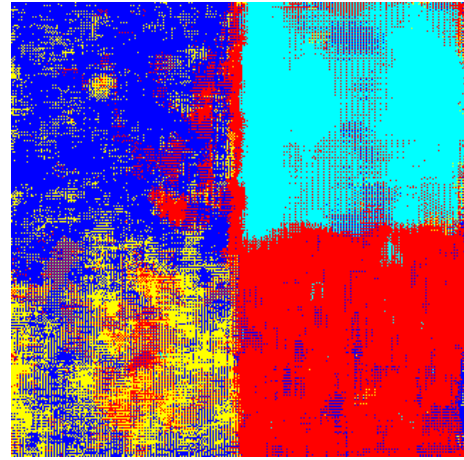
(f) using db6 Wavelet, K=2

**Figure 6.5 : WBCT BT Segmentation Results.**

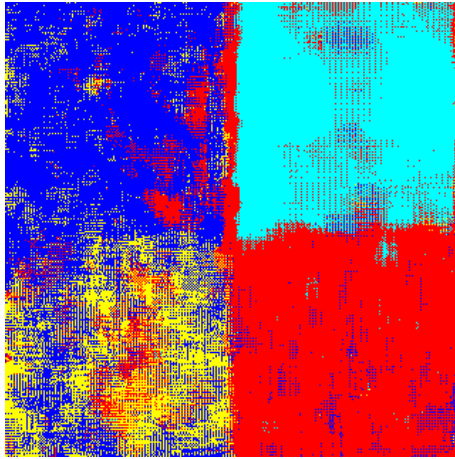
## 6.6 Stationary Wavelet Based Contourlet Transform Brodatz Results



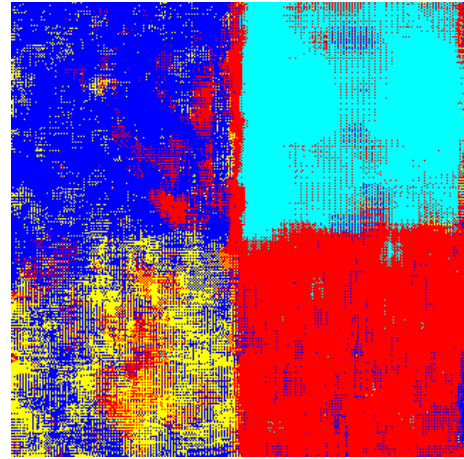
(a) using Haar Wavelet, K=1



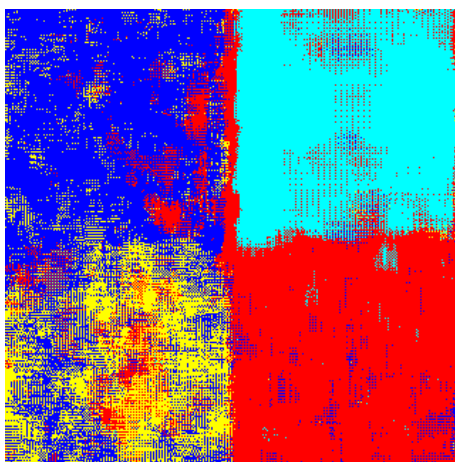
(b) using Haar Wavelet, K=2



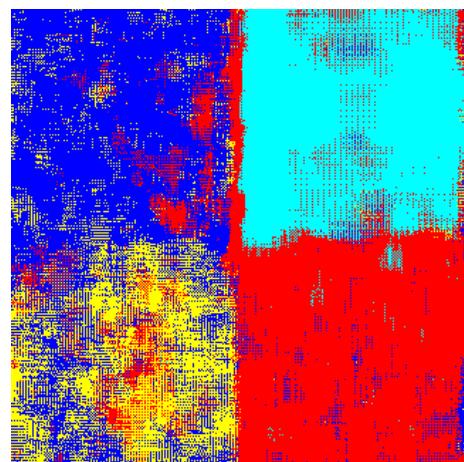
(c) using db4 Wavelet, K=1



(d) using db4 Wavelet, K=2



(e) using db6 Wavelet, K=1



(f) using db6 Wavelet, K=2

**Figure 6.6 : SWBCT BT Segmentation Results.**

## 6.7 Brodatz Results and Discussion

The common observations from the results for the BT are that there exist tolerable misclassification bands on the boundaries between the class regions and the top-right, top-left and bottom-right class regions were classified most successfully. Additionally, the results demonstrate that there were small differences between the classification performances with different Wavelets. In general, the Daubechies-4 and Daubechies-6 Wavelets performed equally as the most whereas the Haar Wavelet did as the least successful. The Hybrid Transform methods provided significantly worse results compared to the other ones and the nonsubsampling transform methods except the SWBCT resulted in much clustered segmentations compared to the subsampled ones.

The DWT results for the BT demonstrate that the Daubechies-4 Wavelet performed as the most whereas the Haar Wavelet did as the least successful in this transform method. In all class regions, there were misclassified pixels belonging to all other classes. The most successful segmentations occurred on the top-right class region whereas the least successful segmentations occurred on the bottom-left class region.

The SWT for the BT greatly outperformed the DWT counterpart. The redundancy of the SWT resulted in much clustered segmentations. There were almost no differences between the results with the Daubechies-4 and Daubechies-6 Wavelets whereas it is noticeable that more misclassified pixels occurred on the upper class regions with the Haar Wavelet. The Daubechies-6 Wavelet performed as the most whereas the Haar Wavelet did as the least successful in this transform method. The most successful segmentations occurred on the top-right class region having been classified better than the DWT counterpart whereas the least successful segmentations again occurred on the bottom-left class region.

The CT for the BT performed better than the DWT counterparts except the Haar Wavelet one; whereas some additional pixels distributed over the class regions were misclassified as well. The reason for this is that since the CT has more directionality than the DWT counterparts, the training features were scattered over many directions, resulting in less successful segmentations on some parts as well, noticeably on the top-right and bottom-left class regions. The Daubechies-4 Wavelet performed as the most whereas the Haar Wavelet did as the least successful in this



transform method. The most successful segmentations occurred again on the top-right class whereas the least successful segmentations again occurred on the bottom-left class region.

The NSCT for the BT greatly outperformed the CT counterpart and its performance was also better than the SWT counterpart with the Haar Wavelet. The redundancy of the NSCT resulted in much clustered segmentations. There were almost no differences between the results with the Daubechies-4 and Daubechies-6 Wavelets whereas it is noticeable that less misclassified pixels occurred on the upper class regions with the Haar Wavelet. The Haar Wavelet performed as the most whereas the Daubechies-6 Wavelet did as the least successful in this transform method. The most successful segmentations occurred on the top-right class region having been classified better than with the DWT counterpart whereas there was still a tolerable band of misclassification on the boundary between this region and the top-left class region. The least successful segmentations again occurred on the bottom-left class region.

The WBCT for the BT provided the worst results among all transform methods. The used Wavelets affected the segmentations of the most misclassified class region, the bottom-left one. The Daubechies-6 Wavelet performed as the most whereas the Haar Wavelet did as the least successful in this transform method.

The SWBCT for the BT compensated the flaws of the WBCT counterpart marginally and its segmentation performances are almost independent of the Wavelets used. Still, it was not powerful enough to compete with the other Transform Methods. The Daubechies-6 Wavelet performed as the most whereas the Haar Wavelet did as the least successful in this transform method.

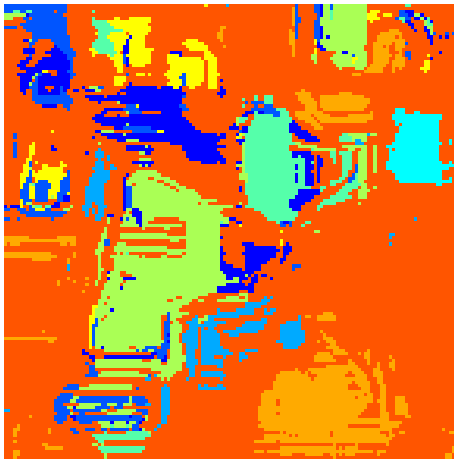
## 6.8 Discrete Wavelet Transform AVIRIS Results



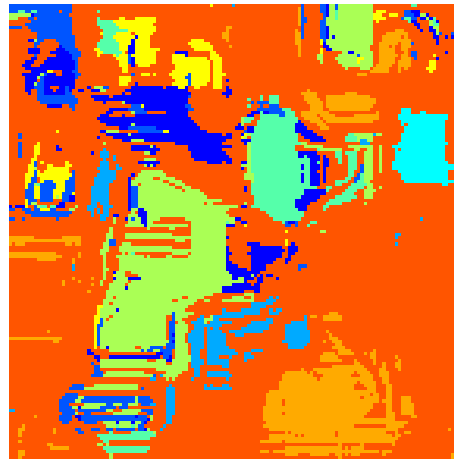
(a) using Haar Wavelet, K=1



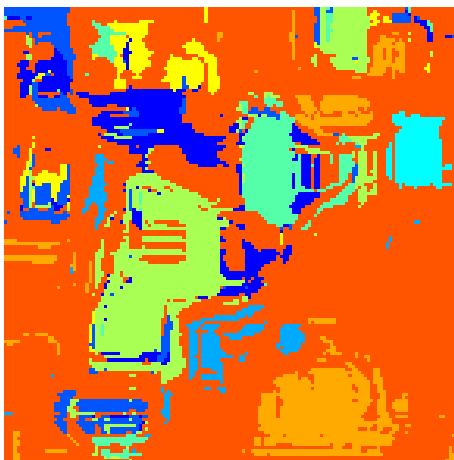
(b) using Haar Wavelet, K=2



(c) using db4 Wavelet, K=1



(d) using db4 Wavelet, K=2



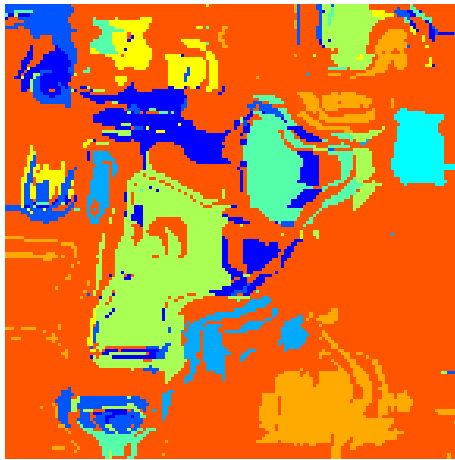
(e) using db6 Wavelet, K=1



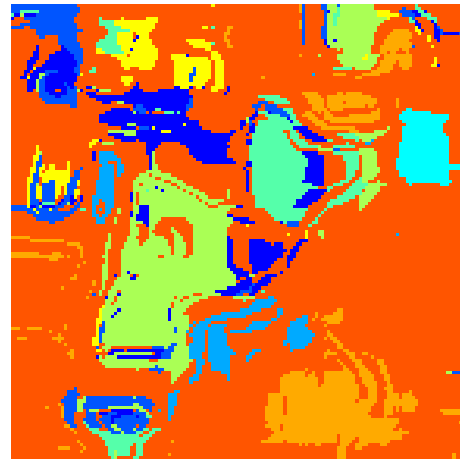
(f) using db6 Wavelet, K=2

**Figure 6.7** : DWT AVIRIS Segmentation Results.

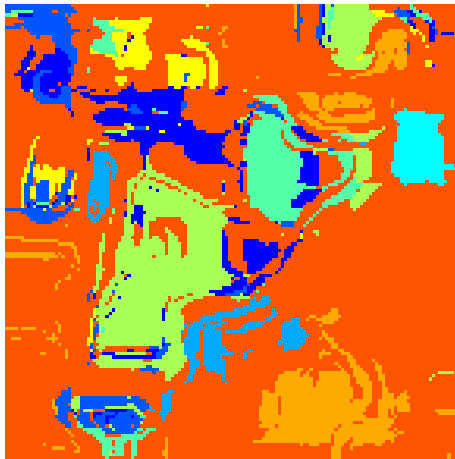
## 6.9 Stationary Wavelet Transform AVIRIS Results



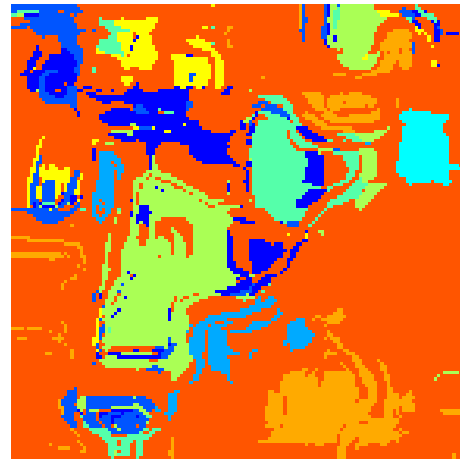
(a) using Haar Wavelet, K=1



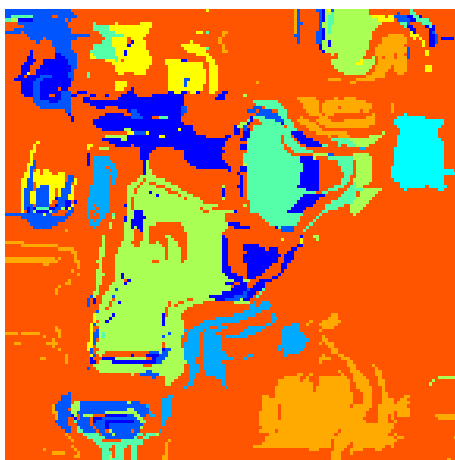
(b) using Haar Wavelet, K=2



(c) using db4 Wavelet, K=1



(d) using db4 Wavelet, K=2



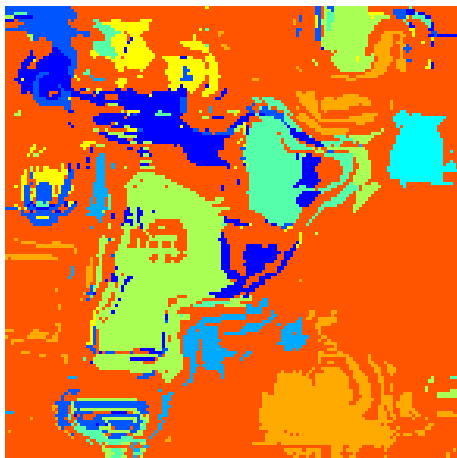
(e) using db6 Wavelet, K=1



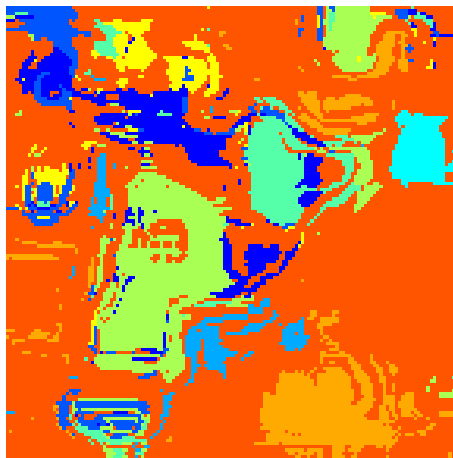
(f) using db6 Wavelet, K=2

**Figure 6.8 :** SWT AVIRIS Segmentation Results.

## 6.10 Contourlet Transform AVIRIS Results



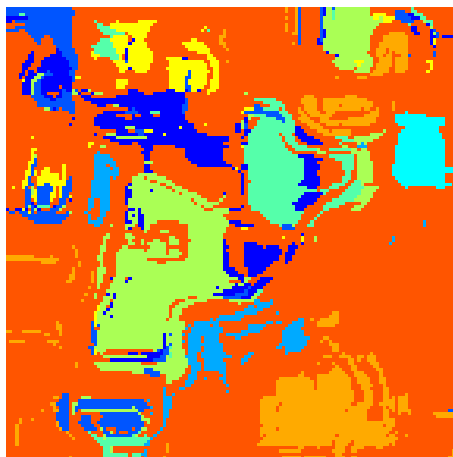
(a) using Haar Wavelet, K=1



(b) using Haar Wavelet, K=2



(c) using db4 Wavelet, K=1



(d) using db4 Wavelet, K=2



(e) using db6 Wavelet, K=1

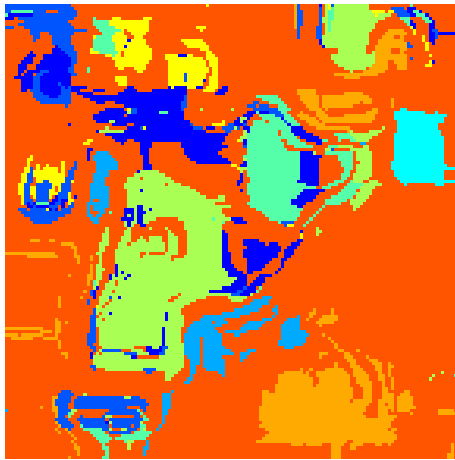


(f) using db6 Wavelet, K=2

**Figure 6.9 :** CT AVIRIS Segmentation Results.



### 6.11 Nonsubsampled Contourlet Transform AVIRIS Results



(a) using Haar Wavelet, K=1



(b) using Haar Wavelet, K=2



(c) using db4 Wavelet, K=1



(d) using db4 Wavelet, K=2



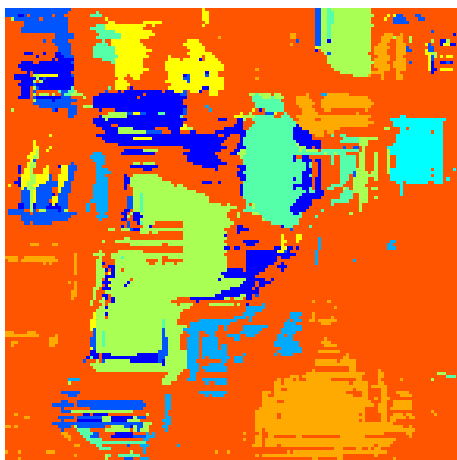
(e) using db6 Wavelet, K=1



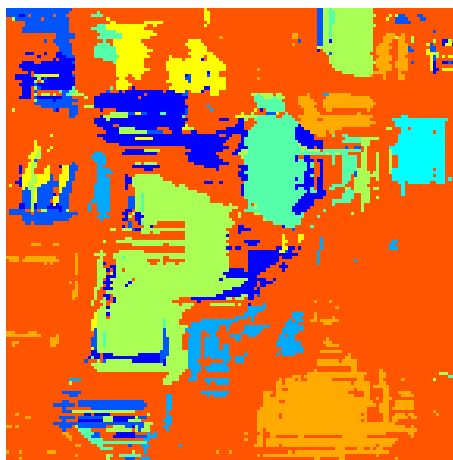
(f) using db6 Wavelet, K=2

**Figure 6.10** : NSCT AVIRIS Segmentation Results.

## 6.12 Wavelet Based Contourlet Transform AVIRIS Results



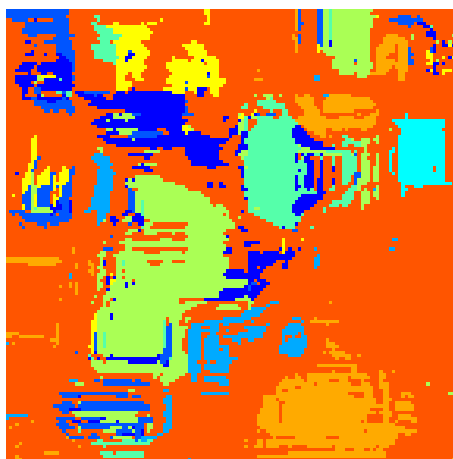
(a) using Haar Wavelet, K=1



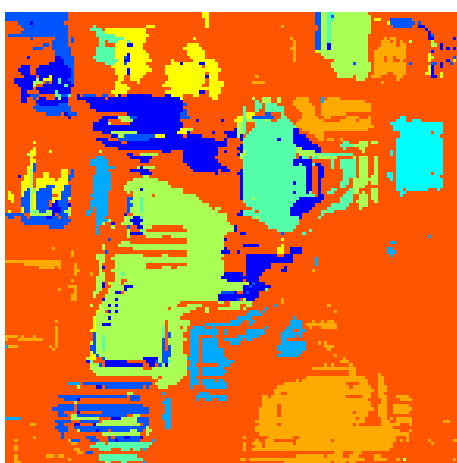
(b) using Haar Wavelet, K=2



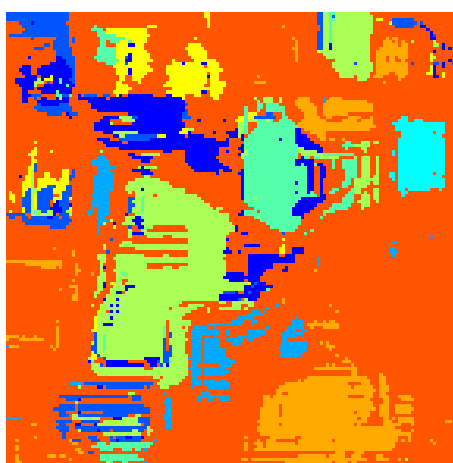
(c) using db4 Wavelet, K=1



(d) using db4 Wavelet, K=2



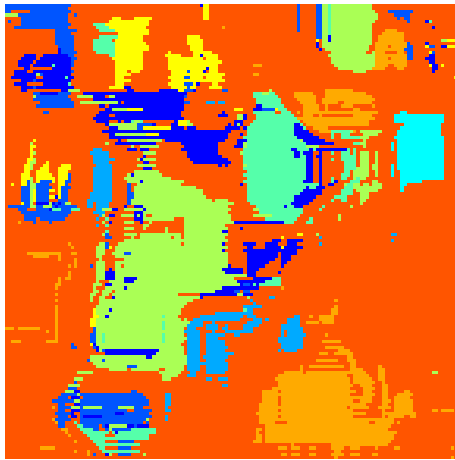
(e) using db6 Wavelet, K=1



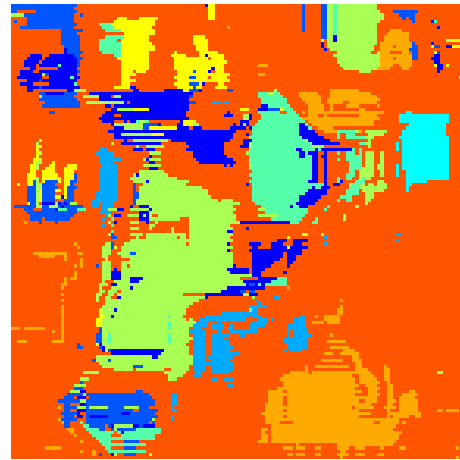
(f) using db6 Wavelet, K=2

**Figure 6.11** : WBCT AVIRIS Segmentation Results.

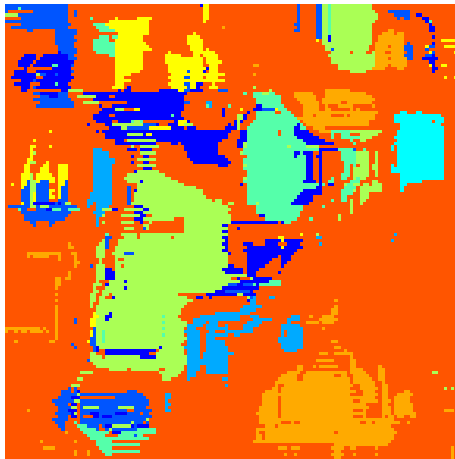
### 6.13 Stationary Wavelet Based Contourlet Transform AVIRIS Results



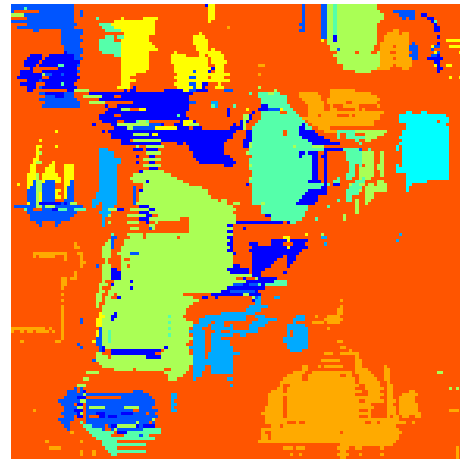
(a) using Haar Wavelet, K=1



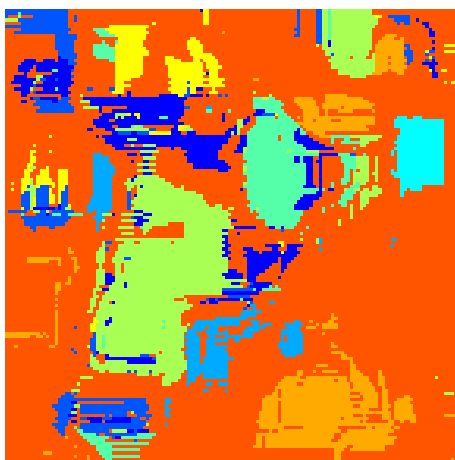
(b) using Haar Wavelet, K=2



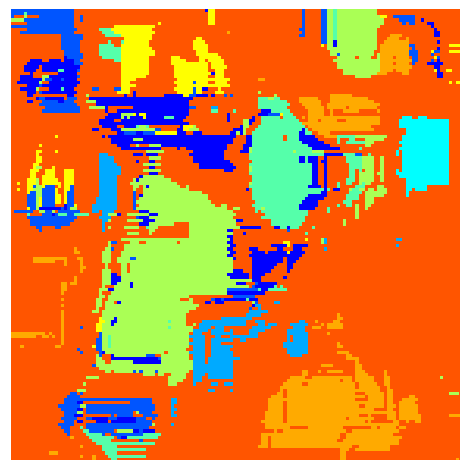
(c) using db4 Wavelet, K=1



(d) using db4 Wavelet, K=2



(e) using db6 Wavelet, K=1



(f) using db6 Wavelet, K=2

**Figure 6.12 :** SWBCT AVIRIS Segmentation Results.

## 6.14 AVIRIS Results and Discussion

The results for the AVIRIS Hyperpectral Data demonstrate even smaller differences between the classification performances with different Wavelets. In general, both the Daubechies-4 Daubechies-6 Wavelets performed equally as the most whereas the Haar Wavelet did as the least successful. Unlike the BT case, the misclassified pixels occurred on all the class regions belonged to a single class, the background class 17. It was also noticeable that the vanished classes after the class reduction process were partially detected and assigned to the nearest classes different than the background class. Finally, the Hybrid Transform methods did not face significant performance drops as in the BT case. In fact, the SWBCT provided the most successful results in all Wavelet choices.

The DWT results for the AVIRIS Hyperpectral Data demonstrate that the best results were obtained using the Daubechies-6 Wavelet. The Haar and Daubechies-4 Wavelets provided less successful results in this transform method.

The SWT for the AVIRIS Hyperpectral Data outperformed the DWT counterpart due to its redundancy. The Haar Wavelet performed as the most whereas the Daubechies-4 and Daubechies-6 Wavelets did equally less successful in this transform method.

The CT for the AVIRIS Hyperpectral Data outperformed the DWT counterpart due to its increased directionality. The Daubechies-6 Wavelet performed as the most whereas the Haar Wavelet did as the least successful in this transform method.

The NSCT for the AVIRIS Hyperpectral Data outperformed the CT counterpart due to its increased directionality. The Daubechies-6 Wavelet performed as the most whereas the Haar Wavelet did as the least successful in this transform method.

The WBCT for the AVIRIS Hyperpectral Data outperformed the DWT counterpart due to its increased directionality. The Haar Wavelet performed as the most whereas the Daubechies-6 Wavelet did as the least successful in this transform method.

The SWBCT for the AVIRIS Hyperpectral Data outperformed all the other transform methods due to its redundancy and increased directionality. The Daubechies-6 Wavelet performed as the most whereas the Haar Wavelet did as the least successful in this transform method.

The overall results are presented on Tables 6.1 and 6.2.

**Table 6.1 :** BT Classification Results.

Waveform	K	DWT %	SWT %	CT %	NSCT %	WBCT %	SWBCT %
haar	1	84.63	89.81	84.21	90.43	72.79	75.30
haar	2	84.63	89.81	84.21	90.43	72.79	75.30
db4	1	85.04	90.52	86.17	90.33	74.00	76.88
db4	2	85.04	90.52	86.17	90.33	74.00	76.88
db6	1	84.26	90.76	85.80	90.30	76.54	77.66
db6	2	84.26	90.76	85.80	90.30	76.54	77.66

**Table 6.2 :** AVIRIS Hyperspectral Data Classification Results.

Waveform	K	DWT %	SWT %	CT %	NSCT %	WBCT %	SWBCT %
haar	1	76.76	78.88	77.19	78.99	78.07	79.27
haar	2	76.76	78.88	77.19	78.99	78.07	79.27
db4	1	76.76	78.78	78.66	79.15	78.04	79.67
db4	2	76.76	78.78	78.66	79.15	78.04	79.67
db6	1	78.16	78.78	78.73	79.17	77.86	79.80
db6	2	78.16	78.78	78.73	79.17	77.86	79.80

At the first glance, the classification performances clearly show that the performances do not depend on the parameter K for the values 1 and 2. However, the omitted K values from 3 to 5 showed small variations during the simulations. Most importantly, the BT classification performances are superior to the AVIRIS Hyperspectral Data classification ones on all transform methods except the Hybrid Transform ones.

As the second observation, the nonsubsampling transform methods greatly outperformed its nonsubsampling counterparts. The Hybrid Transform methods performed superior in AVIRIS Hyperspectral Data but fell short in BT case. The BT features have diverse frequency spectrum characteristics compared to the AVIRIS Hyperspectral Data and the Wavelet subband decomposition divides the frequency plane into smaller directional subbands than the LP/NSLP; hence, the BT features become scattered over many different directions, resulting in poor performance of

the DFB/NSDFB used by the Hybrid Transform methods. On the contrary, the AVIRIS Hyperspectral Data features stayed concentrated and in addition to that, the classes in the AVIRIS Hyperspectral Data case were closed to each other; thus, the used windows contained many different classes. The Hybrid Transform methods performed well in those cases.

Finally and most importantly, the CT and NSCT performed better than the DWT and SWT respectively for all AVIRIS Hyperspectral Data cases and for some BT cases. Benefiting from increased directionality of the CT and famous performance of the DWT, the Hybrid Transform methods provided promising and encouraging results in hyperspectral data classification.

## 7. RESULTS OVERVIEW AND CONCLUSION

Considering the BT classification results, the CT outperforms the DWT with the Daubechies-4 and Daubechies-6 Wavelets; the NSCT outperforms the SWT with the Haar Wavelet. This shows that the classification algorithm benefits from increased directionality but the redundancy is more dominant. It is contradictory to this observation however, that the WBCT and the SWBCT perform poorer than all the other transform methods. The main reason for this is that the BT features are scattered over many different directions, resulting in poor performance of the Hybrid Transforms on those smaller chunks.

Considering the AVIRIS Hyperspectral Data classification performance, the CT and NSCT outperform the DWT and SWT in all Wavelet choices. Unlike in the BT classification, the SWBCT performances are superior and the WBCT performs comparable to the other transform methods. In fact, the SWBCT is the best transform method for the hyperspectral data classification benefiting from the increased directionality and redundancy. The data difference between the BT and AVIRIS Hyperspectral Data clearly shows that the usage of the increased directionality property of the CT on more clustered and smooth class regions with decreased resolution, hence with many classes near the same regions, improves hyperspectral data classification performance.

These results overall demonstrate that the extraction of the directional features during the classification of the single-band regular textures is crucial with the avoidance of the decomposition into too many directions, which is on the contrary desirable in the hyperspectral data classification. The Hybrid Transform family is to be considered as the promising successor of the CT benefiting from its advantages.

As the next future work, modern Wavelet Transforms like the Directional Wavelet Transform can be added for comparisons; the CT and NSCT can be applied to RADARSAT images taken from UHUZAM and Haralick features like contrast, energy, entropy, local homogeneity etc. can be used to improve the classification performances [37].





## REFERENCES

- [1] **Mallat S. G.**, 1989: A Theory for Multiresolution Signal Decomposition: The Wavelet Representation, *IEEE Transactions on Pattern Analysis and Machine Intelligence*, vol. 11, no. 7.
- [2] **Grossman A., Morlet J.**, 1984: Decomposition of Hardy Functions into Square Integrable Wavelets of Constant Shape, *SIAM J. Math*, vol. 15, pp. 723-736.
- [3] **Shensa M. J.**, 1992: The Discrete Wavelet Transform: Wedding the A Trouns and Mallat Algorithms, *IEEE Transactions on Signal Processing*, vol. 40, no. 10, pp. 2464-2482.
- [4] **Bamberger R. H., Smith M. J. T.**, 1992: A Filter Bank for the Directional Decomposition of Images: Theory and Design, *IEEE Transactions on Signal Processing*, vol. 40, pp. 882-893.
- [5] **Park S., Smith M. J. T., Mersereau R. M.**, 1999: A new Directional Filter Bank for Image Analysis and Classification, *Proceedings of IEEE International Conference on Acoustics, Speech and Signal Processing*, pp. 1286-1290.
- [6] **Do M. N., Vetterli M.**, 2002: Contourlets: A Directional Multiresolution Image Representation, *Proceedings of IEEE International Conference on Image Processing*, pp. 357-360.
- [7] **Burt P. J., Adelson E. H.**, 1983: The Laplacian Pyramid as a Compact Image Code, *IEEE Transactions on Communications*, vol. 31, no. 4, pp. 532-540.
- [8] **Do M. N., Vetterli M.**, 2001: Pyramidal Directional Filter Banks and Curvelets, *Proceedings of IEEE International Conference on Image Processing*.
- [9] **Antoine J. P., Carrette P., Murenzi R., Piette B.**, 1993: Image Analysis with Two-Dimensional Continuous Wavelet Transform, *Signal Processing*, vol. 31, pp. 241-272.
- [10] **Kingsbury N.**, 2001: Complex Wavelets for shift-invariant Analysis and Filtering of Signals, *Journal of Applied and Computational Harmonic Analysis*, vol. 10, no. 3, pp. 234-253.
- [11] **Candes E., Donoho D.**, 1999: Curvelets: A surprisingly Effective Nonadaptive Representation for Objects with Edges, *Curve and Surface Fitting*, Vanderbilt University Press.
- [12] **Do M. N., Vetterli M.**, 2005: The Contourlet Transform: An Efficient Directional Mutiresolution Image Representation, *IEEE Transactions on Image Processing*.

- [13] **Majumdar A., Bhattacharya A.**, 2009: A Comparative Study in Wavelets, Curvelets and Contourlets as Feature Sets for Pattern Recognition, *The International Arab Journal of Information Technology*, vol. 6, no. 1.
- [14] **Li S., Taylor J. S.**, 2004: Texture Classification by Combining Wavelet and Contourlet Features, *SSPR & SPR, LNCS 3138*, pp. 1126-1134.
- [15] **Duan R., Man H., Chen L.**, 2001: Rotation Invariant Texture Classification Based on a Directional Filter Bank, *Proceedings of IEEE International Conference on Multimedia and Expo*, pp. 1291-1294.
- [16] **Eslami R., Radha H.**, 2004: Wavelet-based Contourlet Transform and its Application to Image Coding, *Proceedings of IEEE International Conference on Image Processing*.
- [17] **Eslami R., Radha H.**, 2005: New Image Transforms Using Hybrid Wavelets and Directional Filter Banks: Analysis and Design, *ICIP*.
- [18] **Cunda A. L., Zhou J., Do M. N.**, 2006: The Nonsubsampled Contourlet Transform: Theory, Design and Applications, *IEEE Transactions on Image Processing*, vol. 15, no. 10.
- [19] **Hu Y., Hou B., Wang S., Jiao L.**, 2006: Texture Classification via Stationary-Wavelet Based Contourlet Transform, *IWICPAS, LNCS 4153*, pp. 485-494.
- [20] **Tanaka Y., Ikehara M., Nguyen T. Q.**, 2009: Multiresolution Image Representation Using Combined 2-D and 1-D Directional Filter Banks, *IEEE Transactions on Image Processing*, vol. 18, no. 2.
- [21] **Tadjudin S., Landgrebe D. A.**, 1999: Covariance Estimation With Limited Training Samples, *IEEE Transactions on Geoscience and Remote Sensing*, vol. 37, no. 4.
- [22] **Benediktsson J. A., Garcia X. C., Waske B., Chanussot J., Sveinsson J. R., Fauvel M.**, 2008: Ensemble Methods for Classification of Hyperspectral Data, *IGARSS*.
- [23] **Mojaradi B., Emami H., Varshosaz M., Jamali S.**, 2008: A Novel Band Selection Method for Hyperspectral Data Analysis, *The International Archives of the Photogrammetry, Remote Sensing and Spatial Information Sciences*, vol. 37, part B7.
- [24] **Nguyen T. T., Oraintara S.**, 2006: On Aliasing Effects in the Contourlet Filter Bank, *14<sup>th</sup> European Signal Processing Conference*.
- [25] **Alpaydm E.**, 2004: Introduction to Machine Learning, *MIT Press*.
- [26] **Bishop C. M.**, 2006: Pattern Recognition and Machine Learning, *Springer Science & Media*.
- [27] **Kunaver M., Tasic J. F.**, 2005: Image Feature Extraction – an Overview, *EUROCON*.
- [28] **Brodatz P.**, 1966: Textures: A Photographic Album for Artists and Designers, *Dover, New York*.
- [29] **MATLAB 2009b for Windows x64 Edition**, 2009: MATLAB Wavelet Toolbox, <http://www.mathworks.com/products/wavelet/>.

- [30] **Do M. N.**, 2005: Contourlet Toolbox developed by Minh N. Do, <http://www.mathworks.com/matlabcentral/fileexchange/8837-contourlet-toolbox> or <http://www.ifp.uiuc.edu/~minhdo/software>.
- [31] **Cunda A.**, 2006: Nonsubsampled Contourlet Toolbox developed by A. Cunda, <http://www.mathworks.com/matlabcentral/fileexchange/10049-nonsubsampled-contourlet-toolbox>.
- [32] **MATLAB 2009b for Windows x64 Edition**, 2009: MATLAB Parallel Computing Toolbox, <http://www.mathworks.com/products/parallel-computing/>.
- [33] **AVIRIS Hyperspectral Data**, 1992: AVIRIS NW Indiana's Indian Pines 1992 data set, <ftp://ftp.ecn.purdue.edu/biehl/MultiSpec/92AV3C> and [ftp://ftp.ecn.purdue.edu/biehl/PC\\_MultiSpec/ThyFiles.zip](ftp://ftp.ecn.purdue.edu/biehl/PC_MultiSpec/ThyFiles.zip).
- [34] **NVidia CUDA Zone**, 2010: CUDA SDK, Drivers and Guides are available at [http://www.nvidia.com/object/cuda\\_home\\_new.html](http://www.nvidia.com/object/cuda_home_new.html).
- [35] **MATLAB Jacket Engine**, 2010: Commercial MATLAB CUDA Engine called Jacket is available at <http://www.accelereyes.com>.
- [36] **Truc P. T. H., Khan M. A. U., Lee Y., Lee S., Kim T.**, 2008: Vessel Enhancement Filter Using Directional Filter Bank, *Computer Vision and Understanding*, Elsevier.
- [37] **Haralick R. M.**, 1979: Statistical and Structural Approaches to Texture, *Proceedings of IEEE*, vol. 67, no. 5.



## **CURRICULUM VITAE**

**Candidate's full name:** **Bedrettin Erbil KONUK**

**Place and date of birth:** **Turkey / Istanbul 29.07.1977**

**E-mail:** **erbilkonuk@gmail.com**

**Universities and  
Colleges attended:**

**Middle East Technical University**

**Electrical & Electronics Engineering Department**

**Istanbul Technical University**

**Satellite Communication & Remote Sensing**

**Publications:**

▪ **Konuk B. E.**, Gültekin Ö., Erer I., 2010: Hyperspectral Data Classification Using Contourlet Transform, *Unmanned Vehicles 2010 Istanbul, Turkey*.